HYDROLOGICAL EXTREMES IN URBAN ENVIRONMENTS: IMPACT ON WATER QUALITY

by

DANNY CROGHAN

A thesis submitted to the University of Birmingham for the degree of

DOCTOR OF PHILOSOPHY

School of Geography, Earth and Environmental Science

College of Life and Environmental Sciences

University of Birmingham

September 2019

Abstract

Water quality is deteriorating worldwide due to the combined pressures of increasing urbanization and more frequent and severe extreme events. This thesis looks specifically at water temperature and dissolved organic matter (DOM), which despite being master variables of river water quality are not well understood in urban rivers. This thesis aims to increase understanding of how extreme events and urbanization combine to change the dominant processes for water temperature and DOM dynamics. Resultantly research was conducted in a range of headwater streams within Birmingham, UK from June 2016 to September 2018.

Research gaps on the effects of urbanization and extreme events on water temperature and DOM were identified and four research themes were described. Firstly, the effects of precipitation on water temperature surges at 11 sites in an urban catchment were investigated, and the choice of precipitation dataset on the results evaluated. Secondly, the effects of extreme high and low flows on river temperature were analyzed for 27 sites in 3 catchments and the influence of land use evaluated. Thirdly, the impacts of shading and water temperature on photodegradation and biodegradation rates of urban DOM were studied. Fourthly, an *in-situ* fluorometer was used to investigate DOM response to storm events, and the influence of hydrometeorological and land use predictors were investigated. The primary findings were 1) High intensity precipitation events cause water temperature surges in urban catchments, while high temporal and spatial resolution datasets are required to capture this effect, 2) Water temperature anomalies are highest during extreme low flows, while urbanization is related to lower water temperature anomalies during extreme low flows. 3) Shading changes the

composition of urban DOM by preventing photodegradation of the humic pool, however temperature had minimal effect. 4) Urban DOM is source-limited and exhibits exhaustion and dilution effects, with the main predictors of urban DOM during storms being water temperature and antecedent rainfall.

The results indicate new understanding of how a range of extreme events alter water temperature and DOM processes within headwater, urban rivers. The need to change urban land use practices to mitigate the impacts of extreme events on urban water quality is highlighted.

Acknowledgments

Thanks must go to Anne Van Loon who did a fantastic job as primary supervisor. I'm am also very grateful to my other supervisors Chris Bradley, Jon Sadler, and David Hannah for their help and guidance throughout the project.

I am also very grateful for the help of Kieran Khamis and his endless patience guiding me through some unfamiliar technology and guidance on chapters 3 and 4. Other post-docs Val Ouellet and Steve Dugdale also provided guidance at various points.

I would also like to acknowledge funding for the project provided by the Engineering and Physical Sciences Research Council (EPSRC).

For data collection I thank The Nature Centre who provided access for logger sites and were always extremely receptive to the project. Thanks must also go the Environment Agency for providing temperature and flow gauge data.

For providing assistance on some long days of logger installations I would also like to thank Richard Johnson and his unfailing enthusiasm.

I also thank members of the drought research group past and present and in particular Colin Manning, Sally Rangecroft, Doris Wendt, Lucy Capewell for their support and allowing me to bounce ideas off them. I'll particularly remember the writing weeks as some of the most productive times.

My thanks also go to Tanu Singh for assisting with field work and sitting behind me for 3 years, Alex Hurley for his R guru expertise and always being a willing cinema companion, Julia Docherty for helping with field work, as well as Ben Fryer, Nicolai Brekenfeld, and everyone else in office 325.

Finally, I would like to thank my parents for their continuous support in this never ending endeavor.

PUBLICATIONS

Peer- Reviewed Work Accepted for Publication

Croghan, D., Van Loon, A.F., Sadler, J.P., Bradley, C., & Hannah D.M. (2018) Prediction of river temperature surges is dependent on precipitation method. *Hydrological Processes*. doi:10.1002/hyp.13317. (Chapter 2)

In Preparation

Croghan D., Van Loon A.F., Sadler, J.P., Bradley, C., & Hannah D.M. River temperatures higher during low flows but land use buffers effect (In Preparation)

Croghan, D., Khamis K., Van Loon A.F., Sadler, J.P., Bradley, C., Singh T., & Hannah D.M. Mesocosm experiments show stream burial inhibits Dissolved Organic Matter processing by reducing photodegradation (In Preparation)

Croghan, D., Khamis K., Van Loon A.F., Sadler, J.P., Bradley, C., & Hannah D.M. High-frequency in-situ fluorometry indicates the control and source dynamics of Dissolved Organic Matter during stormflow events in urban systems (To be submitted to Science of the Total Environment)

Table of Contents

List of Figures

Chapter 1

Chapter 2

Chapter 3

Chapter 4

Chapter 5

List of Tables

Chapter 2

Chapter 3

Chapter 4

Chapter 5

CHAPTER 1: INTRODUCTION

1.1 Extreme Events and Water Quality in Urban Rivers

1.1.1 Background

Water quality is crucial to the functioning of society and impacts a vast array of sectors ranging from ecology and global health to social well-being, and the economy (UNESCO, 2019). Water pollution is linked to an estimated 1.5m deaths globally every year (Landrigan et al., 2018). In the USA alone, attempts to improve water quality and reduce water pollution have cost $1.9 trillion since 1960 (Keiser and Shapiro, 2019). Water quality is also important for social well-being: clean rivers are important for recreation, and society puts a high utility on clean rivers (Keeler et al., 2012). Water quality degradation is linked to biodiversity loss, and a reduction in the ecological health and functioning of rivers (Vaughn, 2010). Despite the costs of water quality degradation to society, global freshwater water quality is deteriorating (UNESCO, 2019). The main driver of global water quality degradation is land use change such as urbanization and agriculture (Foley et al., 2005), which coupled with climate change is exacerbating water quality issues worldwide (Tu, 2009). Water quality can be defined as the physical, chemical, biological, and aesthetic characteristics of water. The precise quality is then usually determined by a range of indices and metrics relating to specific requirements such as by finding thresholds at which parameters become hazardous to ecology (Environment Agency, 2018). Urbanization is increasing rapidly globally, and the population living in urban areas is expected to rise from 55% in 2018 to 68% by 2050 (United Nations, 2018) with an increase in urban extent of up to 1,500,000 km^2 (Seto et al., 2012). Urbanization is a primary driver of water quality degradation (Fletcher et al., 2013; Brabec et al., 2002; McGrane, 2016): it alters water quality by increasing

pollutant inputs to streams, and by modifying in-stream geomorphology and changing connectivity (Fletcher et al., 2013; Grimm et al., 2008). Stream chemistry within urban areas tends to be unique as a result of inputs from the wider catchment (Halstead et al., 2014). These inputs contribute to the "urban stream syndrome" where streams draining urban catchments are usually associated with poor ecological health (Walsh et al., 2005).

Extreme events (floods and droughts) are one of the main mechanisms of water quality change within urban streams (Miller and Hutchins, 2017; Mosley, 2015; Whitehead et al., 2009). The amount of urban land exposed to droughts and floods is expected to increase 2 and 2.7 times respectively by 2030 (Güneralp et al., 2015). Consequently, there is an increasing risk of water quality change in urban areas due to extreme events. The effects of floods on water quality in urban streams are more commonly studied than those of droughts (Fletcher et al., 2013). Contaminants tend to build up in urban catchments, therefore, flood events are a common cause of water pollution due to increased surface runoff from impermeable surfaces (Brabec et al., 2002; Miller and Hutchins, 2017). Drainage systems in urban catchments convey stormwater into streams rapidly which can lead to rapid perturbation of water quality variables (Mallin et al., 2009). Droughts meanwhile are characterized for rivers by hydrological low flows and are known to alter water quality as the concentration of pollutants increases at low flow due to less dilution (Zwolsman and van Bokhoven, 2007). Droughts are expected to increase in severity and frequency (Güneralp et al., 2015), and can further degrade water quality by increasing pollutant concentrations due to less dilution at low flows (Sprague, 2005). Droughts are often coupled with extreme high temperature events which induce further water quality change (Stott et al.,

2016; Ummenhofer and Meehl, 2017). However, understanding of the effects of drought on urban water quality are limited and require further work.

Water quality is characterized by several variables. In urban areas a wide number of variables including nutrients, heavy metals, pH, dissolved Oxygen, turbidity, suspended sediments and conductivity are all liable to change due to extreme events in urban rivers. In this research however, the focus is on temperature and dissolved organic matter (DOM). In the following sections I will discuss the rationale for choosing these variables, the relevant processes and the effects of urbanization and extreme events.

1.1.2 Defining Water Quality

Water quality has generally been defined and regulated using thresholds and indices developed by governmental agencies. In the UK water quality targets are mainly set in relation to the EU Water Framework Directive (WFD) (Giakoumis and Voulvoulis, 2019). The WFD is a piece of legislature that aims to restore the physical, chemical, and biological water quality of surface and groundwater in the EU, with the overall aim to achieve "good quality" in all these aspects (Brack et al., 2017).

To define water quality, indices were developed as part of the WFD. The indices judge water quality on a five-point scale with the following classifications: bad, poor, moderate, good and high. Water quality indices have been developed to assess rivers based on chemical quality and ecological quality, with waterbodies expected to reach at least "good" standard for each (Brack et al., 2017). The chemical and ecological indices work by using a threshold-based approach to classify water quality for a range of water quality parameters. Thresholds are set by classifying

the range of values that define “bad” to “high” status for each water quality parameter. The chemical quality indices using abiotic metrics such as nutrient concentration and the ecological indices uses biotic metrics such as species richness alongside physical-chemical metrics to ascertain overall water quality. Each indices then defines the quality of a river by the worst performing parameter (European Commission, 2019). Hence, if one water quality parameter in the chemical indices is defined as “bad”, the overall chemical quality of the river would be defined as “bad”. The idea is based around the one out, all out principle which considers that water quality is reliant on a range of parameters, anyone of which may act as a barrier to achieving a healthy stream.

In the WFD, water temperature is used as one of the indicators for the ecological water quality indices (UKTAG, 2008).The thresholds for water temperature vary by river and country, with thresholds mainly relating to tipping points thresholds of economically important fish such as Salmonids. The temperature exceedance thresholds are based around temperature levels that have been shown to have a deleterious effect on target species, as temperature influences fish habitat range strongly (Réalis-Doyelle et al., 2016). In the UK, river temperature thresholds are set for individual rivers based on the river typology, which is classified dependent on the fish community present. In order to achieve at least “good” status, the following indices are monitored: water temperature is measured downstream of points of thermal discharge and must not exceed a greater than 1.5 ºC increase for rivers with Salmonids, or 3 ºC for rivers with Cyprinids, and temperatures must not exceed 21.5 ºC for more than two percent of the time, while during breeding season rivers with cold water species should not exceed 10ºC (UKTAG, 2008). The use of these exceedance-based approaches reflects their ease of use, however they

may be insufficient at identifying short term temperature stressors such as thermal surges (Nelson and Palmer, 2007).

With regards to DOM, no specific legislature currently exists for regulating DOM in the UK, highlighting the paucity of research and importance for further study. This is mainly because the main regulations such as the WFD use measurements that are easy to undertake and commonly found (European Commission, 2019), whereas characterizing DOM requires specialist equipment. However, the WFD chemical and ecological indices use a threshold-based classification for metrics as Dissolved Organic Carbon (DOC), which correlates with the amount of humic-like organic matter, while Biological Oxygen Demand (BOD) is used within the regulations and has been shown to correlate to proteinaceous organic matter (Environment Agency, 2018). Further, using threshold-based approaches for DOM is generally problematic, as commonly used methods of characterizing DOM such as fluorescence have instrument specific biases as such results are not directly comparable between sites. One means of overcoming this is the use of indices that compare ratios of fluorescence peaks, such as the protein-humic ratio proposed by Baker et al., (2003) wherein organic pollution can be identified identifying protein-humic ratios that are protein dominated. Though such ratio indices are widely used in academic literature, they have not yet been used to develop DOM standards. The use of lower cost methods of characterizing fluorescence in-situ as undertaken in this thesis may instead offer a way of incorporating DOM into wider water quality indices and standards by making measurement of DOM easier and quicker.

1.2 Water Temperature:

1.2.1 Rationale

Water temperature is considered a master variable of water quality due to its influence on a wide range of stream processes and effects on many other water quality variables (Hannah et al., 2008; Caissie, 2006). Temperature influences the solubility of solids and gases in water (Kobe and Dutton, 1961): higher temperatures are associated with reduced dissolved Oxygen concentrations and changes in the nutrient and contaminant levels in streams with this relationship described by the Arrhenius equation wherein the rate constant generally increases rapidly with increased temperature (Harvey et al., 2011). Temperature is particularly important to the ecological functioning of streams as it controls the metabolism of the biota in rivers (Demars et al., 2011), growth rates of biota which tend to have a parabolic relationship with temperature (O'Gorman et al., 2016), decomposition of organic matter by microbial activity (Fierer et al., 2005), life cycles such as when spawning of fish occurs (Woodward et al., 2010b), and habitat ranges as habitat is constricted by a species' preference for water temperature (Freitas et al., 2016).

1.2.2 Processes

Water temperature is determined by a number of processes which can be grouped into atmospheric conditions, topography, stream discharge, and streambed factors (Caissie, 2006). These processes occur over a range of spatial and temporal scales (Webb et al., 2008) and water temperature changes are governed by energy and water fluxes across the atmosphere-surface water and streambed-surface water interface (Kelleher et al., 2012).

Atmospheric conditions mainly influence water temperature through exchanges of shortwave and longwave radiation at the atmosphere-surface water interface (Kelleher et al., 2012). Air temperature acts as a proxy of exchanges of shortwave and longwave radiation at the surface-water interface and is commonly used as a predictor of water temperatures (Webb et al., 2003). Heat loss from rivers is often driven by atmospheric conditions, with evaporation and convective heat flux being important drivers of energy loss at the atmosphere-surface water interface (Caissie, 2006). Precipitation also influences water temperature, as the temperature of precipitation runoff is often different to river temperature (Tilburg et al., 2015; Hofmeister et al., 2015). Precipitation inputs often cause short-term heat fluxes, which can cause thermal pulses to surge through rivers (Somers et al., 2016; Wilby et al., 2015).

Topography influences water temperature by influencing atmospheric conditions (Caissie, 2006). In smaller streams topography largely influences water temperature through shading. Dense riparian zones increase shading and reduce the amount of shortwave-radiation reaching the stream thereby reducing the energy available for heat exchange (Rutherford et al., 1997; LeBlanc et al., 1997). Stream orientation has also been shown to have an important influence on temperature, with stream orientation influencing exposure to solar inputs (Garner et al., 2017). Altitude also influences water temperatures, as air temperatures are reduced at higher altitudes due to reduced adiabatic lapse rates, which subsequently leads to lower water temperatures (Hrachowitz et al., 2010; Jackson et al., 2015). Further, catchment geology is an important influence on rivers, as river temperatures in high permeability catchments are controlled by the temperature of groundwater discharge (Tague et al., 2007).

Conditions at the streambed influence water temperature through hyporheic exchange and groundwater inputs (Caissie, 2006). Groundwater temperatures tend to remain relatively stable throughout the year, therefore in winter groundwater inputs act to increase river temperature, while conversely during summer groundwater acts as a moderating force on river temperatures (Alexander and Caissie, 2003; Constantz, 1998). The effects of groundwater upwelling and hyporheic exchanges are often highly localized with minimal influence downstream of upwelling zones (Krause et al., 2012). Friction between flow and the streambed can also increase water temperatures, with higher velocity flows leading to increased friction (Hannah et al., 2004). However, this effect is minimal in comparison to other processes.

Stream discharge impacts water temperature by altering the thermal capacity of the water (Sohrabi et al., 2017). Increases in stream discharge increase the amount of heat required to alter water temperature, and hence at higher discharges streams are less influenced by the air-water surface interface (Webb et al., 2003). Floods and droughts are characterized by large changes in discharge and are therefore expected to be first-order drivers of water temperature change, but this relationship has not been explored in detail (Brown and Hannah, 2007; Zwolsman and van Bokhoven, 2007).

1.2.3 Urbanization and Extreme Events as Drivers of Change

Urbanization and extreme events modify the processes controlling water temperature (Figure 1.1). Atmospheric conditions, topography, discharge & streambed conditions are all modified. Urbanization influences the atmospheric processes of water temperature. The urban heat island effect can lead to increased air temperature, with mean annual air temperatures up to

5.9 °C higher than surrounding area air temperature (Soltani and Sharifi, 2017). This occurs because solar inputs in urban areas tend to be absorbed by buildings and impermeable surfaces (Mohajerani et al., 2017). Subsequently, during intense precipitation events rainfall runoff can heat substantially. Rainfall runoff has been measured at up to 7 °C warmer than river temperatures in urban areas (Pluhowski and Pecora, 1970; Nelson and Palmer, 2007; Somers *et al.*, 2013). Urbanization has also been found to increase the frequency of intense precipitation events, particularly the short-duration high-intensity events which often lead to water temperature surge events (Golroudbary et al., 2019).

Urbanization also changes the topographic controls of river temperature (O'Driscoll et al., 2010b; Miller et al., 2014; Miller and Hutchins, 2017). Changes in riparian zones are common during urbanization. In some cases riparian zones are deforested, which reduces shading and can lead to increased warming of rivers (Garner et al., 2017). Other aspects of urban infrastructure such as buried streams and bridges/tunnels may increase the amount and frequency of shading in urban rivers (Elmore and Kaushal, 2008). Further, the impact of catchment geology is often reduced within urban streams due to reduced connectivity with groundwater as a result of urban river engineering. Modifications such as concreting river beds limit groundwater exchange reducing the moderating effect on water temperature (Tam and Nga, 2018). Drought events particularly impact urban rivers due to the reduced groundwater connectivity (O'Driscoll et al., 2010b), although to a certain extent other aspects of urban river management, such as stream burial, may offset the effects on water temperature. During high flows, the increased area of impermeable surfaces increases surface runoff which increases

peak flows and potentially water temperature surge events (Nelson and Palmer, 2007; Somers et al., 2013).

Changes in land-use can cause substantial changes in stream discharge (McGrane, 2016; Fletcher et al., 2013). During high flow events urbanization increases the speed to peak flow, and overall peak flow values as a result of increased surface runoff from impermeable surfaces (Miller & Hutchins, 2017; O'Driscoll et al., 2010). Further, urban drainage infrastructure tends to channel stormflow into rivers quickly with reduced infiltration and storage within urban catchments (Braud et al., 2013). During high flows this is likely to alter stream discharge as a control of water temperature as higher discharges have higher thermal capacity (Webb et al., 2003). For particularly large events, urbanization may lead to reduced water temperature variability, although the extent to which urbanization alters river temperature regimes compared to rural rivers is not well understood. Reduced baseflow discharge is also a commonly reported side effect of urbanization although evidence for this is conflicting (Bhaskar et al., 2016; Finkenbine et al., 2000). During periods with no rainfall this effect is exacerbated as the influence of the atmosphere on water temperature increases due to the lower thermal capacity of the water at low flows (Folegot et al., 2018). However, the extent to which inflows from urban sources such as pipe leaks and sewage outlets influence water temperatures at baseflow is not known.

Streambed conditions in urban rivers are regularly altered through hard engineering (Walsh et al., 2005; Fletcher et al., 2013). Concreting of stream beds and channelization are common approaches in flood engineering, which can reduce the influence of streambed conditions on water temperatures (King et al., 2010). During high flows this leads to rapid transport of water.

This can increase the friction with the streambed which slightly influences water temperature (Hannah et al., 2004). However, the effects from altering streambed conditions are most likely to be evident during extreme low flow conditions. Streambed alteration reduces groundwater and hyporheic upwelling and reduces these moderating effects on water temperature at low flow (Constantz, 1998).

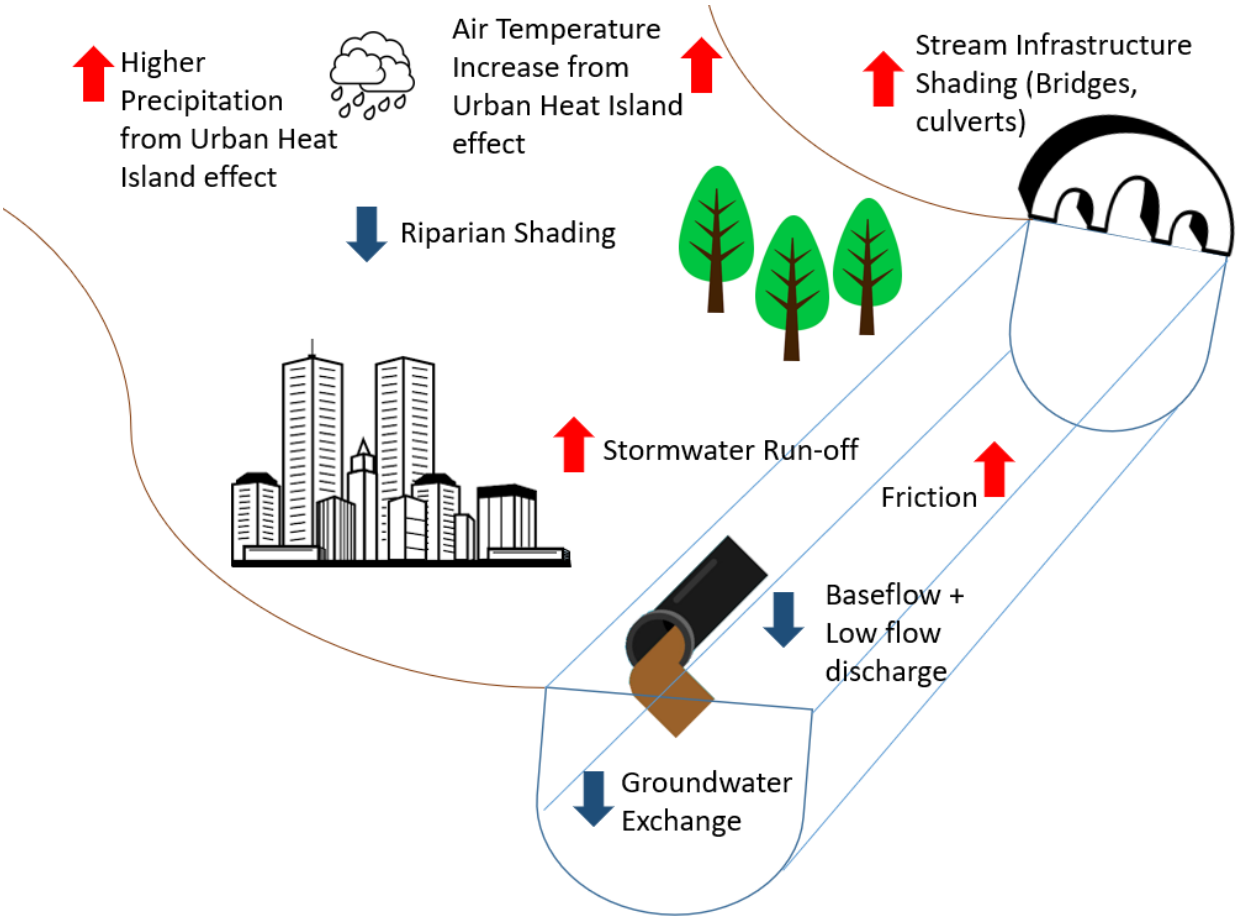

Figure 1.1. Potential effects of urbanization on processes controlling water temperature during Summer. Red arrows show increase in process (for example increase in air temperatures in urban areas), blue arrows show decrease.

1.3 Dissolved Organic Matter

1.3.1 Rationale

Dissolved Organic Matter (DOM) provides one of the largest sources of energy and nutrients in streams (Wymore et al., 2016). Microbial activity accounts for most of the biological uptake of DOM in streams, however DOM is an important resource at all higher tropic levels. DOM is critical to support food webs (Arango et al., 2017; Meyer and Edwards, 1990) and plays an important role in the transport and mobilization of pollutants in streams (Hansen et al., 2016). The chemical make-up of DOM determines its role and interactions within the environment, with characteristics such as reactivity and lability determining to what extent it acts as an energy resource within streams (Hudson et al., 2007). The quality of DOM is highly variable, and characterization of DOM is important in order to understand its role within the environment. DOM is strongly influenced by terrestrial-aquatic linkages (Massicotte et al., 2017), therefore, changes to the terrestrial environment through land use change like urbanization are a particularly strong control on DOM dynamics (Khamis et al., 2018).

1.3.2 Processes

The main processes controlling DOM amounts and composition in streams are terrestrial inputs and biodegradation and photodegradation (Del Vecchio and Blough, 2002; Hansen et al., 2016).

Allochthonous DOM from terrestrial sources is usually the main input of DOM to streams and most river fauna considered heterotrophic (Tank et al., 2010). The importance of terrestrial sources of DOM is central to the “river continuum concept” where upstream inputs of terrestrial carbon and nutrients from processes upstream are vital to the functioning of rivers

downstream (Vannote et al., 1980). The characteristics of DOM in rivers reflects processes in the wider catchment and is heavily influenced by land use. DOM in the terrestrial catchment builds up over time and is usually transported to streams during storm events, which is termed the “flood-pulse concept” (Tank et al., 2010). DOM transport during storm events can be through direct overland flow, however storms may also activate shallow sub-surface flow pathways which represent a further source of DOM (Fork et al., 2018).These slower activated pathways tend to be associated with labile, high-molecular-weight material and with DOM inputs reaching the stream over longer time periods (Dosskey and Bertsch, 1994).

The types of DOM from the terrestrial environment are wide ranging and highly variable in quality and are strongly dependent on surrounding land use. Humic DOM tends to be produced by decomposition of leaf litter which provides an important source of labile material to streams. This is particularly prominent during autumn when leaf-fall is highest (Meyer et al., 1998; Singh et al., 2014). Meanwhile proteinaceous terrestrial material is often associated with anthropogenic inputs, such as sewage effluent (Baker and Inverarity, 2004). Other forms of allochthonous DOM are derived from atmospheric deposition. This occurs through wet deposition (precipitation) and dry deposition (where gases and particles settle on the surface). (Monteith et al., 2007; Countway et al., 2003).

Autochthonous processes influencing DOM in streams include autotrophic production, adsorption and desorption (Ye et al., 2018). Autotrophic production of DOM occurs mostly from phytoplankton and bacterial production, and through breakdown of material by grazers (Descy et al., 2017; Brett et al., 2017). Autotrophs produce DOM through photosynthesis, and this is usually subsequently released through respiration or grazer activity (Thorp and Delong, 2002;

Bunn, 1986). Respiration releases DOM through extracellular release, which provides high-quality labile material to streams (Baines and Pace, 1991). Proteinaceous materials from cyanobacteria release is also a source of low lability material that is considered a major pollutant (Henderson et al., 2008; Qu et al., 2012). Grazer species are important to DOM processing as they feed on autotrophs such as algae and phytoplankton and subsequently release and transform DOM (Thorp and Delong, 2002). Adsorption and desorption meanwhile are key transfer processes within streams, as DOM can bind to suspended sediments which provides a key mechanism for transport downstream and for contaminants entering the food chain (Ye et al., 2018). Autochthonous material is taken up preferentially within the aquatic ecosystem (Sieczko et al., 2015), but it is not able to support food webs within streams, and terrestrial inputs of DOM are also required (Kritzberg et al., 2004)

The main removal and transformation processes for DOM are biodegradation and photodegradation (Hansen et al., 2016). Biodegradation refers to the loss and transformation of DOM through decomposition from microbial activity. In streams the most labile, low-molecular weight, aliphatic material tends to be taken up preferentially by microbes, thus fresh material in streams tends to be degraded relatively rapidly (Moran and Zepp, 1997). Biodegradation also leads to the production of new DOM material, with aromatic, high-molecular materials often produced as a byproduct of activity from heterotrophs (Stepanauskas et al., 2005). Photodegradation refers to the breakdown and transformation of DOM through exposure to light sources. Photodegradation causes DOM to alter from large to small molecules, with an associated increase in lability for the smaller molecules (Moran and Zepp, 1997; Helms et al., 2008). These molecules are often quickly removed from the DOM pool through uptake by

microbes or through volatilization. Photodegradation can also transform DOM and create by-products by producing higher molecular weight, lower lability material (Hansen et al., 2016). Photochemical oxidation of DOM meanwhile causes increases in the release of nitrogen rich-compounds, which in turn increases the potential for biodegradation of humic materials as nitrogen is often limiting in riverine environments (Bushaw et al., 1996).

1.3.3 Urbanization and Extreme Events as Drivers of Change

Urbanization and extreme events drive changes in the processes controlling DOM in a multitude of ways (Figure 1.2). The processes impacting allochthonous DOM in rivers are drastically altered by urbanization (Fork et al., 2018; Kaushal et al., 2014). The processes of DOM transport are different within urban catchments. Engineered sewage and storm drainage networks are the main pathways for allochthonous DOM within urban catchments (Hosen et al., 2014; Kaushal and Belt, 2012). Sub-surface runoff is often reduced in urban areas due to the extent of impermeable surfaces (Khamis et al., 2018). Resultantly, there are reduced inputs of humic-like DOM, while inputs of fresh, proteinaceous materials that are quickly routed through storm drainage systems are often increased (Carstea et al., 2009). This alteration of flow pathways leads to changes in the character of allochthonous DOM in urban rivers compared to rural rivers. Although DOM in rural rivers are usually dominated by humic materials, urban rivers tend to be dominated by proteinaceous DOM (Chen et al., 2017; Hosen et al., 2014; Khamis et al., 2018). Transport of allochthonous material mainly happens during high flows due to activation of terrestrial flow paths. In urbanized catchments, the increased peaks and quicker time-to-peaks as a result of modified flow pathways lead to greater quantities of DOM transport into urban rivers (McGrane, 2016; McElmurry et al., 2014). During low flows the

terrestrial – aquatic linkage is reduced, lowering the input of DOM to urban streams (Petrone et al., 2011).

Urbanization also changes the autochthonous processes influencing DOM (Hosen et al., 2014; Lambert et al., 2017; Parr et al., 2015). Autotrophic production of DOM is altered in urban streams as they have different autotrophic communities (Pereda et al., 2019). High Nitrogen loads are commonly found in urban rivers and can increase production of DOM due to increases in the population of autotrophs (Lavelle et al., 2019). Subsequently, in these Nitrogen-rich systems, increased autotrophic microbial activity leads to increases in microbially-derived humic DOM (Zhou et al., 2018). Greater suspended sediment concentrations also increase DOM adsorption, which increases DOM transport in urban rivers (Ye et al., 2018). This poses a concern as pollutants such as heavy metals form a higher portion of the suspended sediment in urban streams and the higher adsorption rates can increase pollutant bioaccumulation (Warren and Zimmerman, 1994).

Extreme low flows increase the importance of autochthonous production as a resource of DOM, as connections to the terrestrial environment are limited. However, in urban rivers this is often not the case due to steady inputs of allochthonous DOM from drains (Petrone et al., 2011). During high flows, the importance of autochthonous processes tends to be reduced, and allochthonous DOM tends to dominate urban rivers (Khamis et al., 2018).

Photodegradation and biodegradation rates are potentially altered as urbanization changes the composition of DOM (Carstea et al., 2010, 2009). In urban streams, DOM tends to be of low lability, high-molecular weight and dominated by proteinaceous material (Khamis et al., 2018).

Urban DOM is generally not very bioavailable, thus reducing rates of biodegradation for urban streams. Similarly, for photodegradation, large portions of the DOM pool are less photoreactive than in rural streams, with proteinaceous material found to be less prone to photodegradation than humic-like materials that dominate in rural streams (Hosen et al., 2014; Hudson et al., 2007). Urbanization changes the rate of shading in streams in various ways. For example, in buried streams there is total shading therefore photodegradation cannot remove or transform DOM (Beaulieu et al., 2014; Johnson and Wilby, 2015). Land use in riparian zones may also change, increasing or decreasing the amount of shading hence altering photodegradation rates (Larson et al., 2007).

Extreme low flows have the potential to increase photodegradation rates as reduced flows allow greater light penetration (Harjung et al., 2019). Extreme low flows are also often coupled with extreme temperature anomalies (Manning et al., 2018), and the extreme (high) temperatures during drought events may increase photodegradation and biodegradation rates (Harjung et al., 2019). In high flow events, increased turbidity is likely to reduce photoexposure of the DOM pool. However, the high transport of terrestrial material to the system leads to increased biodegradation. This is likely exacerbated in urban rivers where terrestrial – aquatic linkages are particularly strong (Coble et al., 2016).

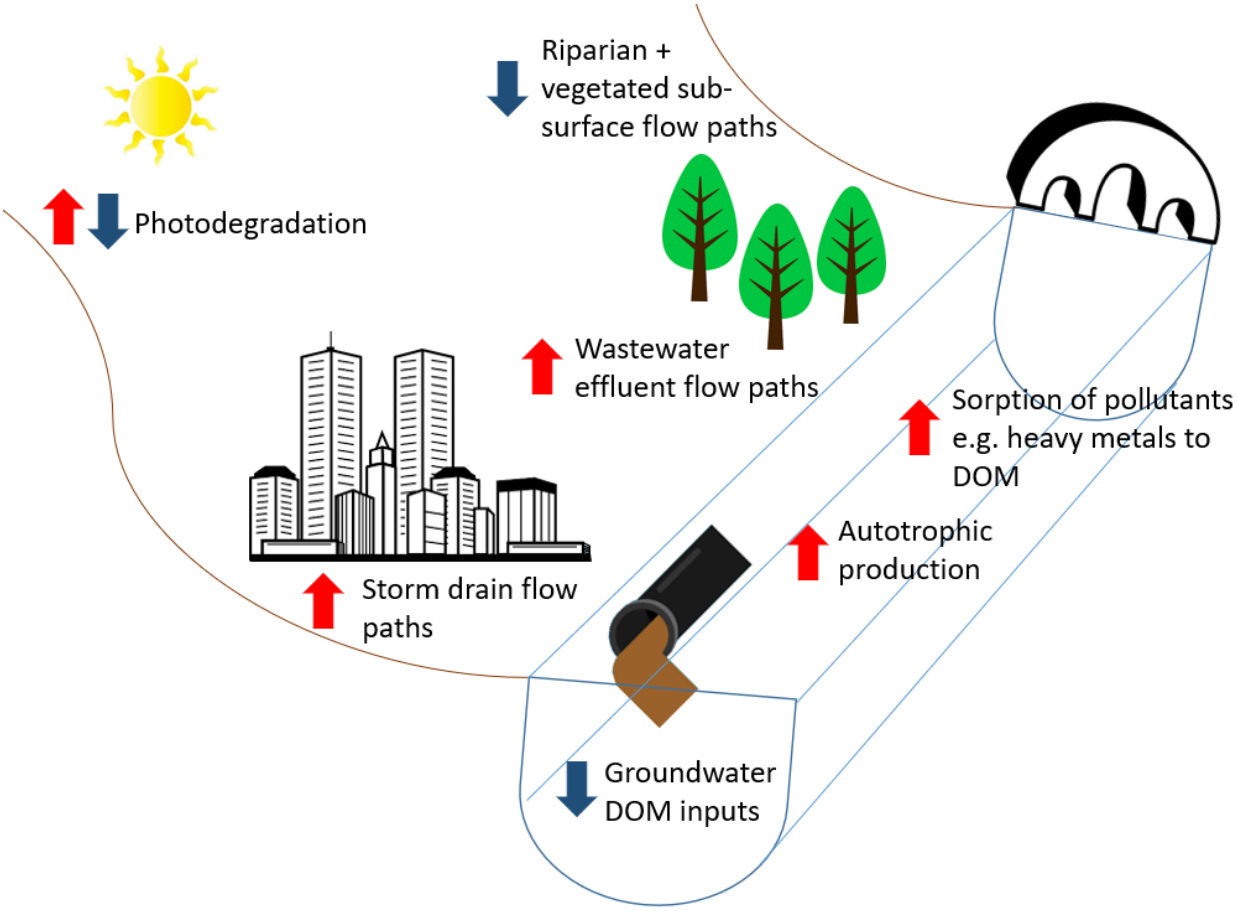

Figure 1.2. Potential effects of urbanization on processes controlling DOM. Red arrows show increase in process, blue arrows show decrease.

1.4 Research Gaps

Urban water quality is a major concern globally, and water quality problems are often exacerbated by extreme events (United Nations, 2018; McGrane, 2016; Fletcher et al., 2013). Resultantly, water quality in urbanized rivers often deteriorates during extreme events (Kaushal et al., 2018a). Water quality degradation in urban rivers is expected to increase in the future as urbanization is increasing rapidly worldwide, while climate change is expected to increase the frequency and severity of extreme events (Güneralp et al., 2015). Despite this, key

knowledge gaps exist on the impact of extreme events on water quality in urban areas for many variables. Understanding of the underlying processes is particularly limited (Blöschl et al., 2019).

In this thesis the variables of focus are water temperature and DOM. Both are important determinants of water quality, and they are likely to be especially impacted by the effects of urbanization (Fork et al., 2018; Kelleher et al., 2012). Despite this, the impact of extreme events on both variables is largely unstudied in an urban context (Hofmeister et al., 2015; Somers et al., 2013; Hosen et al., 2014). Given the importance of water temperature as a master variable controlling many stream processes (Caissie, 2006), and DOM's importance as an energy resource in streams (Hudson et al., 2007), understanding the effects of extreme events on their controlling processes is required in order to facilitate urban stream remediation. Strong linkages exist between the two variables, as temperature is an important control of DOM production and dynamics within rivers (Raymond and Bauer, 2000). Hence an improved understanding of the impacts of extreme events and urbanization on water temperature feeds into greater understanding of the impacts of extreme events and urbanization on DOM.

Water temperature research has been limited till relatively recently, with the importance of water temperature on water quality processes often overlooked (Hannah et al., 2008). Resultantly, multi-year water temperature studies are relatively rare, while water temperature dynamics within the headwaters are also poorly understood (Webb et al., 2008). Most prior catchment scale water temperature studies have also been within rural catchments which have differing controls and processes to urban systems (Somers et al., 2013). A need therefore exists to conduct water temperature studies at the catchment scale. High spatial and temporal resolution datasets are required to better understand water temperature response at the

catchment scale. Particularly during extreme events when water temperature changes may be more rapid both spatially and temporally (Nelson and Palmer, 2007).

DOM dynamics have been poorly characterized for extreme events in urban rivers due to constraints in sampling technology (Khamis, Bradley and Hannah, 2018). DOM can vary over sub-hourly timescales, however most studies on urban DOM have used coarser timescales (Baker et al., 2003; Hosen et al., 2014; Hudson et al., 2007). As extreme events lead to rapid changes in DOM dynamics, sampling at higher frequencies is required to understand the processes driving DOM variability at sub-daily scales.

Furthermore though headwater streams have been identified as crucial for influencing downstream water quality (Ockenden et al., 2016), the effects of urbanization in headwater streams are poorly understood, while extreme events are also likely to influence headwater streams disproportionately (Fork et al., 2018; Imholt et al., 2013). Therefore, improved understanding of the effects of extreme events within headwater streams is required.

This research aims to investigate how extreme events impact the processes controlling water temperature and DOM dynamics in headwater, urban streams. Previous attempts to study water quality during extreme events have been hindered by low resolution datasets. For storm events particularly, high temporal resolution monitoring is required, yet high-frequency monitoring of extreme events is often limited. Therefore, in high spatial and temporal datasets were used where possible.

To identify research gaps for specific aspects detailed literature reviews were undertaken and presented within chapters 2-5.

1.5 Aims, Objectives, and Hypotheses

The main aim of this thesis is to investigate the effects of urbanization and extreme events on river water quality. Specifically, the research considers how extreme events and urbanization alter the hydrological processes controlling water temperature and DOM dynamics by considering a range of spatial and temporal scales using high resolution datasets. The specific objectives were:

1) To analyze the process-based links between precipitation intensity and water temperature surges, and to identify which precipitation dataset best represent these processes (Chapter 2). Subsequently, the following hypotheses were developed:

    - Higher intensity precipitation will be linked to higher sub-hourly water temperature surges.
    - The radar catchment dataset will be the best performing model for modelling water temperature surges.
    - Higher daily precipitation amounts will lead to greater daily water temperature changes.
    - All precipitation datasets will model daily water temperature changes similarly.

2) To determine to what extent extreme events, cause anomalies in daily water temperature when compared to average flow conditions, and how land use impacts the

processes controlling water temperature during extreme events (Chapter 3). To achieve these objectives the following hypotheses were tested:

- Water temperature anomalies will be highest during low flows.
- Water temperature anomalies will be lowest during average flow
- Urbanization land use metrics will be correlated to higher water temperature anomalies for low and high flows.
- Urbanization metrics will be the most important predictor of water temperature anomalies for low and high flows.

3) To test how extreme water temperature events and urban stream burial (where streams are culverted) impact photodegradation and biodegradation rates in urban streams (Chapter 4). To test this the following hypotheses were developed:

- Unshaded treatments will increase the loss of humic-like DOM compared to shaded treatments leading to changes in DOM quality and composition.
- Heated treatments will accelerate the decline in the humic-like content of DOM compared to the non-heated treatments.
- Treatments that are both unshaded and heated will have the highest rate of loss of humic-like DOM.

4) To better understand the sources and pathways of urban DOM during high flows by analyzing the Concentration-Discharge (C-Q) relationship and identifying the hydrometeorological and landscape controls on storm DOM dynamics (Chapter 5). To achieve these objectives the following hypotheses were tested:

    - HLF and TLF will be chemodynamic up to a threshold whereupon they will become chemostatic due to exhaustion of material in the system.
    - A range of hysteresis types would be identified for both TLF and HLF, however anti-clockwise hysteresis will be more common for HLF than TLF due to differences in source types.
    - Antecedent conditions will be the strongest control on TLF and DOM dynamics.
    - Urbanization metrics will be the strongest land use metrics associated with TLF and HLF dynamics.

To achieve these objectives, field studies were conducted for Chapters 1, 2, and 4 within Birmingham, UK. These studies were carried out in headwater streams with a range of sites covering a land use gradient from nearly rural to almost entirely urban. Chapter 3 used an experimental approach using water samples from one of the urban streams in the study sites.

1.6 Thesis Structure

The thesis is structured following a paper-based format. Chapters 2-5 are presented as independent pieces of research. Each chapter is self-contained, featuring a detailed literature review, methods, results and discussion and presented in a suitable format for publication. Chapters 2 and 3 examine water temperature, while Chapters 3 and 4 consider DOM. Water temperature also features prominently in Chapters 3 and 4 as a control on DOM. Chapter 6 consists of a conclusions and synthesis chapter summarizing the main results and placing the results in a wider context, while also identifying future directions for research (chapter 6). A full breakdown of the thesis structure is shown in Figure 1.3.

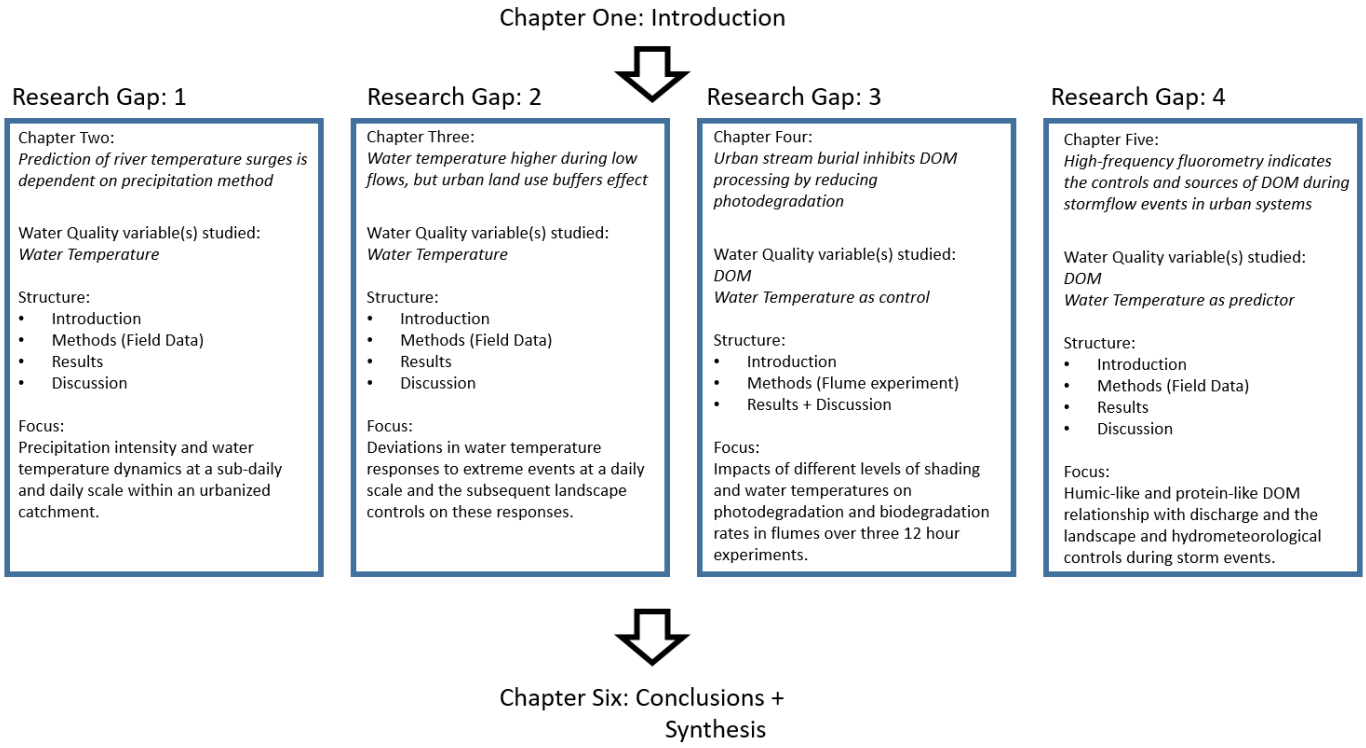

Figure 1.3. Schematic of thesis structure

CHAPTER 2: PREDICTION OF RIVER TEMPERATURE SURGES IS DEPENDENT ON PRECIPITATION METHOD

This chapter has been published in Hydrological Processes:

Croghan, D., Van Loon, A.F., Sadler, J.P., et al. (2018) Prediction of river temperature surges is dependent on precipitation method. *Hydrological Processes*. doi:10.1002/hyp.13317.

2.1 Abstract

Urban river systems are particularly sensitive to precipitation-driven water temperature surges and fluctuations. These result from rapid heat transfer from low-specific heat capacity surfaces to precipitation which can cause thermally polluted surface runoff to enter urban streams. This can lead to additional ecological stress on these already precarious ecosystems. Although precipitation is a first-order driver of hydrological response, water temperature studies rarely characterize rain event dynamics and typically rely on single gauge data that yield only partial estimates of catchment precipitation. This chapter examines three different precipitation measuring methods (a statutory automatic weather station, citizen science gauges, and radar estimates) and investigates relationships between estimated rainfall inputs and sub-hourly surges and diurnal fluctuations in urban river water temperature. Water temperatures were monitored at 12 sites in summer 2016 in the River Rea, in Birmingham, UK. Generalized additive models (GAMs) were used to model the relationship between sub-hourly water temperature surges and precipitation intensity, and subsequently the relationship between daily precipitation totals and standardized mean water temperature. The different precipitation measurement sources give highly variable precipitation estimates, which relate differently to water temperature fluctuations. The radar catchment-averaged method produced the best model fit (generalized cross-validation score (GCV) = 0.30) and was the only model to show a

significant relationship between water temperature surges and precipitation intensity ($P < 0.001$, $R^2 = 0.69$). With respect to daily metrics, catchment-averaged precipitation estimates from citizen science data yielded the best model fit (GCV score = 0.20). All precipitation measurement and calculation methods successfully modelled the relationship between standardized mean water temperature and daily precipitation ($P < 0.001$). This research highlights the potential for the use of alternative precipitation datasets to enhance understanding of event-based variability in water quality studies. We conclude by recommending the use of spatially-distributed precipitation data operating at high spatial (< 1 km^2) and temporal (< 15 minutes) resolutions to improve the analysis of event-based water temperature and water quality studies.

2.2 Introduction

Urban stream water temperatures are highly variable and subject to short-term changes during high-intensity precipitation events. Short duration, event-based changes, hereafter referred to as water temperature "surges", can affect urban stream ecosystem health (Herb et al., 2008; Hester and Bauman, 2013; Hofmeister et al., 2015; Jones et al., 2012; Nelson and Palmer, 2007; Somers et al., 2016, 2013). Water temperature is a controlling factor on a wide range of abiotic and biotic variables. Hence sudden changes can have a cascade effect on a multitude of temperature-driven processes (Webb et al., 2008), particularly in urban catchments where regular surge effects can contribute to the "urban stream syndrome" (Walsh et al., 2005). While water temperature surges occur over short time scales (minutes to hours), precipitation also influences water temperature regimes over longer temporal scales (Hannah and Garner, 2015). The influence of precipitation on diurnal urban water temperature dynamics has not been

studied extensively. Precipitation can lead to the reduced influence of air temperature on water temperature, leading to a distinct diurnal response in water temperature dynamics (Constantz, 1998). Resultantly, large precipitation events may impact river water temperatures change over longer time periods than previously thought.

Urban environments are vulnerable to water temperature surges due to rapid heat-transfer between precipitation and surfaces with a low specific heat-capacity, coupled with changes in surface runoff processes in urban areas (Fletcher et al., 2013; Van Buren et al., 2000; Nelson and Palmer, 2007; Herb et al., 2008). Urban surfaces are typically darker in color and have a low specific heat-capacity; they can heat quickly and reach temperatures that far exceed air temperature on warm days. During precipitation events, heat can be rapidly transferred from these surfaces to surface runoff. As this thermally-polluted runoff enters rivers, rapid increases in river water temperature can occur (Herb et al., 2008; Van Buren et al., 2000). Moreover, the high proportion of low-permeability surfaces in urban areas reduces infiltration, and increases the proportion of precipitation that is conveyed rapidly through the catchment via direct surface runoff and through storm drains (Walsh et al., 2012; Fletcher et al., 2013). Hence a high proportion of urban precipitation is routed rapidly into water courses, with the consequence that thermally-polluted runoff enters rivers in greater quantities than in rural catchments. Furthermore, due to reduced infiltration and changes in subsurface flow pathways, urban streams typically experience reductions in baseflow (Fletcher et al., 2013). This can further increase the vulnerability of urban rivers to precipitation-driven water temperature changes, thereby increasing the influence of runoff temperatures on the temperature of receiving streams.

Characterization of urban precipitation patterns requires high spatial and temporal resolution precipitation data (Berne et al., 2004). However, many studies lack high-density precipitation gauges to quantify urban precipitation accurately (Pedersen et al., 2010; Thorndahl et al., 2017). Consequently, it may be difficult to infer links between precipitation and hydrological processes in urban catchments (Berne et al., 2004). This has implications for a multitude of water quality variables that are influenced by event rainfall (Sandoval et al., 2014; Tilburg et al., 2015).

The analyses of precipitation metrics and water temperature frequently rely on single rainfall gauge data. These are often assumed to be representative of catchments with multiple water temperature logger sites (Lange and Haensler, 2012; Brown and Hannah, 2007; Somers et al., 2013, 2016; Wilby et al., 2015; Hofmeister et al., 2015; Hester and Bauman, 2013). However, precipitation typically exhibits high spatial variability within catchments at different scales (Salvadore et al., 2015; Dixon and Mote, 2003). This is particularly evident in urban catchments where the combination of the urban heat island effect and changes in urban wind field alter precipitation patterns (Salvadore et al., 2015; Dixon and Mote, 2003) leads to variations in rainfall intensity and duration (Pedersen et al., 2010; Gabriele et al., 2017; Villarini et al., 2008; Thorndahl et al., 2017). Consequently, the precipitation processes that drive water temperature fluxes during individual events can be difficult to quantify, particularly when using data from a single rainfall gauge.

Radar and citizen science precipitation datasets may provide a useful alternative to single rainfall gauges (Buytaert et al., 2014; Gabriele et al., 2017; Starkey et al., 2017; Koch and Stisen, 2017; Thorndahl et al., 2017), particularly in urban catchments where high-spatial resolution precipitation data are required, or where catchments are poorly gauged (Berne et al., 2004). Citizen science precipitation databases are increasingly common and can potentially increase the number of precipitation gauges available for catchment studies (Starkey et al., 2017; Koch and Stisen, 2017). However, to-date concerns over data quality have inhibited their uptake for research purposes (Buytaert et al., 2014; Barthel et al., 2016; Starkey et al., 2017). Radar precipitation data can also yield high temporal and spatial resolution precipitation estimates (Golding, 1998; Villarini et al., 2008; Biggs and Atkinson, 2011; Gabriele et al., 2017; Thorndahl et al., 2017). For example, in the UK, the NIMROD system generates radar-derived precipitation estimates at 5-min temporal and 1km^2 spatial resolution (Villarini et al., 2008). These systems can monitor moderate to high-intensity precipitation events well, but they are less accurate in low-intensity precipitation events (Biggs and Atkinson, 2011; Golding, 2000). Previously, five minute temporal resolution radar precipitation has been found to represent spatial variability of rainfall well in small, urban catchments, compared to high-density gauge networks (Berne et al., 2004; Thorndahl et al., 2017). While radar estimates of total precipitation can be variable, the use of radar at a minimum of 5-min temporal resolution can provide good precipitation estimates for urban hydrology applications (Rico-Ramirez et al., 2015; Einfalt et al., 2004).

This chapter investigates the use of different precipitation data sources in urban river water temperature studies, motivated by improving our understanding of water temperature fluxes

during rainfall events. We aim to establish which type of precipitation estimate correlates strongest with sub-hourly and daily water temperature change with the following objectives:

1) Quantify how precipitation captured by citizen science and radar precipitation datasets compare to automatic weather stations providing point-based source estimates in the prediction of river-water temperature fluctuations over sub-hourly and daily timescales.
2) Explore to what extent three precipitation datasets can represent spatial variability in precipitation intensity in relation to a water temperature surge event

2.3 Methods

2.3.1 Study Location

The study was undertaken in the catchment of the River Rea in Birmingham, West Midlands, UK (52.4862° N, 1.8904° W; Figure 2.1a). This headwater catchment is located within the second largest urban conurbation in the United Kingdom (Figure 2.1b). The 74km^2 catchment comprises clay overlying sandstone, with 31% of the catchment defined as highly permeable bedrock, particularly in the center of the catchment (NRFA, 2018). Surface elevations range from 107 to 291m asl, and the catchment has a mean annual precipitation of 781mm (NRFA, 2018). Precipitation in the catchment exhibits a seasonal pattern, with the highest precipitation generally occurring from October to December, with the driest months from February to May (NRFA, 2018). The dominant Lamb Weather Type within the catchment is anticyclonic, with this the dominant weather type throughout the year, although cyclonic conditions occur with increased frequency during the summer months (Zhang et al., 2014). The proportion of the catchment that is urbanized is extremely high (built-up urban: 70.2%) making it an ideal study

catchment for the effects of urbanization: the remaining land use mainly comprises urban green space. The high proportion of storm drains and low-permeability surfaces in the catchment leads to a dominance of rapid flow pathways that route surface runoff quickly to the river during storm events. The presence of widespread low specific heat-capacity surfaces also leads to warming of land surfaces within the summer months, priming the catchment for water temperature surge events. As a result of its land use, the Rea has a flashy flow regime with a mean flow of 0.77 m^3/s and peak flow of 73.8 m^3/s during the study period for a gauge located at the catchment outlet (NRFA, 2018).

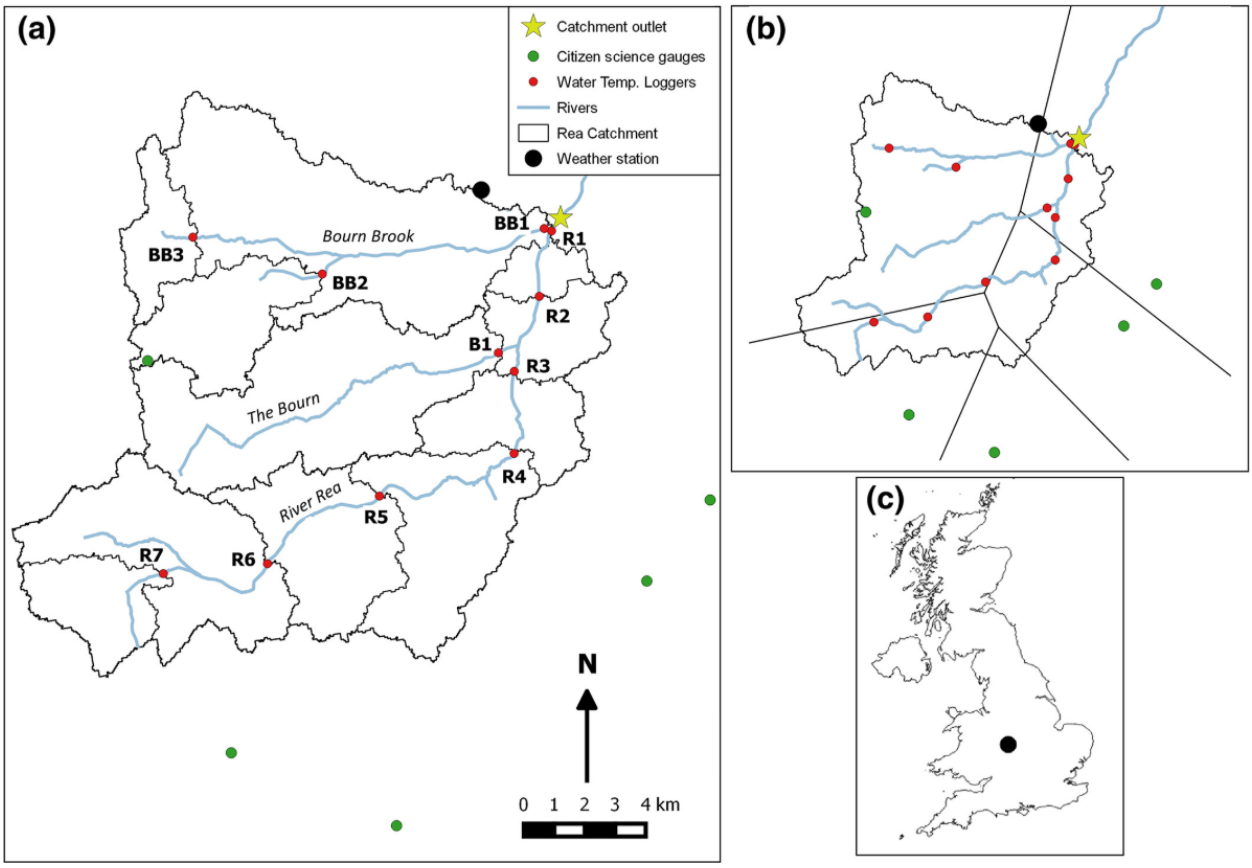

Figure 2.1. The River Rea catchment, UK, showing a) locations of water temperature loggers, automatic weather station, and citizen science gauges within the study catchment, b) the thiessen polygons produced for the citizen science precipitation data, c) the location of the River Rea catchment in the UK.

2.3.2 Water Temperature Data Collection

River water temperatures were monitored using 12 TinyTag aquatic temperature loggers (Gemini Data Loggers, 2017) installed and calibrated using the protocol of Hannah, Malcolm, & Bradley (2009). The TinyTag loggers have a measurement accuracy of +/- 0.2 °C and were calibrated using an ice-bath set at a starting temperature of 0°C in which they were placed for 48 hours with temperature logged at 15-min intervals recording in British Summer Time and starting on the hour, in accordance with the precipitation datasets. The mean water temperature logged in the ice-bath was then determined, and correction factors were calculated for individual TinyTags which either under- or over-estimated water temperatures by more than +/- 0.2 °C compared to the mean. Correction factors were applied post-monitoring.

To monitor the water column temperature, TinyTags were secured to the riverbed in areas of unimpeded perennial flow. The loggers were placed within white radiation shields to prevent atmospheric radiation directly warming the loggers, and placed parallel to the flow to ensure constant flow through the radiation shield (Hannah et al., 2009). Loggers were tied to iron bars buried into the stream bed with wire rope and left free floating in the middle of the river stream, to prevent debris build-up impeding flow to the logger. The length of the wire rope was adjusted to ensure loggers would not be washed out. Loggers were placed evenly throughout the catchment, and at tributary confluences to ensure a high spatial resolution for water temperature monitoring in the catchment. This enabled localized water temperature fluxes to be monitored in line with previous studies of event-based water temperature changes (Somers et al., 2013, 2016; Wilby et al., 2015; Hofmeister et al., 2015). Loggers were installed with a

mean distance between loggers of 2.5km. Placement of loggers in some areas was impeded by lack of access to the river and hence a uniform separation distance between loggers was not feasible. For example, the Bourn tributary (Figure 1) contained only one logger (located at the tributary mouth) as the stream is largely culverted and inaccessible. The loggers were operational during the summer of 2016 (1 June 2016 to 15 September 2016), with river-water temperatures logged at 15-min intervals. Loggers were checked once during the study period to ensure no debris build-up had occurred around the loggers which might have potentially affected the temperature data, however no debris build up occurred during the study period. One logger was lost during the study period, leaving data from 11 loggers available for subsequent analysis (Figure 2.1).

2.3.3 Precipitation Data Collection

Precipitation data were collected from three available sources. First, data were obtained from a weather station (elevation 140m asl) located near the catchment outlet which was installed prior to the study. This is a Met Office (the UK's national weather service) approved station operating at 1-min temporal resolution and providing a dataset which is representative of the precipitation data used in many water temperature studies (Brown and Hannah, 2007; Hofmeister et al., 2015). Data were recorded in Greenwich Mean Time (GMT) and converted to British Summer Time to match the TinyTag water temperature data logging times. Distances from the weather station to individual water temperature sites ranged from 1km to 8.5km. The use of more weather stations would have been desirable, however, further Met Office sites were too far away from the study catchment and the creation of a dense network of gauges would have been expensive and difficult to maintain, as is the case for many water temperature

studies which are reliant on single gauges (Lange and Haensler, 2012; Brown and Hannah, 2007; Somers et al., 2013, 2016; Wilby et al., 2015; Hofmeister et al., 2015; Hester and Bauman, 2013). Air temperature data used in the study were also gathered from the Met Office site within the catchment.

Second, citizen science precipitation data were collected from the Met Office Weather Observation Website (WOW) (Met Office, 2018). The WOW network allows participants to upload data automatically from personal weather stations which can be downloaded freely. Each station in the network contains metadata detailing the degree of exposure, rain gauge type, recording hours, and urban climate-zone of the station. For this study, we used stations with standard precipitation gauges, with records over > 95% of the study period, the minimum threshold for inclusion in the study, and at a sampling frequency of ≤ 15-min. All sites recorded in GMT and were converted to British Summer Time. All stations recorded at time intervals beginning on the hour. This provided a pool of five citizen science gauges (ranging from 2.3 – 4.2 km from water temperature sites), of which four gauges were located outside the study catchment (Figure 2.1a). Rainfall gauges outside a catchment have been successfully used for discharge estimation in ungauged catchments (Samuel et al., 2011), hence the citizen science gauges were considered suitable for use herein. Of the five gauges, one was in the west of the catchment, two to the south, and two to the east. Elevation at the gauges ranged from 110-200m asl, with a mean of 154m asl. As seven of the water temperature loggers are located to the east of the catchment, the gauges to the east of the catchment have a larger weighting on precipitation estimates for these loggers. Although denser networks of citizen science gauges are possible, quality control (e.g. placement of gauges) remains problematic. It should be

recognized, also, that the WOW database is relatively new and is not yet comprehensive. As citizen science gauges are reliant on maintenance and installation by amateurs, data quality are reduced compared to official sources (Buytaert et al., 2014).

Third, high resolution precipitation data from the UK's NIMROD radar system (Golding, 1998) were provided by the UK Centre for Environmental Data (CEDA). Radar data were provided at 5-min temporal and 1km^2 spatial resolution. Data are recorded from the start of the hour onwards and converted from GMT to British Summer Time. Radar data from the NIMROD system have been quality checked and corrected through national scale corrections using gauge data, as described by Harrison, Scovell, & Kitchen (2009). Quantifying uncertainty ranges in radar rainfall has proven difficult as uncertainty propagates from a wide range of sources including, but not limited to, topography, atmospheric conditions, and distance from radar source. An extensive list of uncertainties and errors associated with radar data has been compiled by Villarini & Krajewski (2010). As the study catchment is in a relatively flat area and is situated within 50km of the nearest radar site (the Cleft Hill radar), these uncertainties are reduced for this study.

Point-based and catchment-average estimates were derived for the three precipitation datasets. Point-based data for each water temperature logger site were taken from the nearest weather station (only one weather station was used in this study, resulting in the same data used for each logger site), citizen science gauge, or radar grid cell (at 1km^2 resolution). For catchment-average data, nested catchments for each water temperature logger site were identified from the catchment topography, and precipitation data were averaged over each logger catchment to yield an overall catchment-average precipitation estimate. Consequently,

the catchment data are less variable than point-based data, particularly for the nested catchments. Citizen science gauge precipitation was averaged using the Thiessen method (Figure 2.1b), given its simplicity and widespread use in estimating areal precipitation (Ball and Luk, 1998). The contributing area of each gauge was determined and the contributing percentage of each gauge to each nested catchment precipitation total was calculated to derive estimates for catchment precipitation for each site. Because the weather station data featured only a single gauge, catchment-average precipitation could not be derived for this dataset. For the radar data, the contribution of each grid cell to each sub-catchment were calculated, and catchment-average precipitation was then derived for each logger.

2.3.4 Statistical Analysis

Statistical analysis was undertaken using each of the precipitation datasets to first relate sub-hourly water temperature changes to precipitation intensity; and second, daily water temperature changes to daily precipitation.

2.3.4.1 Sub-hourly analysis

For sub-hourly water temperature changes, the relationship between precipitation and water temperature surges were analyzed. Here water temperature surges were defined as a positive change of at least 1°C in water temperature that occurred after the onset of a precipitation event. The threshold of a 1°C change within a 30 minute time-window, measured from the onset of water temperature rise, was used to identify surges, as has been used in previous studies (Somers et al., 2016). This threshold ensured water temperature changes were caused

by the precipitation event and not by air temperature influence. A total of 48 temperature surges were identified within the study period (Table 2.1).

Precipitation metrics linked to water temperature surges (Herb et al., 2008; Nelson and Palmer, 2007; Somers et al., 2013) were calculated for each precipitation calculation method: maximum precipitation intensity prior to the surge; precipitation in the 30-min before the surge; and the precipitation total for the event prior to the surge. Exploratory analysis revealed that results for each metric were similar; hence only results for maximum precipitation intensity are presented herein. Precipitation intensity was selected given the importance of intense events rather than overall rainfall amount in causing water temperature surges identified in previous studies (Nelson and Palmer, 2007).

Initial analyses showed the relationship between water temperature surge and precipitation intensity to be non-linear, so General Additive Models (GAMs) were chosen for the analysis. GAMs are a class of generalized linear models, and are ideal for semi-parametric datasets given there is no assumption of linearity and are flexible in dealing with differing (non-normal) statistical distributions of the data (Murase et al., 2009). Due to this, GAMs have been particularly useful in modelling environmental effects on water temperature (Laanaya et al., 2017). All models were created using the "mgcv" package in R (Wood, 2018): The equation for GAMs can be written as so:

$$g(E(y)) = \beta\_0 + f1(x1) + f2(x2) + \ldots f_p(X_p) + \varepsilon$$

Where g is a link function, E(y) the response variables expected value, fi(xi) the smoothed function, and ε the error. The link function is a parametric function that enables the Gaussian

error structure to be applied to an exponential family, thereby linking the average of the dependent variables to the predictor variables (Laanaya et al., 2017). The smoothed function defines the regularity of the application of the regression within the model. This is controlled by the basis dimension (k), which represents the dimensionality of the spline basis, and controls the maximum degrees of freedom that can be applied within the model by each term. Higher values of k mean the smoothing function is applied more regularly.

For this study, a two explanatory variable GAM using a Gaussian error structure and identity link function was produced for all precipitation datasets. All water temperature surges in the study period were used for the model (Table 2.1). The difference between water temperature and air temperature was used as an additional variable alongside maximum precipitation intensity, as preliminary analysis for this study had reflected its importance. This was done to achieve better model fits, and to assess how the relative importance of maximum precipitation intensity to the GAM alters depending on the precipitation dataset used. The difference between water temperature and dew point temperature was also calculated, however this was highly correlated with water temperature and air temperature difference so did not feature in the final model. A smoother term was applied to the maximum precipitation intensity variable in all models and the basis dimension (*k* value) was chosen based on generalized cross-validation (GCV) (Wood, 2017). To assess the best model fit for the GAM's generalized cross-validation (GCV) scores were used. GCV scores show the minimized general-cross validation score for each GAM, with a lower score indicating a better fitting model with less predictive error.

For an example storm on 8 June 2016 maximum water temperature surges for each logger site were regressed against maximum precipitation intensity, with models produced for each type of precipitation dataset in the study. The adjusted R^2 was then compared to assess which precipitation dataset had the highest explanatory capability. The 8th June event was chosen as it had the largest water temperature surges in the study period, while the 13 September 2016 event did not feature a regression due to low sample size. A lower intensity event was also analyzed for the 13 September 2016 but did not feature a regression due to low sample size.

Table 2.1. List of water temperature surges in the study period. Site shows the location of the TinyTag logger (Figure 1), water temperature surge (°C) shows the maximum water temperature surge extent for each event, Intensity (mm/hour) refers to maximum precipitation intensity for each surge as recorded by the different precipitation datasets.

Date	Site	Water Temperature Surge (°C)	Weather Station Intensity (mm/hour)	Radar Point Intensity (mm/hour)	Radar Catchment Intensity (mm/hour)	Citizen Point Intensity (mm/hour)	Citizen Catchment Intensity (mm/hour)
07/06/2016 22:30	R2	1.21	2.4	9.48	5.18	0	0.2
08/06/2016 16:30	R5	2.15	0	73.1	34.91	14.24	19.03
08/06/2016 16:30	R2	4.24	0	69.4	34.3	31.52	21.05
08/06/2016 17:00	BB2	3.82	96	107	46.7	31.52	31.52
08/06/2016 17:00	R4	4.19	96	6.4	33.8	31.52	19.03
08/06/2016 17:15	R7	4.93	84	40	36.4	9.12	17.72
08/06/2016 17:30	R1	1.13	14.4	70.5	20.6	7.12	24.52
08/06/2016 17:30	BB3	2.20	14.4	50	30.8	3.08	31.52
08/06/2016 17:30	B1	1.31	14.4	25.8	28.2	7.12	30.07
08/06/2016 18:00	R3	3.20	9.6	25.8	29.6	5.08	18.57
08/06/2016 18:30	R2	1.97	4.8	43.4	22.4	0	21.8
11/06/2016 21:30	R7	1.13	0	0.79	4.64	0	0
11/06/2016 22:00	R4	1.43	0	3.63	9.08	22.36	6.35
12/06/2016 10:15	R7	1.11	4.8	1.97	1.55	2.04	2.94

12/06/2016 16:00	R5	1.27	6.4	32.6	13.6	0	10.24
12/06/2016 16:30	R3	1.07	12.8	12.3	8.9	0	8.62
13/06/2016 23:00	R7	1.21	16	23.2	13.67	4.04	4.51
14/06/2016 15:30	R3	1.12	24	10.7	4.7	1.04	2.91
14/06/2016 18:45	BB2	1.43	0	11.9	6.4	5.08	5.08
14/06/2016 20:00	BB3	1.26	4.8	6.72	6.7	0	5.08
25/06/2016 16:15	R4	1.26	0	51.781	17.5	0	0.04
01/07/2016 18:45	BB2	1.14	0	1.5	20.62	0	9.144
12/07/2016 11:00	BB2	1.49	0	1.4	0.66	2.032	5.08
12/07/2016 14:00	R3	2.34	0	1.6	0.78	0	1.26
28/07/2016 11:45	R7	1.75	4.8	3	2.88	4.064	2.68
28/07/2016 12:45	BB2	1.34	6	2.4	1.52	1.016	4.064
28/07/2016 20:00	BB2	1.44	2.4	25.3	11.97	0	0
29/07/2016 17:00	R6	1.49	0	7.1	4.5	1.016	2.66
29/07/2016 17:15	R7	2.12	0	5.6	4.4	1.016	2.22
19/08/2016 08:30	R7	1.38	4.8	2.18	2.22	2.032	2.68
19/08/2016 10:30	BB2	1.10	2.4	2	2.18	2.032	4.064
25/08/2016 03:00	BB2	1.51	4.8	3.75	4.38	5.08	5.08

25/08/2016 13:45	BB2	1.34	2.4	9.78	9.16	2.032	5.08
25/08/2016 20:30	BB2	1.01	19.2	9.78	9.16	3.048	5.08
27/08/2016 16:30	BB3	2.87	0	20	17.62	0	4.064
28/08/2016 18:15	R7	1.56	0	15.8	7.9	0	0
28/08/2016 19:30	R5	1.09	0	21.8	12.4	0	0
03/09/2016 11:15	BB2	1.64	36	11.1	9.8	18.56	18.56
03/09/2016 11:30	BB3	1.87	36	8.6	10.6	18.56	18.56
10/09/2016 06:45	R3	1.37	28.8	6.4	13.3	16.4	15.2
13/09/2016 16:30	R7	2.23	0	21.6	12.8	0	0.44
13/09/2016 16:45	BB2	2.82	6.4	7.2	21.2	8.128	8.128
13/09/2016 16:45	BB3	1.70	6.4	16.5	15.6	8.128	8.128
13/09/2016 17:15	R2	1.10	25.6	11.2	18.8	18.56	11.4
13/09/2016 17:30	B1	1.05	25.6	8.8	9.12	4.96	18.56
13/09/2016 16:45	R6	1.71	19.2	14.16	8.56	9.04	15.52
13/09/2016 17:15	BB1	1.13	19.2	13.32	11.28	16.256	4.88
13/09/2016 17:30	R1	1.10	19.2	13.32	11.04	16.256	9.44

2.3.4.2 Daily analysis

For daily water temperature variability, the following temperature metrics were calculated: daily maximum, daily minimum, daily mean, and daily range. All metrics, and associated precipitation data were calculated from midnight to midnight across the study period. The influence of seasonality was removed by subtracting a 10-day moving average (5 days either side) for each metric from the corresponding metric for each day. GAMs, with a Gaussian error structure and identity link function, were used to link standardized water temperature metrics to the precipitation total following the same model described in 2.3.1. Only precipitation days > 4mm were included in the analysis, to include only events that produced enough storm water to have a substantial effect on discharge. This threshold was derived based on a sensitivity analysis of discharge to precipitation, with 4mm of daily precipitation being the threshold where daily discharge was consistently twice that of baseflow. The threshold discharge amount was hence decided as 1.49 m^3/s. As a similar relationship is shown between all calculated temperature metrics and daily precipitation, only the GAMs for the daily mean temperature metric are presented here as an example. GCV scores were again used to assess the model with the best fit.

2.4 Results

2.4.1 Thermal, meteorological, and hydrological context

Time-series for precipitation, discharge, air temperature, and water temperature are shown for the study period at site R1 in Figure 2.2. June was notably the wettest month in the study period, registering 174mm of rainfall, whilst July was driest registering 24mm. Air temperature

during the study ranged from 7 to 32 °C, with a mean of 16.3 °C, whereas water temperature ranged from 11.1 to 21.7 °C, with a mean of 15.9 °C. Discharge had a minimum flow of 0.14 m^3/s, with a peak flow of 61.8 m^3/s.

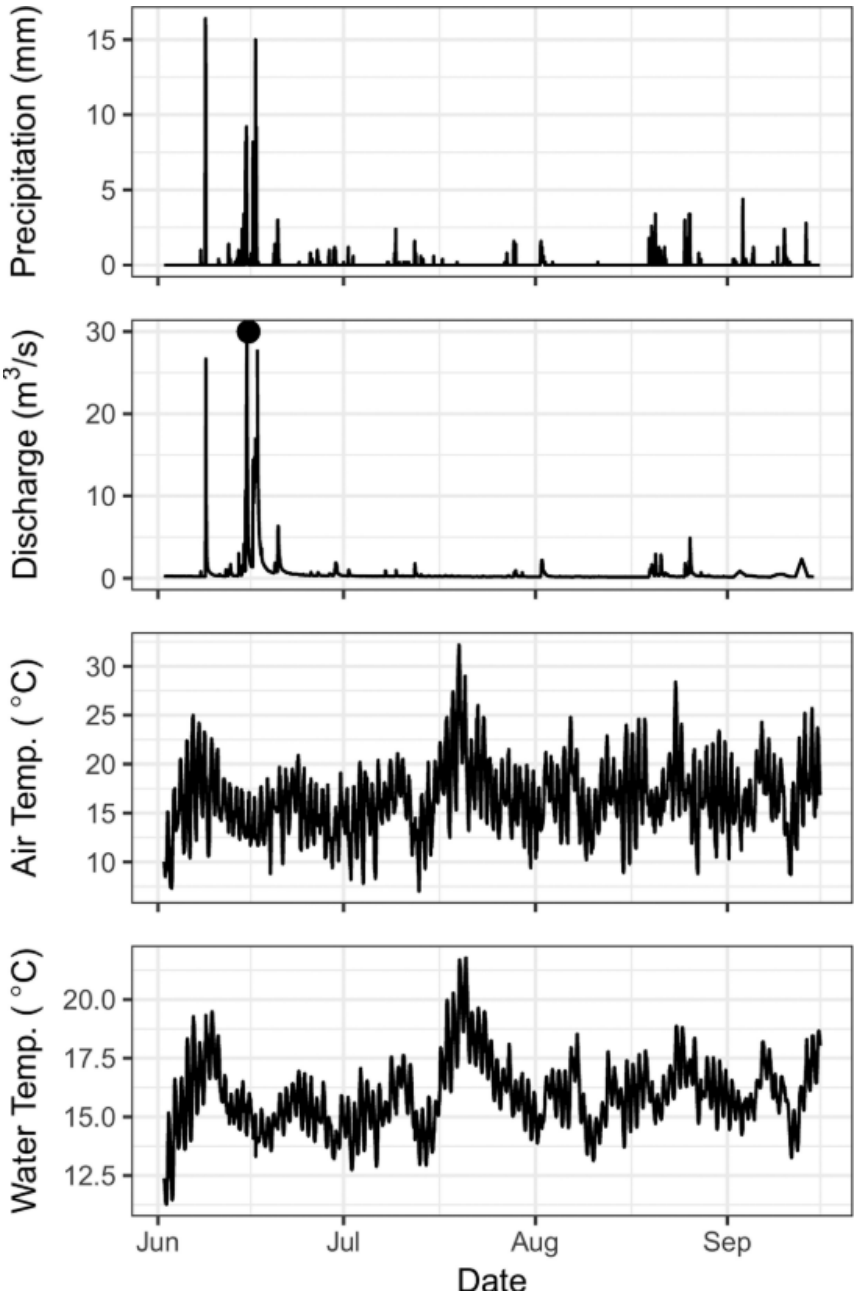

Figure 2.2. Time series of water temperature for site R1 (see Figure 2.1), air temperature and precipitation as recorded at the weather station, and discharge as recorded as recorded at the catchment outlet. The black dot on the discharge graph shows a particularly large event that peaked at 62 m^3/s, outside the limits of the y-axis.

2.4.2 Comparison of precipitation methods

Monthly (Table 2.2) and daily (Figure 2.3) precipitation totals are shown for June, July, and August for the weather station location. The study period included months with very high (June), low (July), and mean (August) rainfall, providing a wide range of event types. Table 2.2 gives the percentage difference in estimated precipitation for the different precipitation methods and the weather station. In the wettest month (June) high variation was apparent. Both citizen science methods considerably underestimated precipitation in comparison to the weather station, whilst both radar methods overestimated precipitation, but by a much smaller amount than citizen science methods. In the driest month (July), all methods measured relatively similar precipitation totals, although percentage differences are large given the small precipitation totals. In August, both radar methods underestimated precipitation in comparison to the weather station, particularly the radar point-based data. In August, citizen science data produced values closest to those of the weather station. The catchment citizen science data slightly underestimated compared to a slight overestimation for the citizen point-based data.

Table 2.2. Precipitation (Precip) measured in mm for summer months in 2016 at the weather station site. Citizen = Citizen Science data, Catchment = Catchment-average, Point = Point-based.

	June Precip (mm)	% Difference to weather station	July Precip (mm)	% Difference to weather station	August Precip (mm)	% Difference to weather station	Total Precip (mm)	% Difference to weather station
Radar Average	166	-6.6	17	-23.5	47	-9.1	230	-9.1%
Radar Point	194	+8.8	20	-5	39	+0.8	253	+0.8%
Citizen Average	120	-47.5	23	+8.7	52	-28.7	195	-28.7%
Citizen Point	128	-38.2	26	+19.2	58	-18.3	212	-18.3%
Weather Station	177	NA	21	NA	53	NA	251	NA

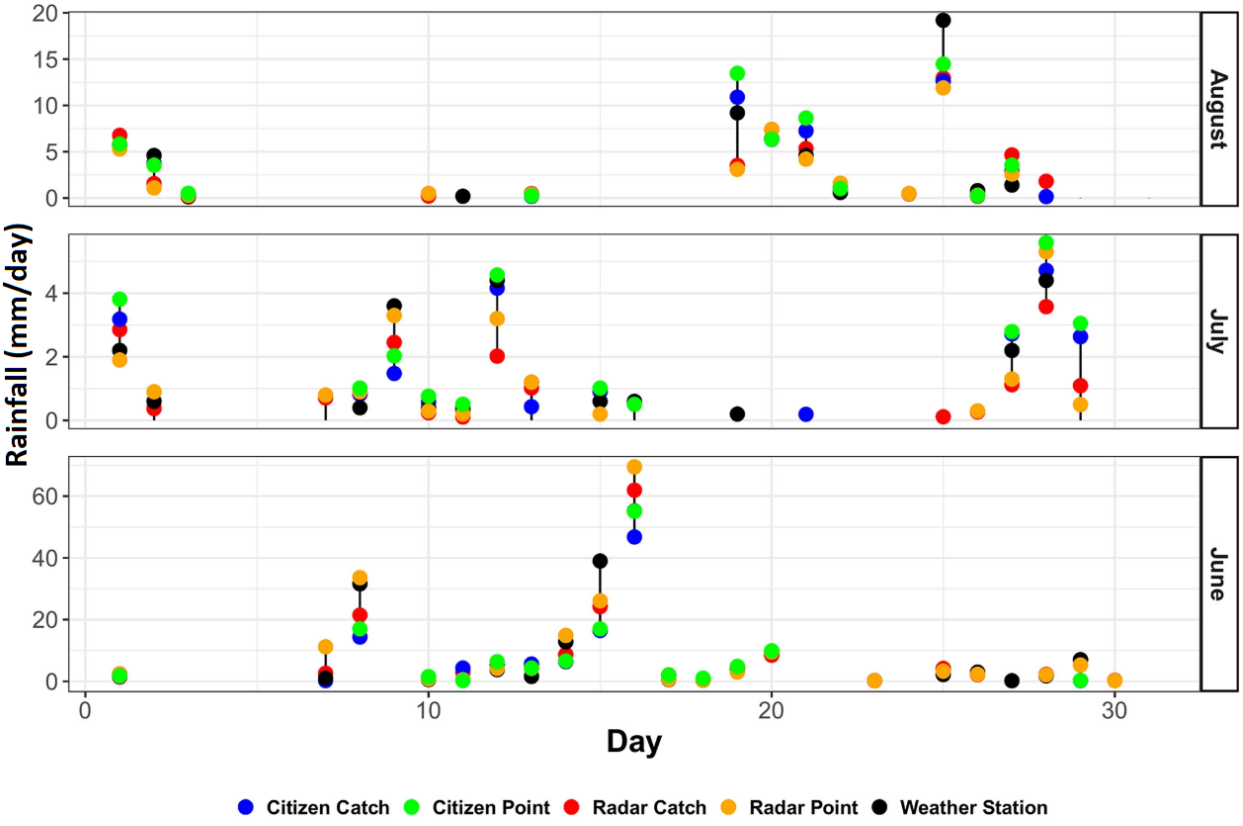

Figure 2.3. Daily precipitation totals (mm/day) for the study catchment. Black bars represent the daily precipitation range. Colored dots represent the different precipitation methods used in the study.

2.4.3 Sub-Hourly Water Temperature Change

Summaries of the GAM's modelling water temperature surge using the predictors maximum precipitation intensity and air/water temperature differences are shown in Table 2.3. Maximum precipitation intensity was found to be a significant predictor ($P < 0.001$) of water temperature surges only when using radar catchment-average precipitation data. In contrast, maximum precipitation intensity was not found to be significant ($P > 0.05$) in any of the other GAMs. The deviance explained varied between models ranged from 72.7% for the radar catchment-average data, to 64.5% for the citizen science point-based data. Adjusted R^2 values ranged from 0.69 for the radar catchment-average GAM to 0.60 for the citizen point-based GAM. GCV score, which can be used as a means of estimating prediction error in models, was lowest for the model using radar catchment-average precipitation data (0.30) and highest for the model showing the citizen point-based precipitation data (0.39).

The GAM featuring radar catchment-average precipitation (Figure 2.4a) shows a non-linear threshold response, with increased water temperatures only at the higher maximum precipitation intensities. A similar non-linear trend is observed in both the weather station data (Figure 2.4e) and citizen point data (Figure 2.4d). In contrast, a linear trend is observed within the radar point (Figure 2.4b) and citizen catchment (Figure 2.4c) models.

Table 2.3. Validated GAM models for maximum precipitation intensity calculated by different precipitation sources against water temperature surges. Citizen = Citizen Science data, Catchment = Catchment-average, Point = Point-based.

	Radar Catchment			**Radar Point**			**Citizen Catchment**			**Citizen Point**			**Weather Station**		
Adjusted R^2	0.69			0.62			0.65			0.60			0.61		
Deviance Explained (%)	72.7			66.7			69.5			64.5			65.4		
GCV Score	0.30			0.37			0.34			0.39			0.38		
Sample Size	48			48			48			48			48		
Covariate	**Df**	**K**	**p-value**	**df**	**k**	**p-value**	**df**	**k**	**p-value**	**df**	**k**	**p-value**	**df**	**k**	**p-value**
Maximum Precipitation Intensity	1.7	3	<0.001	1.7	3	0.30	1.7	3	0.056	1.4	3	0.36	1.15	3	0.17
Starting Water/Air Temperature Difference	3.9	5	<0.01	3.9	5	<0.001	3.9	5	<0.001	3.9	5	<0.001	3.9	5	<0.001

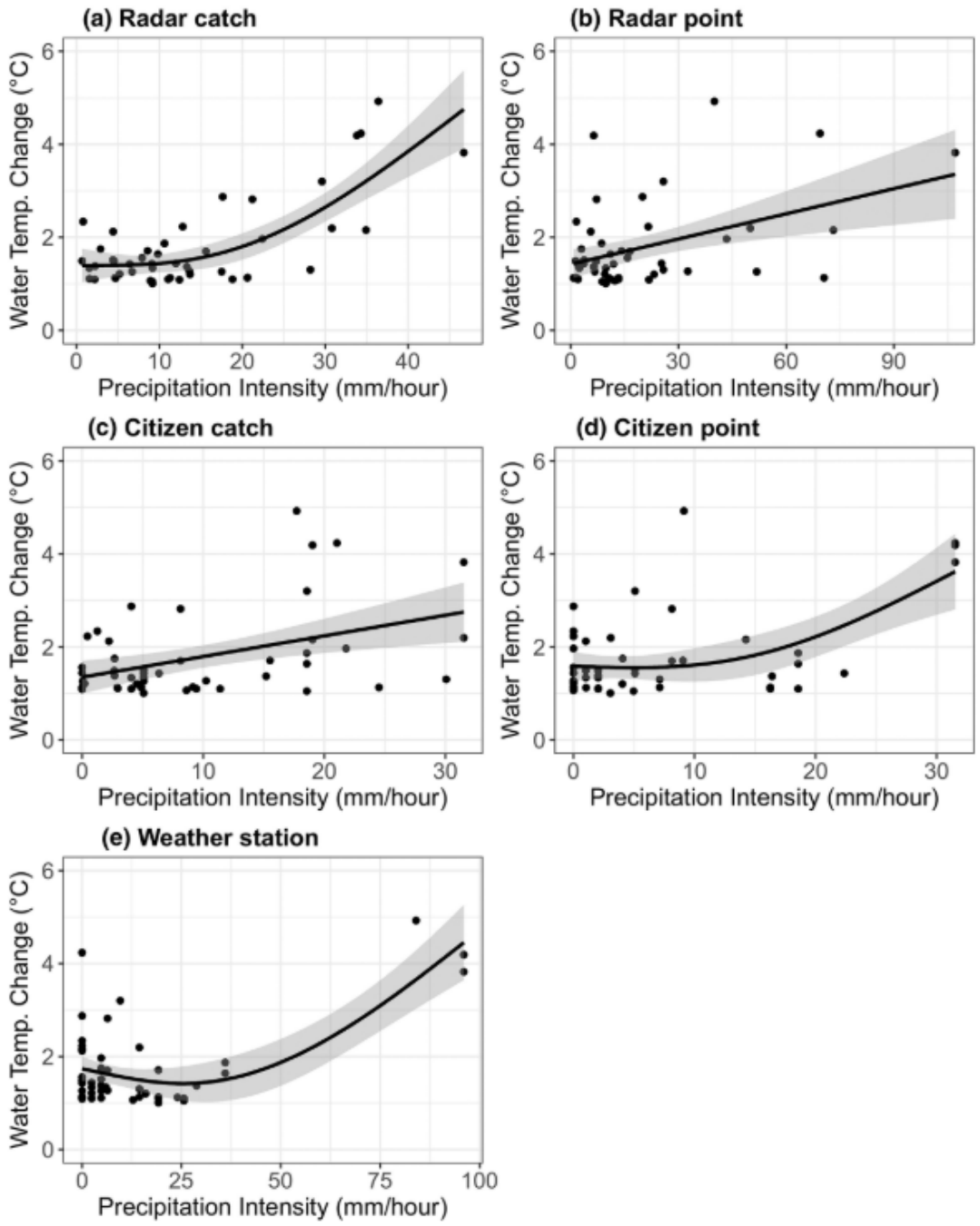

Figure 2.4. GAM's of maximum precipitation intensity and water temperature surge determined by the different precipitation sources. The black line shows the fitted line of the GAM, while the shaded grey area shows the 95% confidence interval.

2.4.3.1 High-Intensity Example (8 June 2016)

Spatial and temporal variation in precipitation for an event on 8 June 2016 and the associated water temperature surges are shown in Figure 2.5. The timing of precipitation differs substantially between precipitation methods. The weather station data provides only one rainfall value across the catchment with heaviest rainfall occurring at 16:45 and 17:00. By contrast, both radar datasets show high spatial and temporal variations in rainfall across the catchment, with peak rainfall for logger sites varying between 16:15 and 16:45. The timing of peak rainfall differed markedly for logger sites between the point-based and catchment-average radar methods. Both the citizen science datasets showed minimal rainfall until 17:00, with both datasets showing peak rainfall at 17:15 for all logger sites.

The initial water temperatures surges shown at 16:15 and 16:30 appeared to occur without the onset of rainfall when using the weather station or citizen science datasets; however, both radar datasets showed rainfall correspond with these surges. Only surges occurring at 17:00 corresponded with peak rainfall at the weather station, however, substantial prior precipitation was also shown with both radar datasets. The final water temperature surges occurred by 17:15, corresponding with peak rainfall in the citizen science dataset, compared to minimal rainfall in the weather station and radar datasets.

Linear regression models show the relationship between maximum precipitation intensity and water temperature surges for the different precipitation methods in the 8th June event (Table 2.4). Maximum precipitation intensity was shown to be a significant predictor only for modelled radar catchment-average data ($P < 0.01$, $R^2 = 0.54$). When using weather station, radar point-

based, and citizen sciences datasets, maximum precipitation intensity was not significant with low explanatory capability shown ($P > 0.05$, $R^2 =$ -0.10 to 0.14).

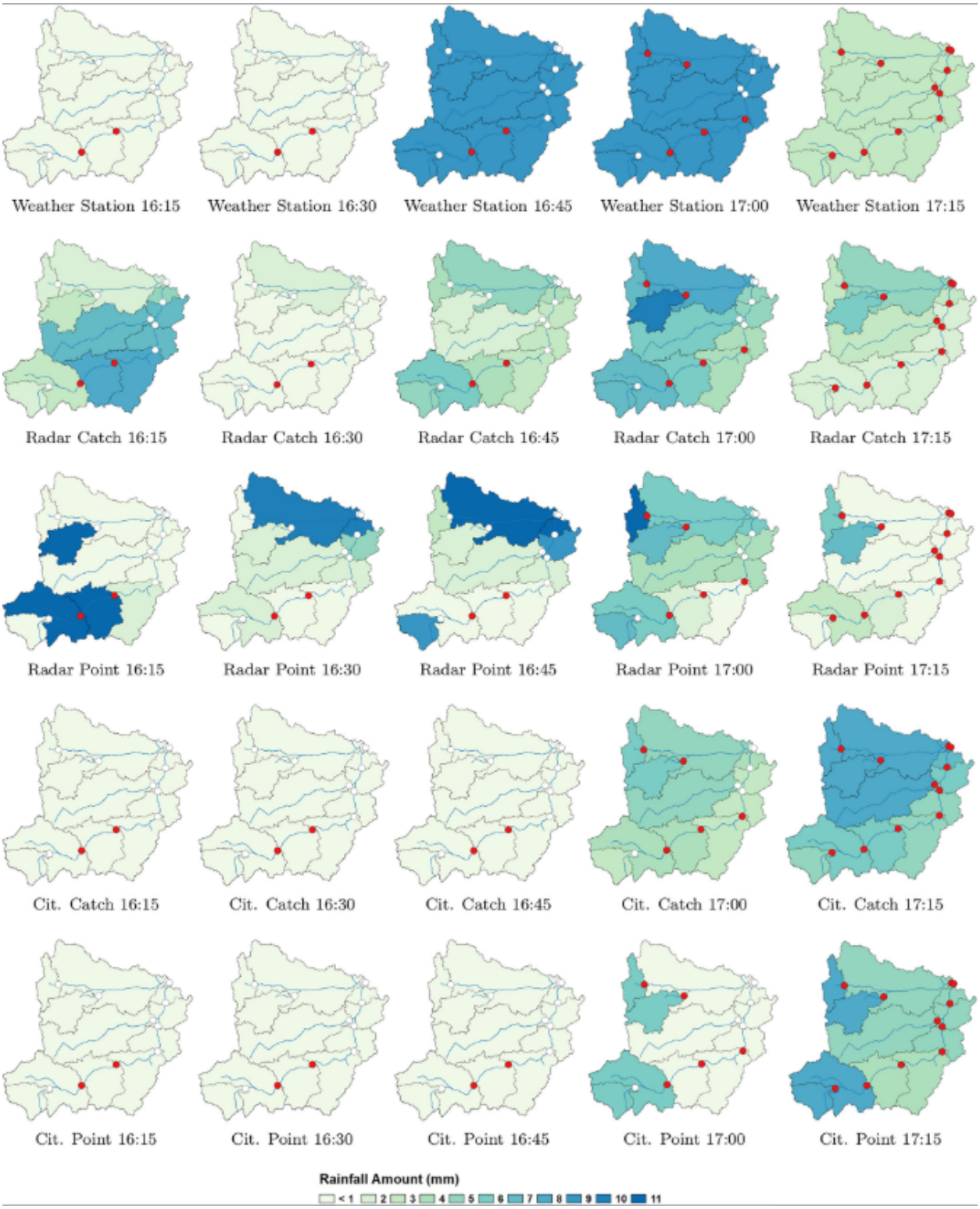

Figure 2.5. Temporal development of the 8 June 2016 event for the different precipitation methods: white circles show no water temperature surge; red indicate > 1° rise in water

temperature for that site. Colors indicate precipitation in mm. Maps created in GIS by coloring in each logger nested catchment with corresponding precipitation amount for time period.

Table 2.4. Linear regression coefficients and adjusted R^2 for maximum precipitation intensity against water temperature surge in the 8th June event. The sample size for all models is 11.

	Estimate	Standard Error	t-value	p-value	Adjusted R^2
Intercept	2.25	0.50	4.49	0.001	0.14
Weather Station	0.15	0.01	1.63	0.138	
Intercept	-1.96	1.37	-1.43	0.185	0.54
Radar Catchment	0.16	0.05	3.56	0.006	
Intercept	3.03	0.90	3.34	0.008	-0.10
Radar Point	0.00	0.01	-0.26	0.796	
Intercept	5.24	1.80	2.90	0.017	0.08
Citizen Catchment	-0.10	0.07	-1.37	0.202	
Intercept	2.12	0.59	3.55	0.006	0.11
Citizen Point	0.04	0.02	1.49	0.169	

2.4.3.2 Low-Intensity Example (13 September 2016)

Spatial and temporal variation in precipitation and water temperature for a low-intensity event for 13 September 2016 are shown in Figure 2.6. Temporal variation through the event was lower than for the 8th June event, with all precipitation datasets suggesting that most of the precipitation occurred between 16:45 and 17:15. Again, the weather station provided a single value across the catchment, suggesting almost all precipitation fell between 17:00 and 17:15 (after the first temperature surge event occurred). In contrast, both radar and citizen science methods indicate substantial rainfall in the south-west of the catchment prior to this, although only the radar methods capture precipitation corresponding to the initial water temperature surge at 16:30. Both citizen science and radar methods capture precipitation in the north-west

of the catchment, which is the location of the subsequent water temperature surge. Large differences in precipitation estimation are noticeable at 17:00. Both citizen science methods suggest minimal precipitation at this point, however this was the time of peak rainfall within both radar methods and at the weather station site in the north of the catchment. By contrast, peak rainfall in the citizen science sites occurred at 17:15. For the citizen science catchment method, peak rainfall is shown within the south-east of the catchment, where no surge events were identified. By contrast, both radar methods suggest minimal precipitation in this location. Two further surge events were captured at this point, with citizen point and radar point suggesting the heaviest precipitation corresponding with these. By 17:30, all methods show the event to have ended.

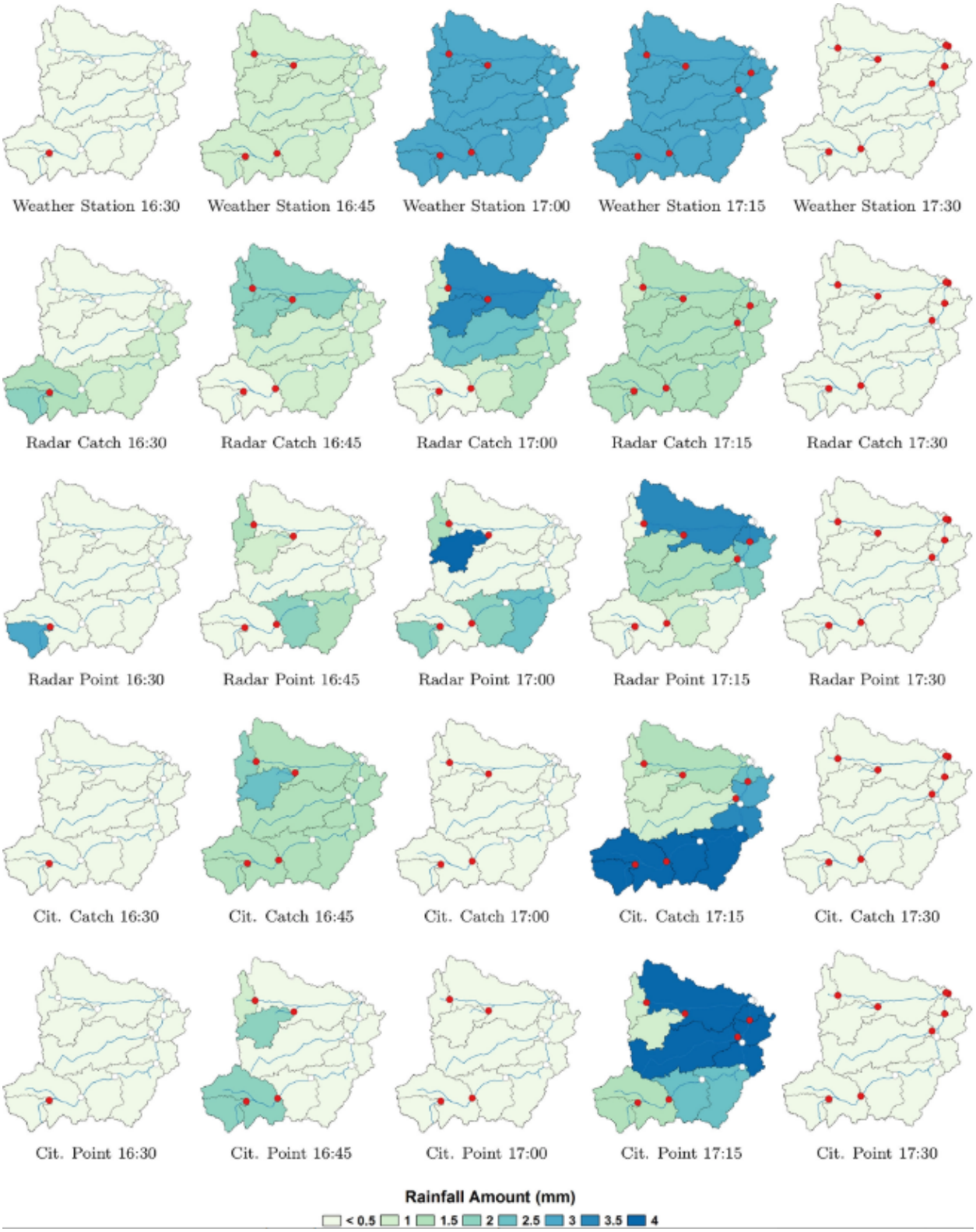

Figure 2.6. Temporal development of the 13 September 2016 event for the different precipitation methods: white circles show no water temperature surge; red indicate > 1° rise in

water temperature for that site. Colors indicate precipitation in mm. Maps created in GIS by coloring in each logger nested catchment with corresponding precipitation amount for time period.

2.4.4. Daily Water Temperature Variability

Summaries of the GAM's modelling deviation from mean water temperature using daily precipitation amount are shown in Table 2.5. In all models, daily precipitation was found to be a significant predictor for standardized daily mean water temperature ($P < 0.001$). The explained deviance varied widely between models, ranging from 20.7 % for the radar catchment-average GAM, to 52.2 % for the weather station GAM. Adjusted R^2 ranged from 0.18 for the radar catchment-average GAM to 0.50 for the weather station GAM. GCV was lowest for the citizen catchment-average precipitation model (0.20) and highest for the radar catchment-average precipitation model (0.33). A non-linear response was evident with an initial rise in standardized mean water temperature with higher precipitation totals up to a threshold around 20mm which is followed by a fall in standardized mean water temperature for the highest daily precipitation totals was shown by all models (Figure 2.7).

Table 2.5. Validated GAM models for standardized mean daily water temperature against daily precipitation as determined by the different precipitation sources. Citizen = Citizen Science data, Catchment = Catchment-average, Point = Point-based.

	Radar Catchment			**Radar Point**			**Citizen Catchment**			**Citizen Point**			**Weather Station**		
Adjusted R^2	0.18			0.20			0.41			0.41			0.50		
Deviance Explained (%)	20.7			22.2			42.5			30.2			52.2		
GCV Score	0.33			0.31			0.20			0.26			0.20		
Sample Size	127			151			155			150			152		
Covariate	**Df**	**k**	**p-value**	**df**	**k**	**p-value**	**df**	**k**	**p-value**	**df**	**k**	**p-value**	**df**	**k**	**p-value**
Maximum Precipitation Intensity	3,2	5	<0.001	3.5	6	<0.001	4.9	6	<0.001	4.7	6	<0.001	4.9	5	<0.001

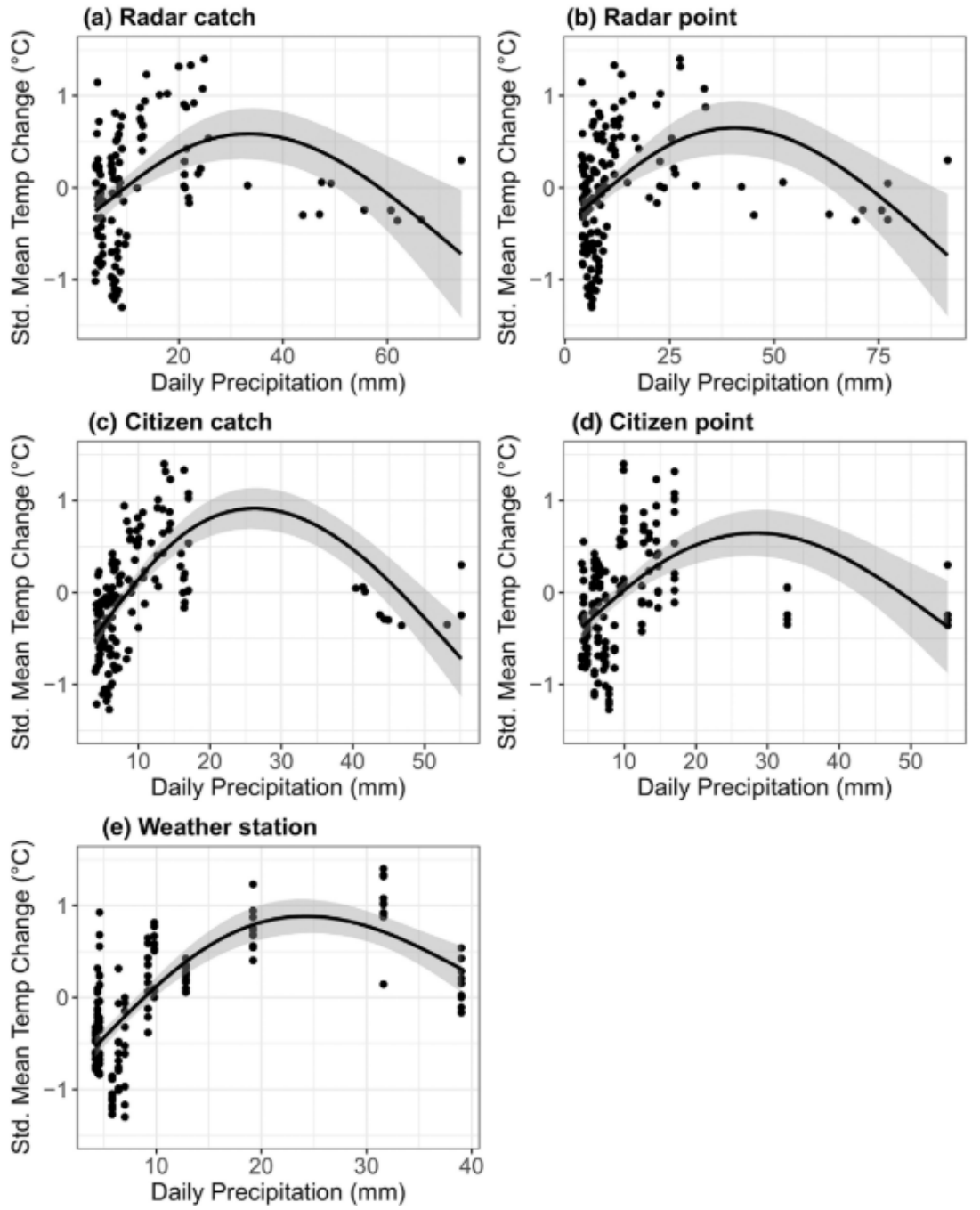

Figure 2.7. GAM's of daily precipitation and standardized mean daily water temperature determined by the different precipitation sources. All TinyTag sites are combined for the purposes of these plots. The black line shows the fitted line of the GAM, while the shaded grey area shows the 95% confidence interval.

2.5. Discussion and conclusions

2.5.1 Precipitation estimate differences between datasets

Differences in precipitation between datasets (weather station, citizen science and radar) were more pronounced than the differences between point-based and catchment-average calculation methods, which reflect precipitation variability over short distances during the events. Single precipitation gauge data are, therefore, often unrepresentative of multiple water temperature sample sites unless strict consideration is given to catchment size and strategic siting (Villarini et al., 2008; Gabriele et al., 2017; Thorndahl et al., 2017).

Citizen science estimates of precipitation displayed large differences with respect to percentage difference in total rainfall amount when compared to estimates at the weather station site location during high-intensity events suggesting it may be inaccurate. This possibly resulted from high spatial variability in precipitation within the catchment that was not adequately accounted for by the citizen science gauges (Pedersen et al., 2010). These errors may also propagate from siting issues as meteorological standards for gauge site siting may be difficult to adhere to for citizens in urban areas due to lack of unobstructed space, which may lead to underestimation of precipitation (Muller et al., 2013). Radar data were most accurate in the wettest month (August), but exhibited substantial discrepancies from the weather station gauge in the driest month (June), possibly as radar data have larger uncertainty at lower precipitation intensities as radar data struggles to identify drizzle (Golding, 2000).

2.5.2 Sub-Hourly Water Temperature Changes

The best model fit was achieved using the Radar catchment-average precipitation dataset. Catchment-average precipitation estimates account for precipitation falling across the catchment so are more spatially representative of 'true' precipitation patterns input into the river system (Walsh et al., 2012; Fletcher et al., 2013). Radar data have previously also been shown to monitor high-intensity events accurately (Biggs and Atkinson, 2011). Consequently, the higher predictive capability of the radar catchment-average model compared to the citizen catchment-average model reflects the higher spatial and temporal resolution of the radar dataset (Gabriele et al., 2017). As water temperature surges are more likely to occur where there is rapid surface and shallow sub-surface drainage (Nelson and Palmer, 2007; Somers et al., 2013), the radar catchment dataset is likely to be more representative of thermally-polluted water in the river than alternative precipitation datasets. Furthermore, as the process of heat exchange between low-heat capacity surfaces and surface runoff occurs over short durations (Herb et al., 2008), this effect is likely to be better captured by the highest temporal resolution datasets. In contrast, point-based methods provide inaccurate precipitation estimates as they fail to account for variations in storm intensity across the catchment, which may result in high spatial variation in rainfall, particularly in urban areas (Thorndahl et al., 2017). Point based methods are unlikely to be an adequate proxy of thermally charged surface runoff, as they fail to represent the export of heated water from individual sub-catchments. Hence point-based methods are particularly ineffective in urban environments, as they lack the spatial representativeness required to account for drainage systems that rapidly route water from the entire sub-catchment to the river rapidly (Jones et al., 2012), which in turn leads to water

temperature surges. This is particularly evident during convective storms which are responsible for most events causing water temperature surges (Hofmeister et al., 2015; Wilby et al., 2015; Nelson and Palmer, 2007). Consequently, point-based methods are unlikely to be representative, therefore, catchment-average radar precipitation datasets are recommended for use in water temperature studies focusing on high-intensity events.

In the example water temperature surge events, both point-based and catchment-average radar estimation methods represented the relatively higher accuracy of radar data in spatially and temporally representing a high-intensity event. The close temporal proximity of the onset of high-intensity precipitation event to the water temperature surges in urbanized catchments as shown by the radar data have been observed in previous studies (Anderson et al., 2010; Nelson and Palmer, 2007; Hofmeister et al., 2015; Somers et al., 2013) which noted the quick onset of surges after localized precipitation, with a longer lag time downstream due to dissipation of heat pulses from upstream (Wilby et al., 2015; Somers et al., 2013). Alternatively, the transit time of water from the point in the catchment where the rain fell to the river may also explain the seemingly delayed water temperature surge at the most downstream sites. It is further important to consider that water temperature dynamics such as water temperature surges are also controlled by numerous other variables such as dew point temperature that are not accounted for by solely using precipitation data (Herb et al., 2008). In contrast, for the low-intensity event, both radar methods provided a relatively accurate description of precipitation associated with water temperature surges, which contrasts with previous studies suggesting that radar data are less effective at lower rainfall intensities (Biggs and Atkinson, 2011; Golding,

2000). Furthermore, both point-based and catchment-based radar methods also gave similar estimates, suggesting lower spatial variability in the low-intensity event.

From the weather station data only constant precipitation across the catchment could be derived, which misleadingly showed water temperature surges taking place before any precipitation was observed in both the high-intensity event and the low-intensity event. The assumption of a constant precipitation value across the catchment is likely to be highly inaccurate and lead to difficulties quantifying precipitation-driven processes (Thorndahl et al., 2017). The degree to which water temperature surges are controlled by precipitation may be underestimated or masked entirely when using single gauge data depending on catchment area, river network properties, storm direction, and rate of passage through the catchment.

Both citizen science point-based and catchment-average methods suggested that the precipitation peak occurred after the water temperature surge at five of the ten logger sites within the high-intensity event. This represents the influence of gauges to the east of the catchment; with the 8th June storm moving from west to east across the catchment. As most of the water temperature loggers were in the eastern part of the catchment, the precipitation estimate for them was derived from gauges to the east of the catchment. Because the rain reached these gauges later, water temperature surges were already present at these sites before precipitation was measured. Increased density of citizen gauges in the western part of the catchment would likely help better capture similar surge-triggering events. However, without high density gauge networks with relatively even spacing, it appears that using citizen science gauge networks can lead to substantial under- or over-estimations in high-intensity events making links to water temperature data problematic. However, for the low-intensity

event, citizen point data corresponded well with water temperature surges at individual sub-catchments and suggested similar spatial distributions in precipitation as the radar methods. The citizen science catchment method gave substantially different estimations, with high precipitation estimates in the south-east region of the catchment that did not feature any water temperature surges, and minimal precipitation was estimated by the point citizen science method and radar methods. This suggests that the density of citizen science gauges was not high enough to provide reliable interpolations for the low-intensity event.

2.5.3 Daily Water Temperature Variability

All precipitation calculation methods modelled the relationship between mean water temperature and total daily precipitation effectively. Strong fits were provided by all models. This is because daily metrics are less sensitive to issues related to storm timing and duration (Fletcher et al., 2013; Jacobson, 2011). This may be because the main process driving the change in daily temperature dynamics after precipitation is a change in the specific heat-capacity of the receiving waters (Hannah et al., 2008). At higher discharges the specific heat capacity of the stream is increased, and the river is more resilient to atmospheric cooling. As only a small subset of overall events leads to water temperature surges, diurnal temperature fluctuations after precipitation are likely to reflect changes in total discharge. Hence, although lower spatial and temporal resolution datasets may be inadequate for analyses of thermally-polluted waters immediately entering rivers, lower spatial and temporal resolution precipitation datasets can provide a proxy of discharge. Therefore, if the focus of study is daily temperature metrics, then high spatial and temporal resolution precipitation data are not necessarily required.

Although citizen science and weather station datasets showed the strongest model fits, this may be an artefact of the reduced variation in rainfall in the point-based datasets which can lead to misleadingly small error in statistical models. Although radar catchment precipitation showed the worst model fit, the greater spatial variation in precipitation patterns accounted for than other methods in turn may lead to larger errors (Gabriele et al., 2017; Pedersen et al., 2010). As such, caution is required in interpreting the strength of relationships within water temperature models where precipitation is a predictor, particularly where only a single gauge is used. Furthermore, some degree of uncertainty in the analyses was caused by the timing of the events, and the possibility that precipitation from a single event may extend over two days. All logger sites were included in the analyses, meaning headwater and downstream sites were also mixed together, which therefore respond differently to precipitation properties.

2.5.4 Implications and Future Research

This study highlights the value of using radar catchment-average rainfall datasets when modelling event-based water temperature fluxes at short temporal scales. However, when using traditional gauge methods, linking precipitation to water temperature dynamics has much greater potential for error at sub-hourly scales, and the role of precipitation as an important variable driving water temperature dynamic may currently be underestimated or ignored. The errors that propagate from the use of single point-based sources are likely to also occur for other water quality variables where precipitation is a primary driver of water quality dynamics. The use of catchment-average radar rainfall data as a means of analyzing precipitation-led fluxes in water quality variables is therefore encouraged. High spatial and temporal variability precipitation sources such as catchment-average radar is likely to be particularly beneficial in

urban water quality studies, where precipitation is shown to be more localized, and where precipitation linkages to water quality dynamics can often be directly correlated. The alternative catchment-average based datasets are likely to also be advantageous to water quality studies within poorly gauged catchments.

Further research is required in catchments of different sizes and land use types. As the study took place in an urban headwater catchment, it would be useful to assess different precipitation datasets in varying land uses where hydrological and water temperature responses to precipitations events are likely to differ. To build on the findings of this study, more systematic examination of the lag time between precipitation and water temperature surges will further enhance understanding of the link between precipitation and water temperature change. Moreover, further water quality variables that are likely to be responsive to precipitation events and are important contributors to water quality such as suspended sediments, pH, conductivity, and heavy metals concentrations could be analyzed to ensure greater transferability of the results of this study to future water quality studies. Variables with a clear first flush effect, such as nutrients, organic matter, and heavy metals are of interest for further study given their links between catchment transport of these variables and precipitation intensity.

CHAPTER 3: WATER TEMPERATURE HIGHER DURING LOW FLOWS BUT LAND USE BUFFERS THE EFFECT

3.1 Abstract

Discharge-related river temperature changes are increasingly likely due to increasing urbanization and increases in the frequency of extreme events. Despite this, understanding of the effects of extreme flows on river water temperatures is limited and the effects of urban land use on river temperatures are not well known. To address these research gaps, we installed 27 water temperature loggers in 3 rivers spanning a gradient of land uses in Birmingham, UK for 3 summers from 2016-2018. We identified low flow, high flow, and average flow periods using $95^{th,}$ 5^{th}, and 50^{th} percentile flow duration curve values respectively for all sites and calculated mean, maximum, and mean temperature anomalies at a daily temporal resolution for all sites. We found low flow periods to have significantly higher maximum, minimum and mean water temperature anomalies compared to average flow and high flow periods. No significant difference was found between high flow and average flow. To identify the main landscape controls on water temperature anomalies during extreme events we used multiple linear regression. For low flow, land use characteristics, specifically road buffer and 1km urban buffer were found to be the main controls, with a negative relationship observed. For high flows, however, elevation was found to be the main control. Overall, we find that low flows lead to increased extreme water temperature, although this effect is reduced in more urbanized areas. Extreme high flows were found to be less related to extreme diurnal water temperatures anomalies. The study highlights that low flow can lead to higher frequency of

extreme water temperature events, however more urbanized streams are less likely to experience extreme water temperature events during extreme flows.

3.2 Introduction

Water temperature is a controlling variable for a multitude of abiotic and biotic processes within streams (Caissie, 2006). For biota within streams, factors such as growth rates, metabolic activity, reproduction cycles and habitat ranges are all governed by temperature (Woodward et al., 2010a; Hogg et al., 1995). Water temperature therefore exerts a strong control on ecosystem health for aquatic organisms. Subsequently, alterations in water temperature can lead to drastic changes in ecosystem health (Mohseni et al., 2003). Water temperature alterations are governed by four main processes: atmospheric conditions, stream discharge, topography, and streambed conditions (Caissie, 2006). Changes to these processes can lead to water temperature change.

Extreme events such as floods and low flows can impact the water temperature dynamics within rivers (Van Vliet et al., 2013; Zwolsman & van Bokhoven, 2007). Due to the unique landscape properties of urban catchments, urban rivers are especially likely to experience water temperature change during extreme events. For example, during high-intensity precipitation, urban rivers can experience water temperature surges (Somers et al., 2013; Croghan et al., 2018; Nelson and Palmer, 2007). Urban areas are susceptible to these water temperature surges as impermeable surfaces often warm to higher temperatures than air temperature, therefore, when stormwater is generated, heat exchange occurs with the impermeable surface which can cause large increases in stormwater runoff temperature (Herb et al., 2008). As

stormwater in urban areas is quickly routed to rivers through storm drains, this leaves urban rivers susceptible to sudden increases during storm events This has been found to lead to increases in water temperature of upwards of 7 °C (Pluhowski and Pecora, 1970; Nelson and Palmer, 2007), while elevated water temperatures can subsequently be apparent for hours (Croghan et al., 2018; Wilby et al., 2015). However, most of the research focuses on isolated surge events. In addition to floods, hydrological droughts have been speculated to exert a strong influence on the water temperature of streams although evidence remains limited (Mosley, 2015; Van Vliet & Zwolsman, 2008). Meteorological droughts are defined as periods of below-normal precipitation, and subsequently can cause hydrological drought, which is denoted by low discharge (Van Loon, 2015). The reduced discharge in streams can increase the sensitivity of rivers to changes in air temperature, which during the summer months can cause extreme warming during heatwaves (Hrdinka, Novický, Hanslík, & Rieder, 2012; Van Vliet & Zwolsman, 2008). Urban catchments are likely to experience low flow conditions (Van Loon et al., 2016) as urbanization is often associated with reduced groundwater discharge. Reduced groundwater inputs increase the importance of atmospheric conditions as a control on water temperature (McGrane, 2016). This increases the chances that urban streams experience low flow related water temperature change.

Land use change through urbanization has been found to be a strong driver of thermal regime change (Kaushal et al., 2010; Rice et al., 2011; Arora et al., 2018). Urbanization modifies all the processes that control water temperature. Atmospheric conditions are altered within urban environments, with urbanization linked to increased summer precipitation (Daniels et al., 2016), and warmer air temperatures (Schwarz et al., 2012). Streambed conditions are often

modified due to the hard engineering of rivers in urban environments which is generally linked to reduced groundwater inputs and resultantly less moderation of stream temperature (McGrane, 2016). Topography is greatly altered with a high degree of impermeable surfaces in urban areas, while vegetation and riparian shading are generally reduced (Wang and Kanehl, 2003). Meanwhile, after urbanization, streams generally have lower baseflow and higher peaks and shorter recession times in flood events due to changes in water pathways (Miller and Hutchins, 2017; McGrane, 2016; Fletcher et al., 2013). The extent to which urbanization changes these processes is likely to be particularly exacerbated during extreme events when the greatest changes to atmospheric conditions and stream discharge are most apparent, and the effects of topography change most pronounced.

Although urbanization is noted as an exacerbating factor in the impact of extreme events on other water quality variables, the evidence for water temperature remains sparse (Miller and Hutchins, 2017). Therefore, in order to mitigate the impacts of extreme events on water temperature within urban systems a greater understanding of the land use controls on water temperature is required. Further, where water temperature studies have incorporated land use, urbanization is usually treated as a coarse metric (Rice et al., 2011; Talmage et al., 1999), but urbanization is likely to be reflected in a multitude of metrics beyond impermeability coverage. Hence, in this study we consider the effects of an abundance of metrics associated with urbanization on water temperature response to extreme events.

In this study, we aim to investigate to what extent extreme events alter water temperature dynamics, and how landscape metrics impact on water temperature response during extreme events. We hypothesize that extreme hydrological events would lead to an increase in the

amount of extreme water temperature events, and that catchment land use metrics associated with urbanization would lead to increased water temperature anomalies during extreme events. Hence, the objectives of our study were:

1) Determine the impact of extreme hydrological events on water temperature
2) Determine the influence of urbanization on water temperature anomalies to extreme events in relation to non-urban streams
3) Examine which specific landscape characteristics are associated with the strongest water temperature anomalies during extreme events

To address these objectives, we placed water temperature loggers at 27 sites for 3 years and determined land use for each logger catchment. Subsequently, we used a threshold-based approach to define high and low flow events for each site.

3.3 Methods

3.3.1 Study Site

The study was conducted in three adjacent headwater catchments: the River Rea, River Cole and River Blythe (Figure 3.1). All three catchments are located within the city of Birmingham, West Midlands, UK (52.48 ° N, 1.89° W). The catchments were chosen to span a gradient of land use, with water temperature sub-catchments located in areas ranging from 0% to 82% impermeable surface cover. The River Rea was the most urbanized of the three catchments, with an average impermeable surface cover of 69%, whilst for the Cole this was 34%, and the Blythe 18%. The widely differing urban extent both within and between the catchments therefore make them ideal for studying the impacts of urbanization.

As they are adjacent catchments, atmospheric and weather conditions usually do not vary greatly between the catchments. Precipitation decreases from west to east across the catchments meaning the Rea experiences slightly more annual precipitation, with a mean annual precipitation of 781mm per year. In contrast, the Cole and Blythe catchments receive 743mm and 725mm respectively.

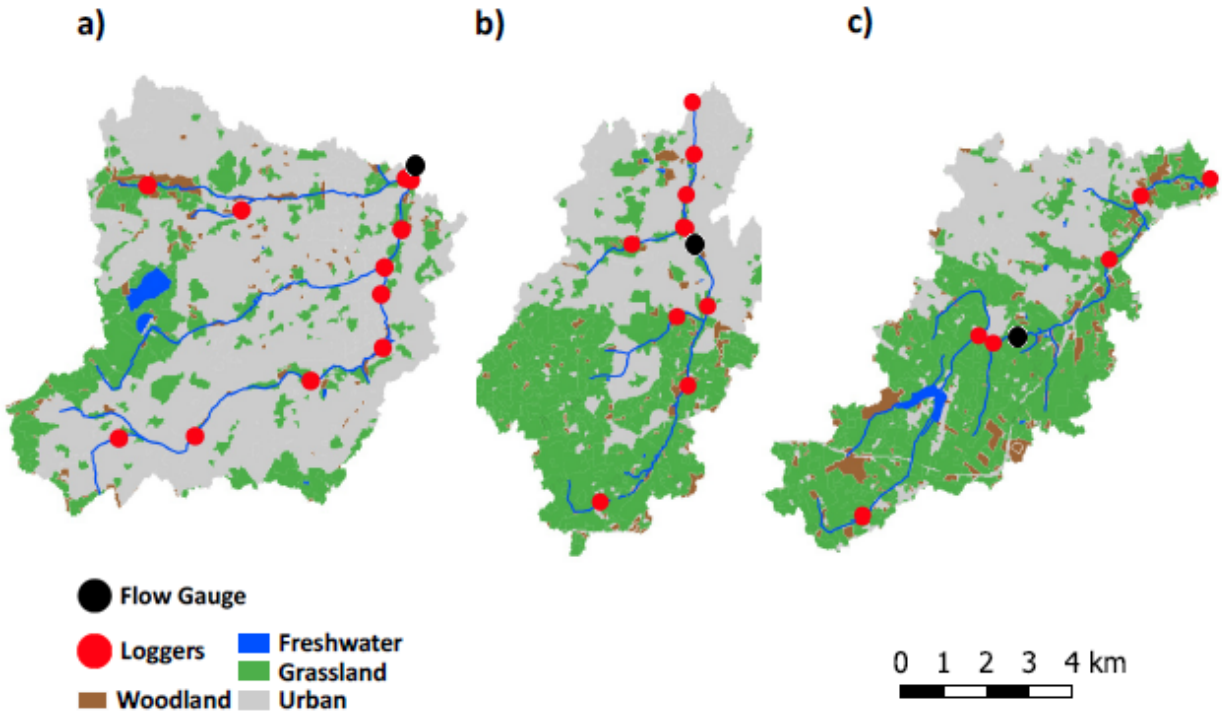

Figure 3.1. Map of study sites – a) River Rea, b) River Cole, c) River Blythe. Land uses classes derived from the Centre of Ecology and Hydrology Land Class 2015 dataset (Rowland et al., 2017). Land use classes were merged to similar classifications in the map for clarity.

3.3.2 Data Collection

3.3.2.1 Water temperature Data

Water temperature data was monitored for a three-year period, from 1st June 2016 to 31st August 2018. Three summers (June, July, and August) of data were collected and analyzed for 27 sites across the three catchments. 11 sites were selected on the River Rea, 10 sites on the

River Cole, and 6 sites on the River Blythe. Sites were selected based on surrounding land use types in order to achieve a strong gradient of land use types for the study. Where possible loggers were also placed with relatively equal spacing between sites to ensure dense coverage of each catchment.

We used TinyTag loggers to monitor Water temperature (Gemini Data Loggers, 2017). These loggers have a measurement accuracy of ±0.2°C and monitored Water temperature at a temporal resolution of 15 minutes. The installation and calibration techniques are outlined in section 2.3.2.

3.3.2.2 Hydrometeorological Data

To identify extreme events, flow and precipitation data were used. One flow gauge providing daily flow data was located within each catchment (Figure 3.1). Flow records were available for the period 2013-2018. For logger sites located away from the flow gauges, we used catchment area weighted averages based on the flow data from the gauges within each catchment. Flow gauge data was hence scaled to each logger's sub-catchment based on sub-catchment area in order to provide estimates of flow for ungauged sub-catchments. This technique has been found to be relatively reliable for providing accurate estimates of flow within small catchments providing there are not vast differences in elevation (Anderson et al., 2010).

3.3.2.3 Land Use Data

A variety of land use characteristics were calculated using GIS. Physical landscape characteristics were chosen as: elevation of logger site, river gradient 1km upstream from logger site, river width at logger site, river depth at logger site, catchment area upstream of

each logger site, and distance of each logger from source. These landscape metrics were chosen as they had previously been identified in regression studies as predictors of water temperature changes (Chang and Psaris, 2013; Imholt et al., 2013; Jackson et al., 2017). A range of land use metrics were calculated: urbanized extent, road density, and woodland extent (measured through tree density). Urbanized extent and road density were included based on identification in prior water temperature and water quality studies as important measures of urbanization (Blaszczak et al., 2019; Somers et al., 2013), while woodland extent has been highlighted as an important proxy for shading in previous studies and a potential control on water temperature (Chang and Psaris, 2013). Land use metrics were analyzed as 50m buffers either side of the stream as the influence of land use has been previously identified as strongest within the riparian extent of the stream (Somers et al., 2013; Malcolm et al., 2008). The land use metrics for the buffer of the entire upstream reach for each logger site were then calculated, as well as the buffer for the 1km upstream of each logger site. The 1km distance was chosen based on use in previous regression studies (Hrachowitz et al., 2010; Imholt et al., 2013; Jackson et al., 2017).

Land use metrics were collated from a variety of sources. Impermeable surface extent, vegetation extent (based on total plant and grassland coverage), and woodland (based on the percentage of catchment defined as forest) data were sourced from the Land Class 2015 dataset (Rowland et al., 2017). Land classes for a wider array of vegetation types were provided by the Land Class dataset, however these were combined into vegetation and woodland classes for the purpose of this study. Road density data was derived from the Europa Urban Atlas 2012 dataset (EEA, 2012). To derive tree canopy data we used LIDAR point cloud data (Environment Agency, 2019), which enabled us to extract tree canopy data.

3.3.3 Analysis

Water temperature data was converted to daily minimum, maximum, and mean temperatures for further analysis. Daily metrics are commonly used within water temperature studies as a means of assessing changing water temperature dynamics (Jackson et al., 2017). In order to reduce the impact of seasonality on results, whereby early within the summer will usually be colder in temperature compared to later in summer, we instead calculated mean, maximum and minimum temperatures as anomalies from two-week moving averages. This provided us with water temperature anomalies for mean, maximum and minimum daily temperature and further allowed better cross comparison between sites by reducing the impact of spatial autocorrelation on the dataset. In this chapter, we refer to these metrics as mean, maximum, and minimum water temperature anomalies.

To identify extreme events, we used fixed 5% and 95% thresholds for flow exceedance for high flows and low flows respectively. The 5% threshold for high flows has been widely used within flood literature for identifying floods, while the 95% threshold is also commonly used within the literature to identify severe low flows (Vicente-Serrano et al., 2017; Whitfield et al., 2009). To identify average flow periods, we used the range of 47.5-52.5% to keep a consistent threshold window between average flow, high flow, and low flow. We considered using precipitation data to further define the extreme events, however as strong correlation existed between the precipitation and flow datasets this was considered redundant. Thresholds were calculated for the three catchments based on flow data from 2013-2018. We used flow data longer than the study period to better put the extreme events identified into a longer-term context. Due to

strong seasonal variations in flow all flow data thresholds were calculated based on summer data.

To identify differences in water temperature anomalies between extreme events and average flow, we paired all the temperature data with flow data for each site by pairing flow gauge data to sites temperature loggers within the same catchment and calculated sub-catchment flows. Data was then subset between low flow, high flow, and average flow. Boxplots were then used to show the difference between water temperature anomalies for each flow type, and one-way ANOVA's used to assess significant differences. We also calculated Z-Scores for the Water temperature anomalies data. Z-scores >+1 or <-1 indicate one standard anomalies from the mean. This threshold was used to identify extreme water temperature events in the distribution of water temperature anomalies data for low flow, high flow, and average flow.

3.3.3.1 Statistical Modelling

We identified the main landscape predictors of water temperature anomalies during extreme events using multiple linear regression (Ordinary Least Squares). The average water temperature anomaly for mean, minimum and maximum water temperature at each site were calculated and featured as the response variables in the models. Initially predictor variables were tested for normality, after which the land use metrics tree buffer, 1km urban buffer, and road density buffer were log transformed. To determine collinearity between the predictor variables we calculated variation influence factors (VIF). If a VIF score was over 3, we removed the highest scoring variable from the dataset till all VIF scores were below 3. Following this process only gradient (GR), elevation (EL), 1km-urban buffer (1km-UB), tree buffer (TB), and

road density buffer (RB) remained as predictor variables taken forward into the final modelling. We used the R package "*MuMin*" to fit all possible combination of models. Due to the sample size of the dataset being less than 40 we used corrected Alkaike Information Criterion (AICc) to rank the models. Models <2 AICc of the highest scoring model were considered the top models of the dataset hence only models < 2 AICc of the highest scoring model are presented herein.

3.4. Results

3.4.1 Effect of Extreme Flows on Water temperature

For anomalies from mean water temperature (Figure 3.2A), a one-way ANOVA was conducted, and a significant difference was observed between groups ($F = 17.3$, $P < 0.05$). A post-hoc Tukey HSD test showed low flow to be significantly warmer than average flow and high flows ($P < 0.05$), however high flow mean temperature anomalies were not shown to be significantly different than average flow mean temperature anomalies ($P < 0.05$).

A one-way ANOVA comparison for anomalies from maximum water temperature (Figure 3.2B) also identified a significant difference between groups ($F = 16.28$, $P < 0.05$). A post-hoc Tukey HSD test was undertaken and showed that anomalies in maximum water temperature were significantly warmer for the low flow data when compared to the average flow and high flow data ($P < 0.05$). However no significant difference was observed between the average flow and high flow groups ($P > 0.05$).

Anomalies from minimum water temperature (Figure 3.2C) also showed a significant difference between the groups ($F = 16.28$, $P < 0.05$) after a one-way ANOVA was conducted. A post-hoc Tukey HSD test observed minimum water temperature anomalies were significantly warmer

during low flow than anomalies under average flow and high flow conditions ($P < 0.05$), however no significant difference was observed between average flow and high flow ($P > 0.05$).

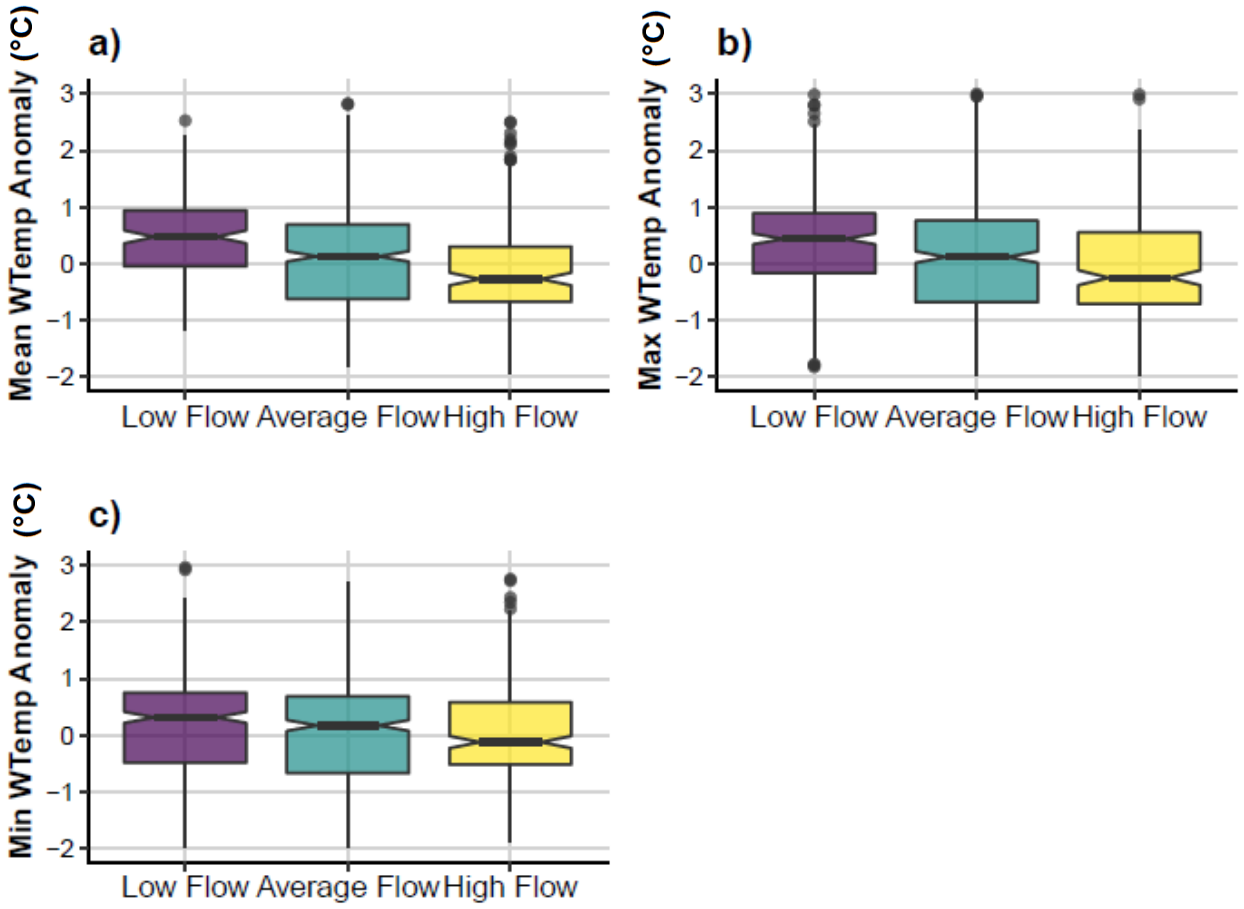

Figure 3.2. Boxplots for moving mean water temperature anomalies (°C) for low flow, average flow, and high flow conditions for a) Mean water temperature, b) Maximum water temperature, and c) Minimum water temperature. Dots show values outside the 95% confidence interval.

A normal distribution for Z-scores was observed for average flow and high flow for the mean water temperature anomalies (Figure 3.3A+C), however in contrast the low flow mean water temperature anomalies skewed to the right (Figure 3.3B). For both average flow and high flow, the distribution of Z-scores greater than one was relatively even between negative and positive anomalies (Table 3.1). However, for the low flow data, there were 43 times more positive Z-

score anomalies greater than one compared to negative anomalies. Furthermore, Z-scores were shown to be considerably more likely within the high flow dataset, with 31.3% of the high flow dataset observed to be above or below the Z-score threshold of one.

For the minimum temperature anomalies, all three flow variables showed a relatively normal distribution (Figure 3.3D-F). Distributions of Z-scores greater or less than one was relatively similar between the three groups, although negative Z-scores were more likely in the average flow data (Table 3.1).

For the maximum temperature anomalies, all three flow variables had a normal distribution (Figure 3.3G-I), although the low flow data (Figure 3.3H) had slight skew to positive temperature anomalies. The average flow and high flow maximum data both had slightly skewed distributions, with more negative Z-scores below -1 than positive Z-scores above 1 (Table 3.1). In contrast, the low flow data had less negative z-scores and a skew to positive anomalies.

Table 3.1. Percentage distribution of extreme temperatures for each water temperature metric within the study.

	% Z-Scores < -1	**% Z-Scores > 1**	**Total**
Average flow Mean	15.8	12.6	28.4
Low flow Mean	0.5	21.5	22.0
High Flow Mean	15.9	15.4	31.3
Average flow Min	17.1	12.7	29.8
Low flow Min	10.1	14.3	24.4
High Flow Min	10.2	14.4	24.6
Average flow Max	16.8	11.1	27.9
Low flow Max	8.2	12.7	20.9
High Flow Max	18.2	12.0	30.2

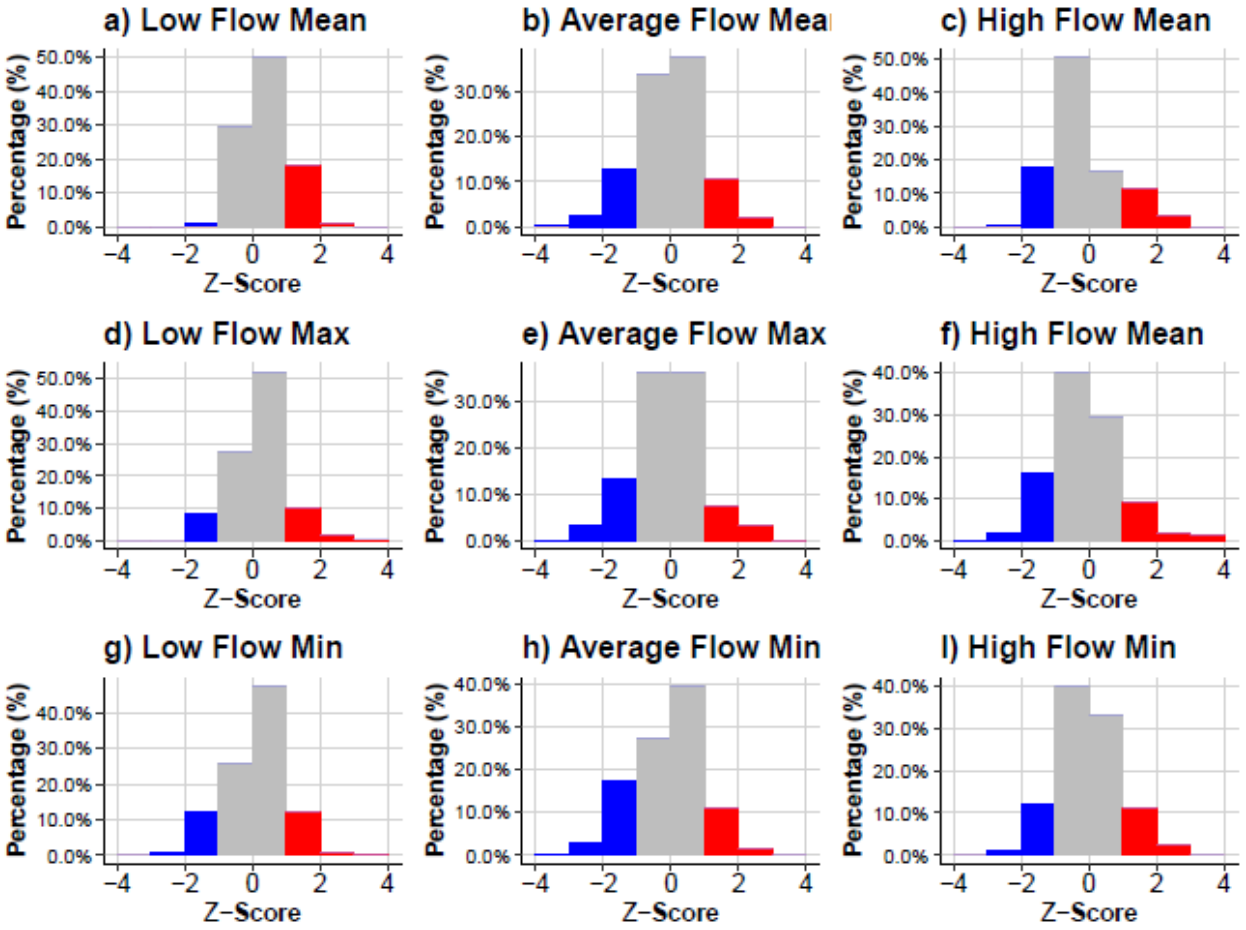

Figure 3.3. Histograms showing Z-scores for moving mean water temperature anomalies for low flow, average flow, and high flow conditions. A – C show mean water temperature, D – F show maximum water temperature, and G – I show minimum water temperature. Red denotes a Z-score greater than one, blue denotes a Z-score less than one.

3.4.2 Impact of land use on Water temperature response

3.4.2.1 Low flow

Landscape predictors showed weak predictive ability for low flow mean water temperature anomalies with the top model's explanatory value ranging between 11-20% (Table 3.2).

However, RB was found to be a significant variable in the top model (Figure 3.4A; $P < 0.05$). The 1KM-UB featured in the second highest model however showed weaker explanatory ability and was not significant ($P > 0.05$). A model featuring RB and 1KM-UB had the highest predictive value, but neither variable was a significant variable ($P > 0.05$, $R^2 = 0.05$). Both RB and 1KM-UB were negatively associated with mean water temperature anomalies. RB and 1KM-UB were found to be of nearly equal importance to the low flow mean water temperature anomalies model, with minimal importance shown for the other predictor variables. (Table 3.3).

In contrast, moderate predictive ability was shown by landscape characteristics for the maximum water temperature anomalies models with explanatory values from 25% to33% (Table 3.2). In both top models, land use variables were featured as predictor variables, whereas neither physical landscape characteristic featured in the best models. In the top model, RB (Figure 3.4B) and TB (Figure 3.4D) were found to be significant predictors ($P < 0.01$), with relatively similar effect sizes (RB = -0.49, TB = -0.43). 1km-UB (Figure 3.4C) also featured among the predictors but was not found to be significant ($P < 0.05$). In all cases, the land use characteristic had a negative relationship with maximum water temperature anomalies. In the second-best model also, both RB and TB featured as significant predictors (RB = $P < 0.01$, TB = $P < 0.05$), therefore RB was observed to be the strongest predictor of maximum water temperature anomalies. When assessing the relative importance of predictor variables (Table 3.3), RB was found to be the strongest predictor (0.78), however TB (0.63) and 1KM-UB (0.50) were relatively strong predictors also.

Moderate explanatory ability was observed in all models for minimum water temperature anomalies, with explanatory ability ranging from 36% to 40% (Table 3.2). Within all three top

models 1KM-UB (Figure 3.4E) was found to be the only significant predictor ($P < 0.01$), with a negative correlation observed. The minimum water temperature anomalies models were the only low flow model to feature a physical landscape characteristic, with EL featuring in the second top model, although it was not found to be significant ($P > 0.05$). In the relative variable importance, 1KM-UB was found to be by far the most important predictor (0.98), with elevation found to be the second most important predictor (Table 3.3).

Table 3.2 - Results of model selection for the anomalies (°C) from low flow mean, maximum and minimum water temperature metrics. Standardized model effect sizes are shown for each variable in each model. Variables deemed significant in each model are bolded. * = <0.05, **<0.01, ***<0.001.

Response	Model Rank	Variables				R^2	AICc	Δ AICc	Weight
		RB	TB	1KM-UB	EL				
Mean Water temperature Anomalies	1	**-0.38***				0.16	11.64	0.00	0.36
	2			-0.37		0.11	11.67	0.03	0.35
	3	-0.29		-0.28		0.20	12.19	0.45	0.29
Max Water temperature Anomalies	1	**-0.49****	**-0.43***	-0.34		0.33	23.57	0.00	0.62
	2	**-0.57****	**-0.37***			0.25	24.56	0.99	0.38
Min Water temperature Anomalies	1			**-0.62*****		0.36	-10.97	0	0.39
	2			**-0.54****	-0.26	0.40	-10.88	0.08	0.38
	3		-0.21	**-0.68*****		0.38	-9.93	1.04	0.23

Table 3.3. Relative variable importance of predictor variables for the anomalies (°C) from low flow maximum, mean and minimum water temperature models.

Response	Road Buffer	Tree Buffer	1km Urban Buffer	Elevation	Gradient
Mean Water temperature Anomalies	0.48	0.20	0.50	0.30	0.20
Max Water temperature Anomalies	0.78	0.63	0.53	0.28	0.20
Min Water temperature Anomalies	0.24	0.34	0.98	0.44	0.20

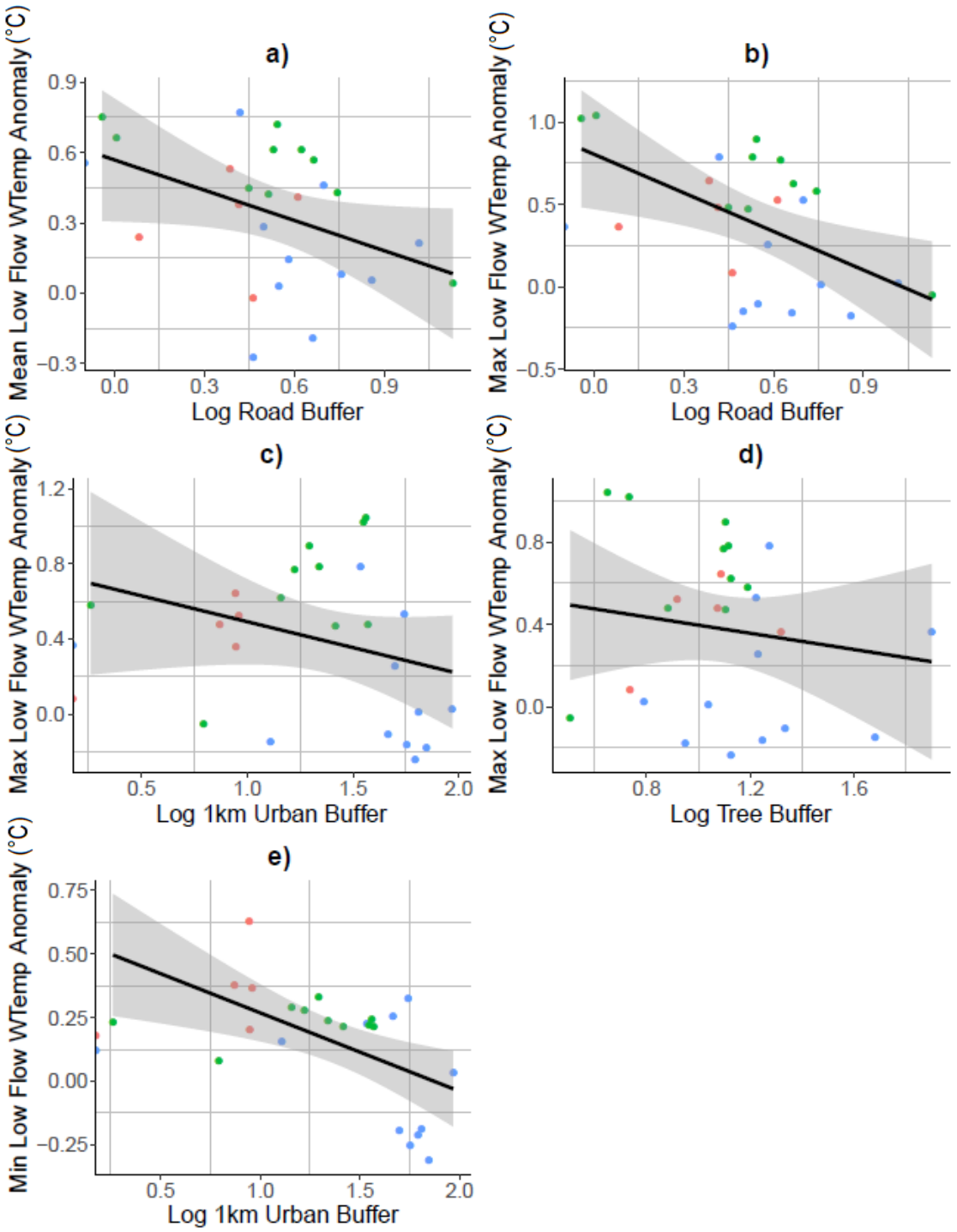

Figure 3.4. Linear regressions of variables featuring in the top model for mean, maximum, and minimum water temperature anomaly (°C) during low flow. Green dots indicate River Cole sites, Blue dots River Rea sites, and Red dots show River Blythe sites. The grey shading represents the 95% confidence interval.

3.4.2.2 High Flows

Landscape predictors showed weak to moderate explanatory ability for the mean water temperature anomalies during high flows, with variation ranging from 14% to 24% (Table 3.4). EL featured as a significant predictor in the three top models (Figure 3.5A; $P < 0.05$) and had the largest effect size. A positive association was found between EL and mean water temperature anomalies. In the model with the highest explanatory capability ($R^2 = 0.24$), 1KM-UB (Figure 3.5B) and TB were also found to be predictors, however only 1KM-UB was found to be significant ($P < 0.05$). Both 1KM-UB and TB were negatively associated with mean water temperature anomalies. EL was found to be the most important predictor variable overall (0.79), although 1KM-UB was by far the most important second predictor variable (Table 3.5).

In the maximum water temperature anomalies model's moderate explanatory ability was shown by the landscape metrics, with explanatory ability ranging between 27% and 30% (Table 3.4). Again, EL (Figure 3.5C) had the strongest effect size in all three models and was significant in all three models ($P < 0.01$), with a positive relation with maximum water temperature anomalies. The only land use characteristic to feature within a model was 1KM-UB (Figure 3.5D), which was not found to be significant ($P > 0.05$), however in contrast to the mean water temperature anomalies model, had a positive relationship with maximum water temperature anomalies. EL was once again found to be the most important predictor with 1KM-UB the second most important predictor (Table 3.5).

Weak explanatory ability was shown by the landscape metrics in the minimum water temperature anomalies models, with explanatory ability at 13% and 18% (Table 3.4). In both

top models, EL was again the predictor with the strongest effect size (Figure 3.5E), although it was not found to be significant in either top model ($P > 0.05$). RB was the only other landscape variable to feature within a top model, although was also not found to be significant ($P > 0.05$). RB was negatively associated with minimum water temperature anomalies during high flows, whereas EL was positively associated. EL was also again found to be the most important variable (0.50) (Table 3.5).

Table 3.4. Results of model selection for the anomalies (°C) from high flow mean, maximum, and minimum water temperature metrics. Standardized model effect sizes are shown for each variable in each model. Variables deemed significant in each model are bolded. * = <0.05, **<0.01, ***<0.001.

Response	Model Rank	Variables					R^2	AICc	Δ AICc	Weight
		RB	TB	1KM-UB	EL	GR				
Mean water temperature anomalies	1			-0.34	**0.51***		0.21	5.92	0.00	0.43
	2				**0.41***		0.14	6.75	0.82	0.29
	3		-0.25	**-0.42***	**0.55***		0.24	6.83	0.90	0.28
Max water temperature anomalies	1			0.32	**0.44***		0.34	16.81	0.00	0.47
	2				**0.54****		0.27	17.73	0.91	0.24
	3				**0.57****	0.25	0.30	18.17	1.36	0.30
Min water temperature anomalies	1	-0.36			0.44		0.18	6.63	0.00	0.53
	2				0.26		0.13	6.84	0.21	0.47

Table 3.5. Relative variable importance of predictor variables for the anomalies (°C) from high flow maximum, mean and minimum water temperature models.

Response	Road Buffer	Tree Buffer	1km Urban Buffer	Elevation	Gradient
Mean water temperature anomalies	0.24	0.30	0.59	0.79	0.20
Max water temperature anomalies	0.35	0.20	0.52	0.83	0.32
Min water temperature anomalies	0.36	0.22	0.23	0.50	0.22

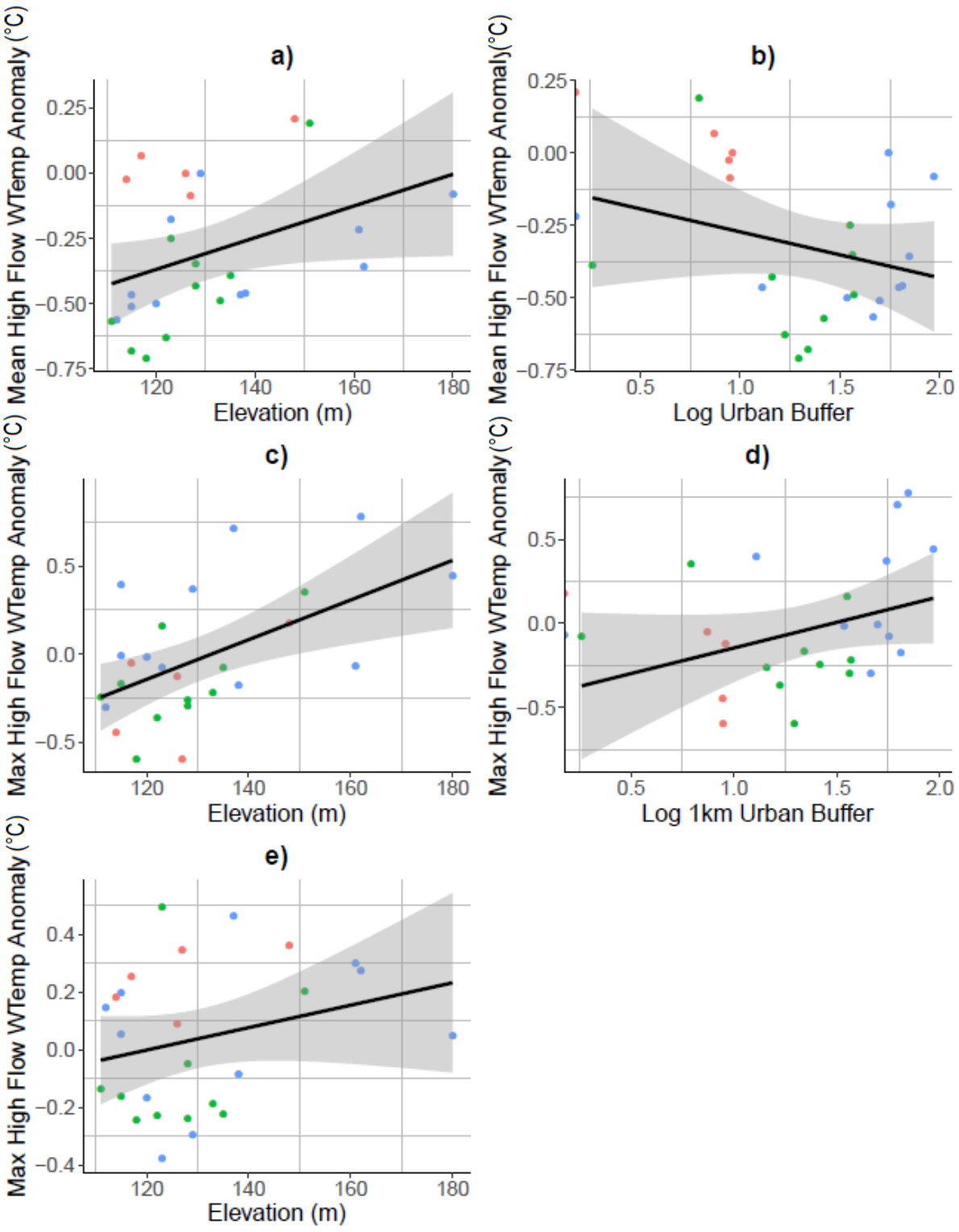

Figure 3.5. Linear regressions of variables featuring in the top model for mean, maximum, and minimum water temperature anomaly (°C) during high flow. Green dots indicate River Cole sites, Blue dots River Rea sites, and Red dots show River Blythe sites. The grey shading represents the 95% confidence interval.

3.5 Discussion

3.5.1 Impact of Extreme Events on Water temperature

Extreme events have been shown to lead to differences in water temperature anomalies compared to average flow, although differences were most apparent under low flow conditions. Although high flow conditions did have on average cooler water temperature anomalies compared to average flow, this was not substantial and may be because at high flow the specific heat capacity of the rivers increases, which increases the amount of heat transfer required to increase water temperature (Hannah and Garner, 2015). Resultantly, variation in water temperature is likely to be minimized during high flow events as a result of the increased thermal capacity. The moderately colder water temperature anomalies observed compared to average flow may reflect that the study took place during the summer months as heat budgets vary by season, with heat gain usually occurring during summer (Wagner et al., 2017; Kelleher et al., 2012). Hence, during high flows in summer, the increased thermal capacity likely leads to slightly cooler on average thermal dynamics than average flow because the main fluxes acting on water temperature are less effective at changing water temperature during higher discharge (Yang et al., 2014).

Differences in water temperature anomalies between average flow and high flow were overall not high, suggesting that high flows do not constitute a strong control on water temperature. Although water temperature surges have been observes in rivers after summer storms (Nelson and Palmer, 2007; Pluhowski and Pecora, 1970), these likely constitute a relatively small subset of overall events that are often not visible on daily timescales. Furthermore, Croghan et al.

(2018) found that although precipitation events in summer can lead to increases in daily water temperature, for the largest precipitation events this effect was highly variable. Overall, the impact of high flows on water temperature appeared to be minimal, with the likelihood of the occurrence of extreme temperature anomalies similar between average flow and high flows.

In contrast to high flow, low flow conditions lead to substantial differences in water temperature anomalies compared to average flow. During low flows, the thermal capacity of streams is reduced and therefore the heat flux required to instigate water temperature change is decreased (Toffolon and Piccolroaz, 2015). Resultantly, low flows are likely to experience increases in water temperature during the summer months due to increased atmospheric influences. Hydrological drought is driven by anomalies in precipitation, and/or high temperatures leading to increased evaporation rates (Van Loon, 2015). Low flows therefore often occur during periods of high air temperatures, which means atmospheric conditions are already favorable to create water temperature increases, while the influence of high atmospheric temperatures increases as flow reduces (Van Vliet & Zwolsman, 2008; Zwolsman & van Bokhoven, 2007). Hence, atmospheric drought conditions during the summer months lead to a cascading effect causing extreme values in both flow and water temperature.

Low flow conditions were almost twice as likely to exhibit positive extreme mean water temperature anomalies which further suggests that low flow can substantially increase the likelihood of rivers experiencing extreme warming. This has substantial implications for river ecology as the increased extreme water temperatures are a stressor to ecological life (Hester and Doyle, 2011), this stress is often exacerbated during low flow conditions where refuges from high temperatures are often reduced due to reduced flows (Bond et al., 2008). The

increased extreme water temperatures hence combine with low flow to provide a dual stressor on ecological life. Overall, the impact of low flows on water temperature can be substantial compared to both average flow and high flow which is likely to lead to degradation of riverine ecosystems.

3.5.2 Impact of land use on water temperature response

The main landscape characteristics predicting anomalies in low flow water temperature anomalies were land use characteristics. Counterintuitively, variables relating to urbanization (road density and 1km urban buffer) were negatively related to maximum, mean, and minimum water temperature anomalies. This suggests urbanization may reduce extreme low flow temperature anomalies. This may be because urban streams are usually found to be warmer than rural streams in the first place due to modifications such as increased discharge of effluents from sewage plants and industry as well as reduced riparian zone extent (Kaushal et al., 2010), therefore as this study looked at water temperature anomalies, it may be the case that as urban streams are comparatively warmer in the first place, the chances of positive temperature anomalies are less likely than in rural streams. Furthermore, infrastructure in urban streams, for example culverts, bridges, and tunnels have been found to reduce water temperatures by providing shading and thereby reducing the influence of atmospheric conditions on river temperatures (Anderson et al., 2010). Road density was found to be a particularly strong predictor of low flow water temperature anomalies. Road density has been found to be a main predictor of other water quality variables (Blaszczak et al., 2019), however has previously been thought to be a proxy of flow routing into streams. In this study it is possible that road density is a proxy of the drainage system, where areas of higher road and

drainage density provide a source of cooled water into urbanized rivers which may act to moderate water temperature. Further, pipe leakages are very common within urban areas in the UK and can provide an important source of groundwater recharge far exceeding natural conditions. This may provide a regular inflow of groundwater which moderates water temperature into more urbanized sites (Wakode et al., 2018), although evidence for the effects of urbanization on groundwater as a whole are mixed (O'Driscoll et al., 2010a). Furthermore, although urbanization is often associated with reduced riparian zones, which would reduce shading and potentially leave the site more responding to water temperature changes during low flow, a difference in riparian zone extent between our urban and non-urban sites was not noted. Tree buffer was also found to be negatively related to low flow temperature anomalies, which is likely due to increased riparian shading in forested areas which reduces temperature extremes (Garner et al., 2017; Dugdale et al., 2019).

For predicting anomalies in high flow temperatures however, physical characteristics were continually the most important predictors with land use secondary or not relevant. Specifically, elevation was linked to increased mean, maximum and minimum temperatures anomalies which suggests that higher elevations are correlated with smaller river width and depth. Where rivers have less discharge, variations in flow and water temperature occur more quickly (Pilgrim et al., 1982), while increases in water temperature surges after storms are also found more in smaller catchments (Somers et al., 2013). Therefore, elevation likely represents increased temperature anomalies in headwater sites during high flow events. Elevation has further been noted as important predictor in water temperature in prior studies (Imholt et al., 2013; Jackson et al., 2017; Chang and Psaris, 2013). In these studies, elevation is noted to have a negative

relationship with water temperature at average flow, however sites with higher elevations usually have cooler water temperatures initially, this increases their susceptibility to warming through storm runoff. In contrast, the main land use characteristics predicting water temperature anomalies during high flows were the 1km urban buffer and road buffer. Surprisingly, urbanization characteristics were negatively associated with mean and minimum anomalies but positively associated with maximum anomalies. This likely represents the water temperature surge effect for maximum water temperature anomalies where initially during some storms there is a surge in water temperature, with this effect strongly linked to urbanization (Somers et al., 2013; Nelson and Palmer, 2007). However, for minimum and mean temperature anomalies, the negative relationship may result from the fact that storm discharge is higher in urban areas (Fletcher et al., 2013), which may lead to reduced temperatures during high flow within the summer months due to increases in thermal capacity during high flow. Overall however, landscape characteristics predicted water temperature anomalies for high flow weaker than for low flow, indicating links between landscape and high flow water temperature are less marked.

3.5.3 Conclusions and Future Research

This study highlights that extreme events can lead to an increase in extreme water temperature anomalies. By providing better understanding of the landscape properties determining water temperature response to extreme events, the results inform urban planning to increase resilience of urban streams to extreme events.

Low flow is the main risk factor for extreme water temperature responses, with the relationship between water temperature and high flows being less marked. As climate change is expected to increase air temperature and the regularity of low flow events (Van Vliet et al., 2013), the impact of low flows on water temperature is likely to become increasingly common and more severe within future years. Further, we also found an impact of land use on water temperature response to extreme events. Urbanization was noted to be negatively related to mean low flow temperatures, which may be because urban streams are usually warmer than natural in the first place hence less susceptible to anomalies in warming. Furthermore, although urbanization is usually noted to degrade water quality, some aspects of urban stream infrastructure such as stream burial and artificial flow paths may reduce the impact of low flows on water temperature. For high flows, elevation, likely acting as a proxy of stream size, and distance to source were noted as strong predictor of high flow water temperature response and may highlight the responsiveness of water temperature in headwater catchments to high flow events.

To increase the applicability of these results, studies featuring a wider range of geographical sites covering a greater range of land uses and river types is required. Further, developing longer water temperature time series is crucial to capture a wider range of flood and low flow events in order to increase confidence in the relationships we have observed.

CHAPTER 4: URBAN STREAM BURIAL INHIBITS DISSOLVED ORGANIC MATTER PROCESSING BY REDUCING PHOTODEGRADATION

4.1 Abstract

Urban landscapes can dramatically change fluvial shading (i.e. by stream burial) and water temperature regimes with significant implications for biodegradation and photodegradation of DOM rates in these ecologically vulnerable systems. However, short-term biodegradation and photodegradation dynamics in urban systems are not well understood, and sub-daily photodegradation has been rarely studied. In this chapter, we conducted 3 flume experiments with the following treatments: unheated and unshaded, heated and unshaded, unheated and shaded, and heated and shaded. The aim was to replicate various shading and temperature conditions to investigate the interaction between stream burial and future increases in climate extremes on photodegradation and biodegradation for urban streams by characterizing DOM using standard optical techniques. Mixed linear effects models were used to establish significant differences between treatments. The results show that photodegradation in unshaded treatments leads to high degradation of the fluorescent DOM pool, with significant ($P < 0.05$) differences in unshaded treatments versus shaded treatments for humic-like components and metrics. A significant difference ($P < 0.05$) between shaded and unshaded treatments for absorbance metrics (slope 275-295nm) indicates a shift to lower molecular weight material organic matter resulting from photodegradation in unshaded flumes. Temperature appeared to have a minimal impact on photodegradation rates when compared to shading, whilst minimal interaction effects were also observed, although some impact was observed for humic-like fluorescent metrics. The study suggests stream burial inhibits

processing of DOM and substantially alters DOM within the headwaters by preventing photodegradation of humic material while biodegradation was not affected by the treatments in this study. Hence, the study provides experimental evidence supporting daylighting as a means of increasing DOM processing in urban streams.

4.2 Introduction

Dissolved organic matter (DOM) is critical to the functioning of stream ecosystems, however urbanization can lead to substantial changes in DOM quality and quantity (Hosen *et al.*, 2014; Parr *et al.*, 2015, O'Driscoll, Clinton, Jefferson, Manda, McMillan, *et al.*, 2010; Beaulieu *et al.*, 2014). Urban landscapes significantly modify the processes controlling DOM production and processing to the extent that urban rivers have been associated with unique DOM compositions (Khamis et al., 2018). However, despite current global trends in urbanization and importance of DOM to stream ecosystem dynamics (Kaushal and Belt, 2012), important removal and transformation processes such as photodegradation and biodegradation remain poorly understood within urban streams.

DOM incorporates a diverse mixture of aliphatic and aromatic compounds including humic and fulvic substances, proteins and phenols, carbohydrates and lipids, and polyaromatic hydrocarbons (Leenheer and Croué, 2003). DOM within urban streams has a distinct composition, with a greater prominence of microbial and proteinaceous materials compared to rural streams (Williams et al., 2016). Portions of DOM are important as an energy source in streams. Whilst DOM can attenuate light penetration into streams, DOM also acts as a reactant

and sorbent, enhancing interactions with anthropogenic pollutants and influencing mobilization rates and bioavailability (Minor et al., 2014).

Processing of DOM is to a large extent controlled by rates of photodegradation and biodegradation (Hansen et al., 2016; Del Vecchio and Blough, 2002). Photodegradation occurs in the photic zone and impacts riverine DOM by transforming DOM molecules to smaller photoproducts with increased lability (Moran and Zepp, 1997), while labile bioreactive compounds can also be transformed to biorefractory compounds (Obernosterer and Benner, 2004). Biodegradation occurs through microbial activity in both the photic and aphotic zones. Biodegradation tends to break down labile low-molecular weight organic matter (OM), while high-molecular weight aromatic materials can also be produced as by-products (Hansen et al., 2016).

In urban catchments stream burial reduces the exposure of urban rivers to solar radiation which is the primary driver of photodegradation (Beaulieu et al., 2014; Gurnell et al., 2007). Urban stream burial has been found to change DOM composition with higher humification identified within open reaches due to increased inputs of terrestrial material compared to buried streams, while greater uptake of recalcitrant humic material was also found within buried streams (Arango et al., 2017). Stream burial has also been found to reduce Nitrogen retention primarily as a result of reductions in transient storage, alongside reductions in primary production and hyporheic exchange, while rates of uptake of Nitrogen are lower in buried streams in general mainly as denitrification rates are lower due to reduced hyporheic sediments (Beaulieu et al., 2014; Pennino et al., 2014). Reduced rates of photosynthesis in buried reaches also reduce labile Carbon production, although Carbon in urban streams is

usually dominated by allochthonous Carbon inputs (Arango et al., 2017). Changes in shading can also drive water temperature change within urban environments: riparian deforestation is a common cause of higher water temperatures, while stream burial can reduce both the magnitude and diurnal range of stream temperatures (Johnson and Wilby, 2015; Anderson et al., 2010). These changes in water temperature can impact photodegradation rates as the dominant pathway of DOM transformation changes with temperature (Porcal et al., 2015). Water temperature changes can also change the rate of DOM biodegradation, as solubility of Dissolved Organic Carbon (DOC) and microbial metabolism increase at higher water temperature (Mao and Li, 2018).

Although stream burial has been identified as an important driver of DOM composition change (Beaulieu et al., 2014; Arango et al., 2017), the impacts of urbanization on instream biodegradation and photodegradation have not been quantified under experimental conditions. Field experiments on biodegradation and photodegradation are often hindered by confounding factors that are difficult to control for in field settings such as terrestrial inputs into the buried stream network (Haag and Matschonat, 2001). Mesocosm experiments are a useful alternative to field studies by allowing much greater control over the influencing factors acting on photodegradation and biodegradation rate (Nélieu et al., 2009). In order to validate findings from field studies and improve understanding of the links between buried streams and degradation processes, mesocosm experiments are crucial to improving our understanding of the impacts of stream burial within urban rivers (Challis et al., 2014).

This chapter addresses this gap by aiming to quantify the impact of landscape-induced changes in shading and temperature on DOM biodegradation and photodegradation rates

experimentally. We hypothesized:

1) Unshaded treatments would increase the loss of the humic-like DOM compared to shaded treatments, leading to changes in both quality and composition of DOM.

2) Heated treatments would accelerate declines in the humic-like content of DOM compared to non-heated treatments.

3) Streams that were both unshaded and heated would lose the highest amount of humic-like DOM due to an interaction effect between temperature and shading.

4.3 Materials and methods

4.3.1 Study site and Experimental Set Up

The research was undertaken in August 2018 at the University of Birmingham Ecolab facility in Birmingham, UK (52.4862° N, 1.8904° W). Three experiments were done across three days. In each experiment, 12 re-circulating flumes were installed outside in an unshaded area. The flumes were oval shaped and constructed of white fiberglass (dimensions 2m x 0.5m). Of the 12, six flumes were subsequently shaded by placing a separate flume on top to prevent solar radiation, while the remaining six flumes were kept unshaded. Three shaded and three unshaded flumes were heated to give a total of four treatments in the experiment. Hence the experiment followed a 2x2 factorial design to enable interactions between variables to be explored. In heated treatments water temperature was set to ~23°C. Climate change is expected to increase 95th percentile river temperatures by up to 2.2 °C by 2100 (Van Vliet et al., 2013), hence the 23 °C represents a likely extreme temperature scenario in the future for the

urban river this study sampled water from, where current maximum temperatures of around 21°C have been observed.

To provide water representative of an urban river, 1000 liters of water was taken from the Bourn Brook, a headwater stream 900m away from the Ecolab facility. The catchment is heavily urbanized (80%), and there have been extensive studies of the stream DOM (Carstea et al., 2010; Baker et al., 2004; Khamis et al., 2018). At baseflow, DOC concentration ranges between 3.1-7.0 mg/L, while DOM has a high proportion of proteinaceous material reflecting inputs of OM associated with inputs from storm sewers (Carstea et al., 2009). Stream water was collected prior to each experiment and stored on-site in a water silo to allow mixing of stream water. The silo had an opaque lid to prevent sample photodegradation prior to the experiment start. Each flume was filled with 80 liters of water, giving each flume a water level of ~15cm, which was representative of the water level in the Bourn Brook.

Each flume was instrumented with a water temperature sensor with ± 0.2 °C sensitivity (Campbell Scientific, Utah, USA), logging at 15-min intervals, and aquarium pumps (Newa 1.6 adj, Loreggia, Italy) to circulate water and prevent oxygen depletion. In the heated flumes, an aquarium heater (NEWA THERM VTX 200W) was used to maintain the higher water temperature.

Each experiment was undertaken for nine hours: from 9am – 6pm, which encompassed most of the daily solar radiation exposure. Most prior studies of photodegradation and biodegradation were completed over a daily or weekly timeframe (Shank et al., 2009; Lu et al., 2013; Moody and Worrall, 2017; Sankar et al., 2019). The shorter duration of our experiments reflected our

intention to replicate likely water transit times through buried streams, or deforested riparian margins given that urban streams comprise a relatively short proportion of the total stream length for many catchments (Napieralski and Carvalhaes, 2016). Furthermore, the majority of DOC degradation occurs rapidly, in the first day of DOM input to a river (Moody et al., 2013), although the temporal resolution of many biodegradation and photodegradation studies has been insufficient to investigate this. Hence our experiment offers an opportunity to replicate and control the effects of shading and temperature on photodegradation and biodegradation rates across the same source water.

Atmospheric conditions affecting photodegradation and biodegradation rates were comparable for photosynthetically active radiation (PAR) and shortwave radiation (SW-Rad) during the three experiments (Table 4.1). PAR and SW-Rad were measured using a weather station set up at the same site of the experiment. Mean water temperatures for each treatment for all 3 experiments are shown in Table 4.1. Shaded unheated flumes were 6.6 °C cooler than shaded heated flumes, while the unshaded unheated flumes were 4.5 °C cooler than unshaded heated flumes. This difference was unavoidable due to the requirement to shield the shaded flumes from UV-exposure which reduced atmospheric influence on temperature dynamics. Despite this, water temperatures within the unheated treatments were substantially closer to one another, than to either heated treatment.

Table 4.1 - Water temperature and atmospheric conditions (photo-synthetically active radiation: PAR; and short-wave radiation) for each experiment during the study (Mean ± SD).

	Daily Mean Water Temperature (°C)					
Experiment	Shaded Heated	Shaded Unheated	Unshaded Heated	Unshaded Unheated	Mean PAR (µmol/s)	SW-Rad Daily Flux (W/m^2)
1	25.0 ± 0.40	18.0 ± 0.6	23.9 ± 0.6	19.5 ± 0.61	549 ± 410	148
2	24.5 ± 0.30	17.7 ± 0.5	23.4 ± 0.70	19.1 ± 0.6	570 ± 372	139
3	21.0 ± 0.3	15.0 ± 0.4	22.2 ± 0.60	16.4 ± 0.5	637 ± 281	152
Experiment Mean	23.5	16.9	22.8	18.4	585	146

4.3.2 Sample collection and analysis

Samples were collected from each flume at 0, 1, 2, 4, 6, and 9 hours during each experiment. Samples were taken at higher frequency during the beginning of the experiment as prior studies, albeit in different environments, have indicated high rates of DOC loss and change within the first hour of photoexposure (Moody and Worrall, 2017). A total of 72 samples were collected during each experiment, giving a total of 216 samples in the study. Samples were immediately filtered using 0.45 µm sterile nylon membrane syringe filters following collection. Filtered samples were refrigerated in the dark in 100 ml sample tubes that were kept in an opaque container and had been acid washed for 24 hours and rinsed with deionized water.

Samples were analyzed within 24 hours of collection. Prior to analysis, samples were raised to 20 °C using a water bath. DOC concentration (mg C L−1) was determined for each sample using a Shimadzu TOC-V series autosampler. Organic Carbon calibration standards were prepared for a range of 2-25 mg C L−1 TOC in accordance following manufacturer's guidelines. Prior to the

analysis, a wash cycle and standard measurement were undertaken. Blank measurements were also taken to give estimates of background noise. After every 10th sample, a replicate and quality check sample were measured, and a wash cycle completed.

DOM quality was quantified by fluorescence using a Varian Cary Eclipse spectrofluorometer with a 1cm path length to produce excitation-emission matrices. Samples were kept at a constant 20 °C using a temperature controller. Prior to analysis, the water Raman peak was determined, and a blank sample containing deionized water was measured. Post-measurement corrections were applied to correct for inner-filter effects, Raman and Raleigh scatter was removed from measurements. The blank measurement was subtracted from each EEM and each EEM was normalized to the Raman measurement (Murphy et al., 2010). All corrections were performed using the "*eemR*" package (Massiccotte, 2017) in R (version 3.5.3).

Absorbance spectra were measured for each sample using a Jenway 6850 spectrophotometer UV-VIS spectrometer, with measurements recorded between 200-700 nm at a 1 nm interval, with a 1 cm path length quartz cuvette. A blank measurement using deionized water was recorded prior to the start of the experiment and subtracted from each sample during post-processing.

4.3.3 Calculation of optical metrics

A range of optical metrics were calculated to characterize DOM decomposition (for details of how to calculate these metrics readers are referred to Table 1 in Hansen *et al.*, 2016).

For absorbance metrics we calculated specific ultraviolet absorbance at 254nm (SUVA254) to indicate sample aromaticity (Weishaar et al., 2003). Spectral slopes at 275-295nm (S275-295),

and 350-400nm (S350-400) were also calculated, with higher slope values generally indicating low-molecular weight DOM (Helms et al., 2008). The slope ratio was also determined as this has been found to increase after irradiation (Hansen et al., 2016).

For fluorescence metrics, we calculated the fluorescence index (FI) where values of ~1.5 indicate microbial activity while values around 1.2 indicate terrestrial DOM, the humification index (HIX) where higher values indicate more humic DOM, and the biological index (BI) where higher values indicate more autochthonous production (Para et al., 2010; Ohno, 2002; McKnight et al., 2001). We also calculated peak ratios for peaks C:T (indicating the relative importance of humic-material compared to proteinaceous DOM), C:A (humic content compared to fulvic content), and A:T (recalcitrant humic material compared to labile material) (Baker et al., 2008; Coble, 1996; Hansen et al., 2016).

The main fluorescence components were identified by Parallel Factor Analysis (PARAFAC) in MATLAB 9.2 (MathWorks, USA) using the "*DOMFluor*" toolbox following Stedmon and Bro (2008). We produced a 4-component model (Table 4.2; Figure 4.1) which was split-half validated. Fluorescence maxima (Fmax) values from each component in the validated model were then exported and are presented herein.

Table 4.2. Description of component characteristics identified in PARAFAC model. Similarity scores based on correlations with observed components in the Open Fluor database are shown in brackets in column 5.

Component	Excitation Max λ (nm)	Emission Max λ (nm)	Description	Identification in previous Studies
C1	<250	396	Humic-like, in-stream production	C2 Søndergaard et al. (2003) (0.99) C4 Osburn et al. (2012) (0.99) C1 Yamashita et al. (2013) (0.98)
C2	260 + 355	466	Humic-like, terrestrially derived, reprocessed	C2 Gonçalves-Araujo et al. (2015) (0.99) C2 Borisover et al. (2009) (0.99) C2 Shutova et al. (2014) (0.99)
C3	345	416	Humic-like, terrestrially derived	C4 Stedmon et al. (2003) (0.97) C2 Liu et al. (2019) (0.97)
C4	280	338	Tryptophan-like, associated with microbial activity	C3 Borisover et al. (2009) (0.99) C5 Peleato et al. (2016) (0.99) C3 Stedmon et al. (2011) (0.93)

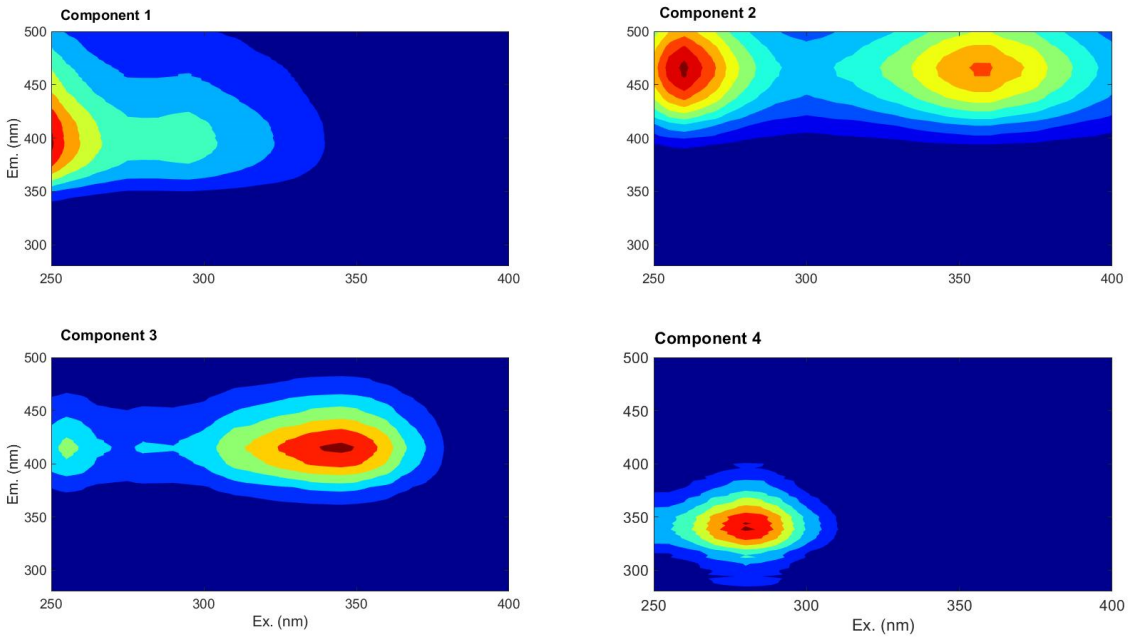

Figure 4.1. Excitation-Emission matrices of PARAFAC components identified in this study.

4.3.4 Statistical Analysis

Results were standardized to percentage change, with values from 0 hours representing 1. All three experiments for same treatments exhibited similar trends in all metrics over time, hence for brevity, graphs represent a pooled dataset.

Differences in degradation rates between treatments were investigated using mixed linear effects models as they allow differences between the treatments to be assessed and have been widely used in experimental studies (Harrison et al., 2018). The response variables in the models are based on the value for each measured variable at the end of each experiment (9-hour value) in order to assess the treatment effects at the endpoint of the experiments. All models were produced using the "nlme" package (Pinheiro et al., 2019) in R (version 3.5.3). In all models, shaded/unshaded and heated/unheated treatments were treated as fixed effects

while models also featured a fixed interaction effect between shaded/unshaded and heated/unheated. Experiment date was treated as a random effect within the models.

4.4 Results and Discussion

4.4.1 Temporal Change in DOC Concentration

In our data, there was no short-term degradation in DOC, DOC did not vary significantly between treatments, and no interaction effect was observed ($P > 0.05$) (Table 4.3). DOC had positive and negative fluctuations within 5% of baseline values over time, suggesting little change in DOC during the experiments (Figure 4.2). Processing rates ranged from -0.28 mg C/l/day to 0.23 mg C/l/day in the experiments suggesting higher processing rates compared to those observed in other urbanized water sources, with 0.0048 ± 0.00339 mg C/l/day identified by Sankar *et al.*

(2019) over a 30-day study, which indicates processing rates are somewhat higher on the first day. In contrast, Moody and Worrall (2017) found rates of -30.1 mg C/l/day to an increase of 3.5 mg C/l/day for a peatland catchment thus highlighting dramatic differences in DOC degradation depending on catchment type. While losses of DOC can occur through biodegradation and photodegradation, the gains in DOC can result from increased production of DOM after photodegradation and biodegradation which can prompt greater autotrophic activity (Catalán et al., 2017).

The minimal degradation of DOC seen in these results likely reflects that urban rivers are relatively DOC depleted and at baseflow the majority of DOC is recalcitrant compared to that typically found in rural rivers (Hook and Yeakley, 2005). Urban DOM is dominated by terrestrial

inputs during storms mainly through storm drain pathways and direct overland flow where there is often a high input of labile material (Coble et al., 2016), however this is rapidly consumed and is unlikely to be present at baseflow which is when water samples were collected for this study.

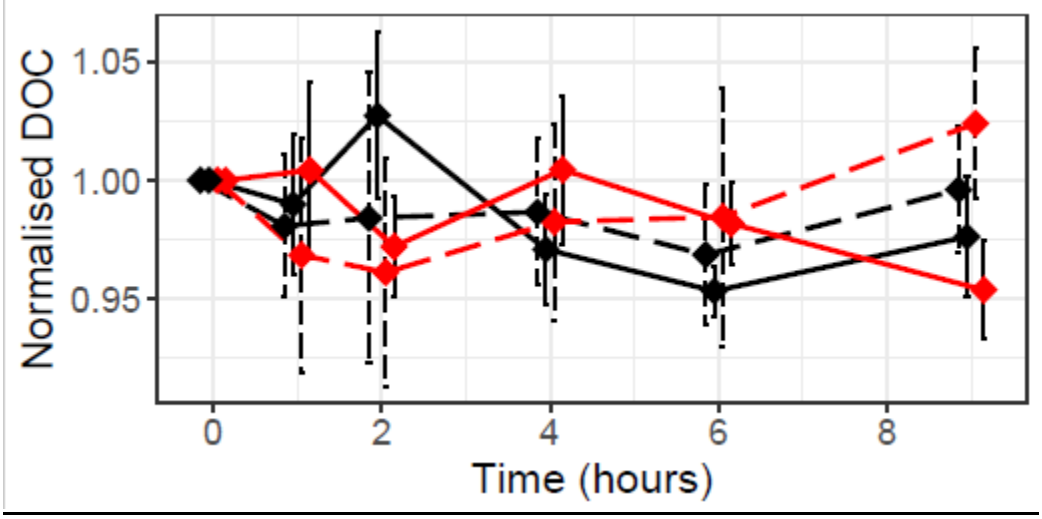

Figure 4.2. Temporal variation of DOC (mg/L) across experiments. Data are normalized across the experiments. Black lines show shaded treatments while red lines show unshaded treatments. Solid lines show heated treatments while dashed lines show unheated treatments. Error bars were calculated at 95% confidence intervals by pooling data from the three experiments.

4.4.2 Temporal Change in Absorption indices

No significant differences in SUVA-254 ($P > 0.05$; Table 4.3) were observed (Figure 4.3A). Minimal positive changes in SUVA-254 following photoexposure were observed in previous studies (e.g. Hansen et al. 2016), suggesting that the aromaticity character of DOM does not change much due to short term photodegradation. Changes in SUVA-254 values have been noted as a result of biodegradation, however usually over a longer timeframe than our study (Fellman et al., 2009).

For S275-295 (Figure 4.3B), there was a significant difference between shaded and unshaded treatments ($P < 0.01$), but no significant difference ($P > 0.05$) between heated and unheated treatments and no interaction effect was observed (Table 4.3). Hence, it appears photodegradation was a significant process in the experiment, while biodegradation was minimal. S275-295 increased by up to 8% in the unshaded treatments, while it decreased by up to 4% in the shaded treatments. The increase in S275-295 values in the unshaded treatments suggests a shift in DOM composition to DOM with a lower molecular weight (Helms et al., 2008). The shift towards lower molecular weight OM after photoexposure has been previously attributed to either disaggregation or an increase in photodegradation by-products (Hansen et al., 2016; Stepanauskas et al., 2005).

In contrast S350-400 (Figure 3C) showed no significant difference between treatments over time ($P > 0.05$; Table 4.3). There was a general decrease in the S350-400 slope: with up to a 20% in the shaded unheated treatment, although large error bars were observed in all cases. Previous studies have found that S350-400 decreases after photoexposure (Spencer et al., 2009; Logvinova et al., 2015; Helms et al., 2008), which we did not observe. It is likely, however, that the S275-295 and S350-400 track different DOM pools which have differing responses to light exposure and microbial activity (Romera-Castillo et al., 2013). Consequently, the pool tracked by S350-400 may be less vulnerable to photodegradation over the short timescale of our study.

With respect to slope ratio (Figure 4.3D), there was a peak increase in the unshaded unheated treatment of 10%, while the shaded, unheated treatment had a peak of 10% decrease. However, these differences were not significant ($P > 0.05$; Table 4.3). Increases in slope ratio

relate to photochemical-induced increases, while decreases arise from microbial processes (Osburn et al., 2012; Helms et al., 2008). The slope ratios were higher in the unshaded treatments for the duration of the experiments, indicating the degradative effects of photoexposure, as higher slope ratios are linked to changes in molecular weight which in this case suggest photodegradation induced changes, however no significant effect was found, likely because there was a relatively large amount of noise with the S350-400 data.

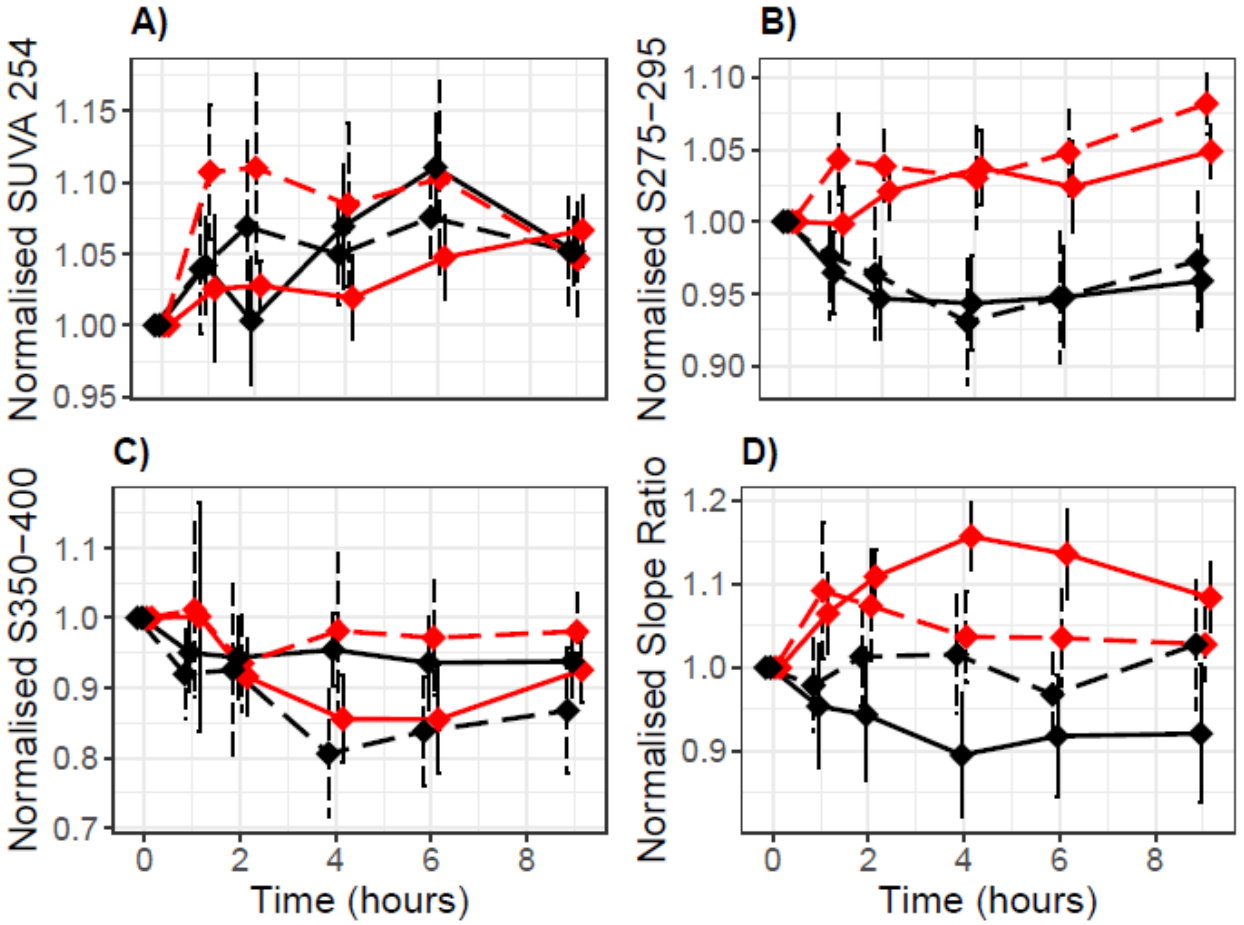

Figure 4.3. Temporal variation of selected absorbance Indices during the study. Error bars were calculated at 95% confidence intervals by pooling data from the three experiments. Black lines show shaded treatments while red lines show unshaded treatments. Solid lines show heated treatments while dashed lines show unheated treatments.

4.4.3 Temporal Change in Fluorescence

A significant difference in the fluorescence index (Figure 4.4A) was found between the shade treatments and a significant interaction effect between shade and temperature was also found ($P > 0.05$, Table 4.3). Fluorescence indices provide an indication of microbial sources, hence the results suggest shading in combination with temperature change lead to a shift in the composition of DOM (Fasching et al., 2015). No clear temporal trend was apparent however, suggesting differences in the fluorescence index at the end point of the experiment may be as a result of natural variability in the treatments. The fluorescence index was not expected to reflect photodegradation given the short time scale of our study (Hansen et al., 2016).

There was a significant difference between shaded and unshaded treatments in the HIX (Figure 4B; $P < 0.01$, Table 4.3) with the HIX of unshaded treatments decreasing over the course of the study by up to 16%, while that of shaded treatments stayed relatively constant. This suggests that photoexposure can lead to rapid decreases in humification (Ohno, 2002). This possibly reflects the presence of allochthonous DOM (e.g. from plant sources) which are more vulnerable to photodegradation (Hansen et al., 2016). HI has previously been identified to be higher in buried reaches than open streams in the summer, however this effect appears to be highly seasonal, with Arango et al. (2017) finding HIX higher in the autumn months due to higher terrestrial inputs of leaf litter in open reaches. In contrast to previous studies which have found SUVA-254 and HIX to co-vary (e.g. Du et al. 2016), the lack of change in SUVA-254 in correspondence with the change in HIX indicates the complexity of the fluorescent DOM pool which may be particularly prone to photodegradation. This is supported by Catalán et al., (2017) who found that the humic-like fluorophores in DOM have widely different reactions to degradation effects. Hence, the main fluorophores contributing to HIX in this study may not be

the same types of fluorophores that are generally linked to SUVA-254 in previous studies. Further, while we observed no significant difference between the heated and unheated treatments ($P > 0.05$), the heated unshaded treatment reached a minimum value substantially quicker than the unheated unshaded treatment. This suggests that higher temperatures in the heated unshaded treatment increased the rate at which humic material was broken down (Porcal et al. 2015).

There was no significant difference in BI (Figure 4.4C) ($P > 0.05$, Table 4.3) between treatments: minimal change was observed during the study with high error bars for all treatments. As BI is reflective of microbial-derived DOM (Para et al., 2010), the lack of change is further evidence that biodegradation was not a primary mechanism of DOM composition change within our study. In literature also no significant differences between BI in buried and open streams has been identified, however in the summer months BI values appear to be higher than other times of year due to higher autochthonous production (Arango et al., 2017).

For the A:T (Figure 4.4D) and C:T (Figure 4.4F) ratios, no significant differences were found between treatments and no interaction effect was found ($P < 0.01$; Table 2). For both A:T and C:T ratios, shaded treatments remained relatively stable throughout the study, although for unshaded treatments decreases of up to 13% and 21% were apparent for the A:T and C:T ratios respectively. Both the A:T and C:T ratios indicate the amount of humic material in comparison to fresh material in the OM pool. Increases in both ratios would be expected after biodegradation, with decreases after photodegradation (Hansen et al., 2016). Though decreases were observed, these were not significant, likely because fluorescence in the peak T and A regions was relatively weak, hence the noise to signal ratio was high between

treatments. The lack of a significant difference between protein and humic ratios between open and buried reaches has also been identified by Arango et al. (2017).

There was significant difference in the C:A ratio (Figure 4.4E; $P < 0.01$; Table 4.3) between the shaded and unshaded treatments with a steady decrease of 13% from baseline values. Peaks C and A represent different DOM pools (Kothawala et al., 2012), and hence the decrease in the ratio in the unshaded treatments suggests that the peak C pool of humic-material is particularly prone to photodegradation as shown in Figure 4.4B. Peak C materials are important to stream ecosystem functioning as an energy source (Hudson et al., 2007), yet peak C has been found to be particularly vulnerable to photodegradation. This suggests that stream burial in urban rivers may have important implications for ecosystem functioning by reducing removal rates of humic material for transport downstream. This effect may, however, be counteracted by higher input

rates of terrestrial materials within open reaches, although this material is often more recalcitrant (Arango et al., 2017).

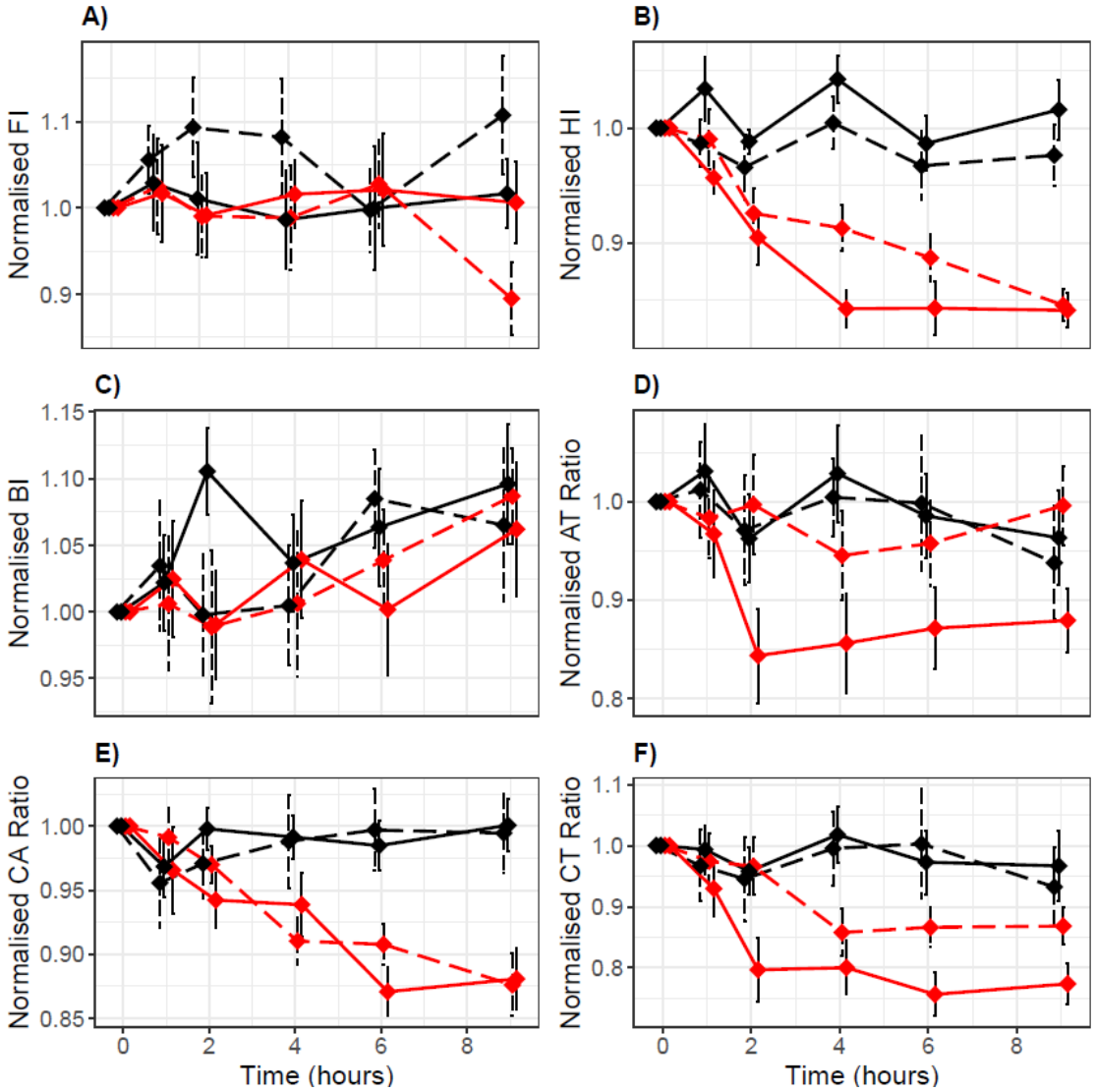

Figure 4.4. Temporal variation of Fluorescence Indices during the study. FI = Fluorescence Index, HI = Humification Index, BI = Biological Index, AT Ratio = Peak A to Peak T ratio, CA Ratio = Peak C to Peak A ratio, CT Ratio = Peak C to Peak T ratio. Error bars were calculated at 95% confidence intervals by pooling data from the three experiments Black lines show shaded treatments while red lines show unshaded treatments. Solid lines show heated treatments while dashed lines show unheated treatment

For components 1 (Figure 4.5A), 2 (Figure 4.5B), and 3 (Figure 4.5C), significant differences ($P < 0.01$) were observed between shaded and unshaded treatments (Table 4.3). Components 1-3

represent distinct pools of humic-like OM and it appears that humic material in the fluorescing pool of DOM is vulnerable to photodegradation over the short timescales of the study. In all cases, C1-3 gradually fell during the study but to varying degrees with reductions of up to 19%, 30%, and 39% for components 1-3 respectively. Differences in the extent of degradation between the humic components reflect the complexity of the urban DOM pool. Humic fluorescence is thus likely to comprise a mixture of natural and non-natural compounds with natural compounds generally relating to breakdown of vegetation materials, while non-natural compounds can exist from inputs from the wider storm drain network where detergents for example also fluoresce in the humic-like region (Williams et al., 2010). C3, which represents a terrestrial DOM pool (Table 4.2), was most vulnerable to photodegradation. The photoreactivity of terrestrially derived humic-like OM has been observed previously (Lu et al., 2013). Hence, systems where terrestrial inputs of humic DOM dominate are likely particularly prone to photodegradation. With respect to temperature effects, C3 showed a significant difference between heated and unheated treatments ($P < 0.05$), although no significant difference was observed for C1 or C2, and no interaction effects were noted ($P > 0.05$). However, in all cases, the heated unshaded treatment was characterized by increased degradation, highlighting the importance of temperature in influencing OM degradation (Porcal et al. 2015).

For C4, significant effects were found for temperature and shading, while the interaction between the two was also significant ($P < 0.05$; Figure 4.5D). Component 4 represents a proteinaceous fluorophore (Table 4.2), which have been found to be more resistant to photodegradation when compared to humic-like material (Phong and Hur, 2015). C4 increased in six hours for both unshaded treatments, indicating there may have been some

photodegradation in the unshaded treatments, however in the heated treatment C4 returned to baseline levels by the end of the experiment suggesting rapid processing by in-stream microbial communities of proteinaceous material at higher temperatures. Unshaded treatments however showed little change over the course of the experiment, likely reflecting that photodegradation was the main potential degradation mechanism to alter proteinaceous materials in the study (Hudson et al., 2007). In contrast to the humic-like components (C1-C3) where photodegradation was apparent within 2 hours, photodegradation was not apparent in C4 till six hours into the experiment, which likely reflects the increased resistance to photodegradation of proteinaceous material compared to humic-like material (Phong and Hur, 2015).

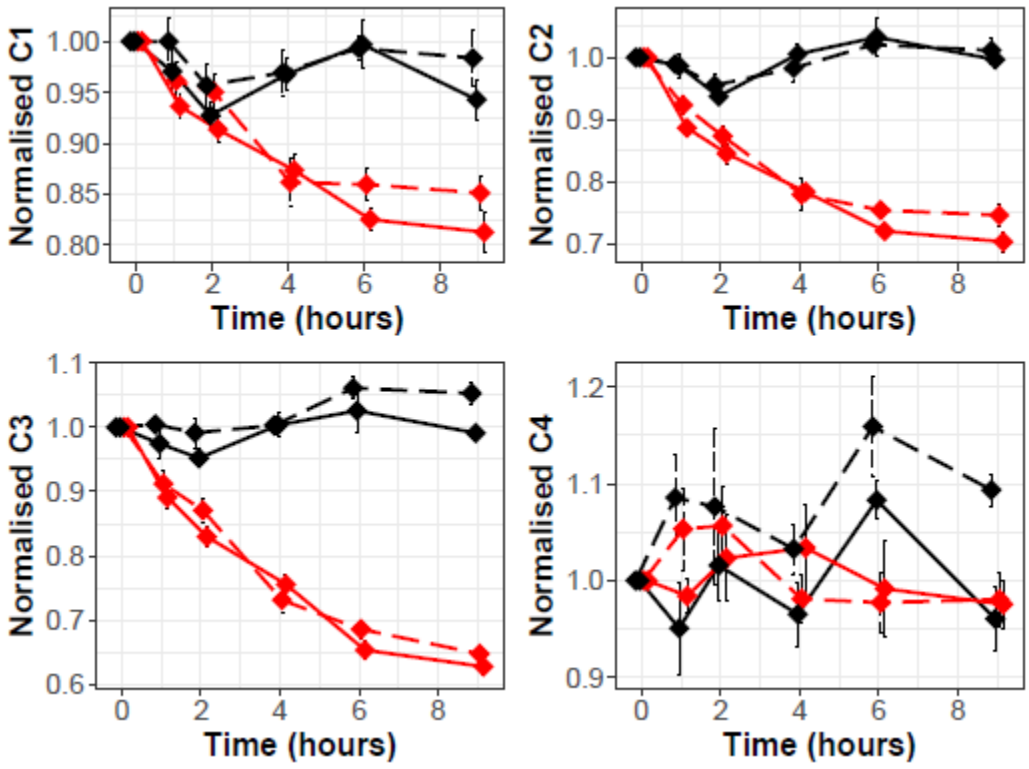

Figure 4.5. Temporal variation of PARAFAC components during the study. Error bars were calculated at 95% confidence intervals by pooling data from the three experiments. Black lines show shaded treatments while red lines show unshaded treatments. Solid lines show heated treatments while dashed lines show unheated treatments

Table 4.3. Linear mixed effects model results for all response variables within the study. Temperature refers to treatments separated into "Heated" or "Unheated" categories, Shade effect refers to treatments separated into "Shaded" or "Unshaded" categories. Interaction refers to the interaction effect between temperature and shading. * denotes significant p-values.

Response Variable	Parameter	Estimate	Standard Error	t-value	p-value
DOC	Intercept	0.99	0.027	36.90	0.00
	Temperature	-0.02	0.037	-0.54	0.60
	Shade	0.02	0.037	0.76	0.46
	Interaction: Temperature and Shade	-0.05	0.052	-0.96	0.34
SUVA254	Intercept	1.05	0.04	27.92	0.00
	Temperature	-0.00	0.04	-0.00	0.99
	Shade	-0.01	0.04	-0.13	0.89
	Interaction: Temperature and Shade	0.02	0.06	0.34	0.73
S275-295	Intercept	0.97	0.04	27.11	0.00
	Temperature	-0.01	0.04	-0.32	0.75
	Shade	0.11	0.04	2.54	0.01*
	Interaction: Temperature and Shade	-0.02	0.06	-0.31	0.75
S350-400	Intercept	0.87	0.09	9.47	0.00
	Temperature	0.07	0.07	1.00	0.32
	Shade	0.11	0.07	1.61	0.12
	Interaction: Temperature and Shade	-0.12	0.09	-1.26	0.22
Slope Ratio	Intercept	1.21	0.11	11.17	0.00
	Temperature	-0.16	0.10	-1.62	0.11
	Shade	-0.08	0.10	-0.79	0.43
	Interaction: Temperature and Shade	0.19	0.15	1.27	0.21
FI	Intercept	1.10	0.05	21.81	0.00
	Temperature	-0.09	0.07	-1.26	0.22
	Shade	-0.21	0.07	-2.96	0.01*
	Interaction: Temperature and Shade	0.20	0.10	1.99	0.05*

HI	Intercept	0.98	0.02	45.62	0
	Temperature	0.04	0.03	1.31	0.20
	Shade	-0.13	0.03	-4.32	0.00*
	Interaction: Temperature and Shade	-0.04	0.04	-1.03	0.31
BI	Intercept	1.07	0.05	22.18	0
	Temperature	0.03	0.07	0.46	0.65
	Shade	0.02	0.07	0.32	0.75
	Interaction: Temperature and Shade	-0.06	0.10	-0.58	0.56
AT Ratio	Intercept	0.94	0.05	20.52	0.00
	Temperature	0.03	0.06	0.39	0.70
	Shade	0.06	0.06	0.90	0.37
	Interaction: Temperature and Shade	-0.14	0.09	-1.56	0.13
CA Ratio	Intercept	98.83	0.27	37.40	0.00
	Temperature	0.01	0.03	0.17	0.86
	Shade	-0.12	0.03	-3.41	0.00*
	Interaction: Temperature and Shade	-0.00	0.05	-0.03	0.98
CT Ratio	Intercept	0.93	0.05	44.49	0.00
	Temperature	0.03	0.07	-1.77	0.62
	Shade	-0.06	0.07	-5.01	0.36
	Interaction: Temperature and Shade	-0.13	0.10	-1.33	0.19
C1	Intercept	0.98	0.03	35.68	0.00
	Temperature	-0.04	0.03	-1.55	0.13
	Shade	-0.13	0.03	-5.03	0.00*
	Interaction: Temperature and Shade	0.00	0.04	0.06	0.95
C2	Intercept	1.01	0.02	46.44	0.00
	Temperature	-0.01	0.02	-0.65	0.52
	Shade	-0.27	0.02	-11.72	0.00*
	Interaction: Temperature and Shade	-0.03	0.03	-0.87	0.39
C3	Intercept	1.05	0.01	75.52	0.00
	Temperature	-0.06	0.02	-3.72	0.00*

	Shade	-0.41	0.02	-24.40	0.00*
	Interaction: Temperature and Shade	-0.04	0.02	1.78	0.08
C4	Intercept	1.09	0.03	41.40	0.00
	Temperature	-0.13	0.04	-3.56	0.00*
	Shade	-0.11	0.04	-3.02	0.01*
	Interaction: Temperature and Shade	0.13	0.05	2.43	0.02*

4.5 Conclusion

The results suggest that shading reduced photodegradation of the humic fluorescent pool of DOM, in accordance with the hypothesis. DOM quantity however did not notably degrade or decrease during the experiments which was contrary to our hypothesis. Over the short timescales of our study, biodegradation appeared to have a minimal impact on DOM composition, with changes seemingly being driven by photodegradation. Furthermore, the effects of water temperature were shown to be relatively minor, which disproved our hypothesis that increased temperature would accelerate photodegradation and biodegradation. This was likely because the range of temperatures was not high enough to cause notable differences in the rates of photodegradation and biodegradation. The interaction effects between temperature and shading were also shown to be weak, which contradicted our original hypothesis. This can also be attributed to the minimal effect of temperature. There were considerable variations in differences in optical metrics: absorbance was generally less responsive than fluorescence which likely reflects the complex and varied OM pool that together constitutes urban river DOM.

These findings have important implications for urban river ecosystem management: the results indicate that shading through actions such as stream burial substantially alters DOM composition in the urban headwaters. Stream burial prevents photodegradation and leads to little compositional change of DOM for export downstream. Previous studies have indicated stream burial also greatly reduces terrestrial inputs of humic material, although this is often more recalcitrant in composition. Therefore, when daylighting streams, it is important to maintain stream shading through riparian coverage to reduce the loss of labile humic material downstream while also maintaining terrestrial inputs. For future research, *in-situ* measurements tracking photodegradation and biodegradation within urban rivers will be useful to increase our understanding of degradation in these relatively little studied, but highly important, river systems. Further, mass spectrometry techniques such as gas-chromatography mass spectrometry (GC-MS) and liquid-chromatography mass spectrometry (LC-MS) may offer a means of better characterizing DOM, in particularly with regards to identifying specific types of Organic Carbon. This will help resolve the complexities involved in understanding the behavior of the DOM pool in relation to biodegradation and photodegradation.

CHAPTER 5: HIGH-FREQUENCY IN-SITU FLUOROMETRY INDICATES THE CONTROL AND SOURCE DYNAMICS OF DISSOLVED ORGANIC MATTER DURING STORMFLOW EVENTS IN URBAN SYSTEMS

5.1 Abstract

Urbanization alters the quantity and quality of Dissolved Organic Matter (DOM) fluxes to river systems during storms, degrading their ecological health. The flashiness of urban flow catchments means synoptic sampling has been a poor method for investigating DOM source dynamics. Resultantly the controls on linkages between DOM sources and flow path are poorly understood, and *in-situ*, continuous monitoring is required to characterize system behavior at a suitable temporal resolution. To address this knowledge gap, we installed an *in-situ* fluorometer in an urban stream (Bourn Brook, Birmingham, UK) for 10 weeks from 8th September to 20th November 2016. Two wavelength pairs were monitored at 5-min resolution: Humic-like fluorescence (HLF) (Ex. 365 nm, Em. 490 nm) and Tryptophan-like fluorescence (TLF) (Ex. 285 nm, Em. 340 nm). Controls on DOM concentration was investigated using log Concentration-Discharge (C-Q) plots. The relationship between discharge and concentration for TLF and HLF were strongly chemodynamic at low discharges but TLF showed chemostatic behavior thereafter suggesting urban DOM can be exhausted during large or frequent events, while figure of eight hysteresis was the most common hysteresis type for both HLF and TLF, indicating that the dominant sources of DOM shifts throughout events. Multiple linear regression was used to identify hydrometeorological and landscape predictors of fluorescence. Water temperature was an important predictor, possibly highlighting the influence of increased microbial activity at higher temperatures on urban DOM dynamics. Seven-day antecedent rainfall was also identified as an important predictor of TLF and HLF change with a negative relationship for both TLF and HLF with

increasing antecedent rainfall (indicating exhaustion of DOM sources). Land use metrics were weaker predictors of DOM dynamics; however, road density and total vegetated areas were important for predicting maximum HLF and TLF, highlighting landscape properties as a control on DOM dynamics. This study enhances mechanistic understanding of DOM controls and sources and highlights the vulnerability of urban rivers to degradation through storm-based inputs of DOM from urban sources.

5.2 Introduction

Dissolved Organic Matter (DOM) represents a pool of complex, heterogeneous material within the carbon cycle that is ubiquitous in riverine systems and critical for ecosystem functioning (Fellman et al., 2010; Hudson et al., 2007). DOM composition and concentration is controlled by a combination of geology, land use, hydrometeorology and *in-situ* conditions such as biological communities and geomorphology (Williams et al., 2010; Coble, 1996). Urbanization can substantially alter catchment permeability, the drainage network, decomposition and the input of terrestrial soil/vascular plant sources of DOM, leading to a distinctive DOM composition in urban catchments (Khamis et al., 2018; Hosen et al., 2014; Kaushal et al., 2014). Urban rivers have previously been found to have a DOM composition in which microbial, proteinaceous compounds dominate, whereas rural systems are typically dominated by humic-like compounds (Smith and Kaushal, 2015; McElmurry et al., 2014; Hosen et al., 2014; Baker, 2001; Kaushal et al., 2018b) . The increased concentration of proteinaceous compounds in urban rivers contributes to oxygen depletion by increasing the biological Oxygen demand (BOD) in streams, which impacts biogeochemical cycling within the stream and can lead to systems becoming anoxic if BOD becomes too high (Paerl et al., 1998; Kaushal et al., 2014). The composition of urban DOM can vary at event-based time

scales when changes in water-flow pathways occur. For example, through the activation of storm drains and combined sewage overflows (CSOs), which can connect the wider catchment and the sewerage system to the stream (Czemiel Berndtsson, 2010; Liu et al., 2019; Zwolsman and van Bokhoven, 2007) . Despite increasing urbanization worldwide (McGrane, 2016), the study of urban DOM has been relatively neglected to date. Improved understanding of the major controls on urban DOM dynamics are required to improve water quality management in urbanized river catchments (Khamis et al., 2018).

A mixture of hydrometeorological and land use controls determine DOM response to individual storm events (McElmurry et al., 2014; Eckard et al., 2017; Blaen et al., 2017; Kaushal et al., 2014). Concentration-discharge (C-Q) relationships can be used to investigate DOM dynamics during storm events (Bowes et al., 2015; Bieroza et al., 2018). The shape of C-Q relationships can be used to infer the dominant catchment characteristics that influence water quality variables. C-Q relationships can be broadly split into two classes: chemodynamic, where source limitation occurs and either a positive or negative relationship is observed, and chemostatic, where no change in concentration with discharge is observed (Godsey et al., 2009). Despite growing interest in the wider water quality literature, little work has been done exploring C-Q relationships for DOM in urban rivers.

Hydrometeorological conditions have also previously been shown to be a major control on water quality dynamics (Worrall and Burt, 2004; Blaen et al., 2017). During storm events the potential nutrient load generated from the catchment is constrained by the precipitation amount and intensity, whilst the subsequent in-stream discharge response can lead to DOM mobilization (Schuster et al., 2007; Saraceno et al., 2009). Antecedent conditions have been highlighted as particularly important controls on nutrient dynamics. Drier conditions lead to

build-up of terrestrial material which can be mobilized during storm events, whilst consistently wet conditions have often been linked to source depletion, and to subdued in-stream response (Carstea et al., 2010, 2009).

Land use is a further control on DOM response during storm events (McElmurry et al., 2014). The characteristics of precipitation events can be highly variable across catchments, particularly in urban catchments (Croghan et al., 2018), hence, DOM may be generated disproportionately at specific points in the catchment (Pedersen et al., 2010). Engineered headwaters, such as storm drains, gutters and pipes can act as sinks for organic material during dry periods but also provide large amounts of carbon and nitrogen to streams during storm events (Fork et al., 2018; Smith and Kaushal, 2015). Hence, in-stream responses are likely to be at least partly controlled by catchment land use in areas where DOM is predominantly mobilized. To date, however, our ability to assess the nature of these controls on urban DOM has been constrained by the limited availability of high temporal resolution data (Blaen et al., 2016; Old et al., 2019). Furthermore, urban land use has been treated as one broad class in previous studies, while urban land cover is variable, with a range of urban metrics influencing hydrological signals (McGrane, 2016).

Historically DOM has been assessed within urban systems by analyzing water samples collected manually (e.g. Carstea *et al.*, 2009). Fluorescence spectroscopy provides detailed characterization of DOM samples, and can be used to assess DOM concentration and quality (Fellman et al., 2010; Hudson et al., 2007). This technique requires the use of laboratory spectrometers or hand-held instruments, and, as a result, the temporal resolution and length of time series at high-resolution has been limited (Blaen et al., 2016). These manual sampling techniques cannot adequately characterize DOM in urban rivers during storm

events, as urban rivers respond rapidly to precipitation events. While some *in-situ* sampling campaigns have been completed (Carstea et al., 2010), they are of limited temporal duration. However, recent developments in optical sensors have included field-deployable *in-situ* fluorometers (Khamis et al., 2017). *In-situ* fluorometers have the capability to monitor fluorescence at high-temporal resolution, allowing monitoring over longer periods and capturing of storm event dynamics (Downing et al., 2012; Saraceno et al., 2017). *In-situ* fluorometers deployed in urban areas tend to monitor Tryptophan-like fluorescence (TLF) and Humic-like fluorescence (HLF) wavelength pairs (Khamis et al., 2018). The TLF signal is predominantly associated with dissolved proteinaceous and phenolic compounds (Beggs and Summers, 2011). However, phenolic compounds are unlikely to be a substantial contributor to the TLF signal in urban streams, which tends to be dominated by proteinaceous material (Baker, 2001). TLF is indicative of organic pollution within streams and strongly correlates with Biological Oxygen Demand (BOD) (Baker and Inverarity, 2004). It has previously been found to be a useful water quality metric in urban streams (Khamis et al., 2018). HLF is associated with humic substances, and provides a proxy for Dissolved Organic Carbon (DOC) (Coble, 1996). To accurately monitor both TLF and HLF *in-situ* it is important that instruments are carefully calibrated and undergo regular maintenance as they can be susceptible to fouling (Downing et al., 2012; Khamis et al., 2017). The technology of *in-situ* fluorometers has, however, great potential to explore DOM dynamics at temporal resolutions that were previously not possible.

Given the research gaps outlined above, the primary aim of this study was to identify the main controls on DOM dynamics (i.e. changes in composition and quantity) during high flow conditions for an urban river. To provide increased mechanistic understanding of DOM storm events dynamics we used high-resolution radar precipitation data, which enabled us

to overcome issues with the spatial patchiness of precipitation, and high spatial resolution land use datasets. Through this we aimed to more accurately link DOM dynamics to the routing of water through engineered drainage infrastructure from discrete parts of the catchment. More specifically, our main objectives were to:

1) Identify the main controls on DOM dynamics during storm events using high frequency, in-situ monitoring of humic-like fluorescence (HLF), and tryptophan-like fluorescence (TLF);
2) Infer source and flow-path linkages based on DOM response to spatially resolved meteorological and land-use variables.

In order to test these objectives, the following hypotheses were developed:

- HLF and TLF will both be chemodynamic up to a threshold whereupon they will become chemostatic due to exhaustion of material in the system.
- A range of hysteresis types would be identified for both TLF and HLF, however anti-clockwise hysteresis will be more common for HLF than TLF due to differences in source types.
- Antecedent conditions will be the strongest control on TLF and DOM dynamics.
- Urbanization metrics will be the strongest land use metrics associated with TLF and HLF dynamics.

5.3 Methods

5.3.1 Study site

The study was conducted during autumn 2017, between September 9 and November 21. Sensors were installed in the Bourn Brook, Birmingham, UK (52°27'N, 1°54'W; Figure 5.1), a headwater stream with a catchment size of 27.9km^2 and elevations ranging from 116 m to 234 m above m.s.l. Although the source of the stream is a natural woodland, most of the catchment is urbanized (77% urban/suburban land use). The stream has a flashy flow regime, typical of urbanized catchments. While no wastewater treatment plant exists in the catchment, the river is vulnerable to Combined Sewage Overflow (CSO) discharges and leakage from the sewerage network (Khamis et al., 2017; Carstea et al., 2009). Chemical water quality in the river has previously been assessed by the Environment Agency as "good", although this does not measure DOM, while biological quality was assessed as "fair", although the river is at risk of diffuse pollution (Carstea et al., 2009).

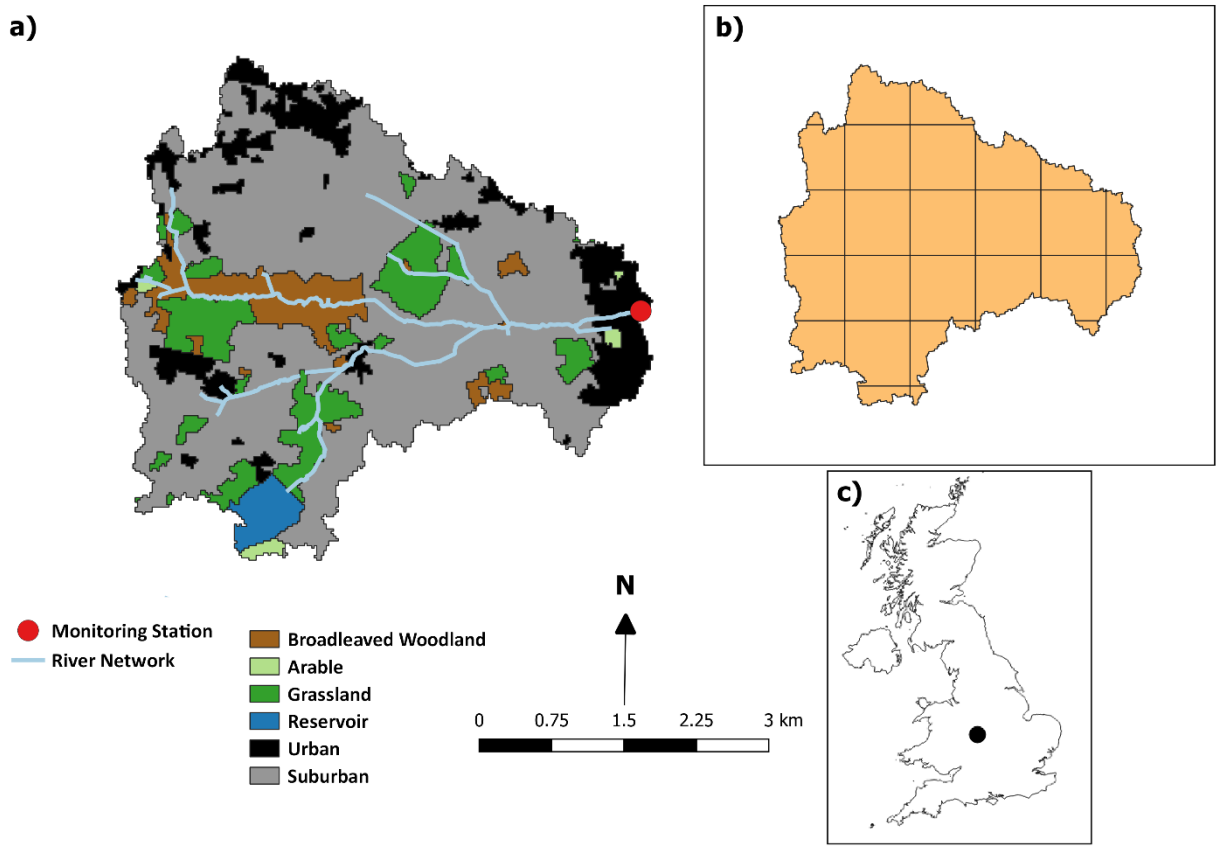

Figure 5.1. A) The Bourn Brook catchment and associated land use derived from the UK Centre of Ecology and Hydrology (CEH) Land Class 2015 (Rowland et al., 2017). B) The distribution of 1km^2 grid cells used to estimate rainfall loads from rainfall radar C) The location of the catchment within the UK.

5.3.2 Stream Data

Water levels in the stream were logged at 5-min resolution over the monitoring period using a Druck PDCR800 pressure transducer (GE, Billerica, USA). Water levels were converted from stage to discharge using a flow rating curve developed for the site, following the velocity-area method. All data from the study were stored on a CR1000 data logger (Campbell Scientific, Logan, USA). A TinyTag Aquatic 2 (Gemini, Sussex, UK) water temperature logger was also installed to monitor in-stream water temperature data (Table 5.1).

A modified GGUN-FL30 fluorometer (Albillia, Neuchâtel, Switzerland) was used to measure *in-situ* fluorescence. The fluorometers instrumentation is composed of an excitation branch

and a detection branch, which runs perpendicular to the excitation branch (Khamis et al., 2017). The instrument monitors wavelength pairs corresponding to Tryptophan-like fluorescence (TLF) and Humic-like fluorescence (HLF) and turbidity (Table 5.1). The turbidity measurements were used to correct for turbidity interference post-monitoring. Sample temperature was measured within the sensor using an internal thermistor, which allowed correction for thermal quenching on the measurements.

Table 5.1. Parameters and corresponding instrumentation with specifications used within study. Accuracy and range are reported for all variables. For TLF, HLF, and Turbidity, wavelengths monitored are reported. MDL = Minimum detection limits, ppb = Parts per billion.

Variable	Instrument	Specification
Water Level	Druck PDCR800	Accuracy = ±0.6%
Water Temperature	TinyTag Aquatic 2	Accuracy = 0.01°C Range = -40°C to +70°C
TLF	GGUN-FL30	MDL = 1.74 ppb Range = 0-1000 ppb Wavelengths monitored = Ex. 285 ± 12 nm (FWHM), Em. 340 ± 15 nm (FWHM)
HLF	GGUN-FL30	MDL = 1.39 ppb Range = 0-1000 ppb Wavelengths monitored = Ex. 365 ± 25 nm (FWHM), Em. 490 ± 30 nm (FWHM)
Turbidity	GGUN-FL30	MDL = 0.8 NTU Range = 0-1000 NTU Wavelength monitored = 660 nm

The fluorometer was secured on the stream bank and water samples were taken from the stream at 5-min intervals. A peristaltic pump (Model 810, Williamson Pumps Ltd, UK) controlled by a CR1000 logger was connected to the sensor and operated through a relay switch. Samples passed through an inlet strainer wrapped in a 250-micron mesh to reduce potential fouling, and then flowed through 3m of silicon tubing (6.4 mm diameter). To minimize contamination between subsequent measurements, samples were pumped through the fluorometer for 3-mins to ensure complete flushing of the measurement cell

before taking three measurements for each wavelength pair. After analysis, samples were returned to the river. Optical sensors are prone to fouling (biological and inorganic) during field deployment, particularly following storm events (Rode et al., 2016), and hence the optical measurement cell of the sensor was cleaned at regular intervals over the monitoring period (i.e. sub-weekly) to reduce fouling-related drift in measurements. When fouling-related drift was observed, which was identified by step changes in measurements following cleaning, this was corrected for using a linear regression model assuming a constant fouling rate. Generally, the regularity of cleaning lead to minimal periods of drift within the dataset.

5.3.3 Instrument Calibration and Data Correction

Raw outputs from the FL 30 (mV) data were converted to ppb or NTU using a six-point calibration curve, over a range of 0-1000 ppb. Prior to each run, a blank reading of the fluorometer was taken using ultrapure water to assess the baseline reading. TLF was calibrated using standards created by dilution of a 100-ppm stock solution (L-Tryptophan, Acgros Organics, 99%). HLF was calibrated using quinine sulphate dehydrate in 0.05 M H_2SO_4, a 100-ppm stock solution was subsequently diluted by ultra-pure milli-Q water. Turbidity was calibrated using a formazine suspension. For all optical parameter's calibration was conducted using 1, 10, 50, 500, and 1000 ppb/NTU standard solutions, which were used immediately after production to avoid deterioration. Each solution was measured in the fluorometer for at least one minute with measurements recorded every 10 seconds and a mean value taken. All measurements were taken at 20°C, and the fluorometer was acid washed and rinsed repeatedly with deionized water between samples to avoid contamination.

Post-monitoring corrections for temperature quenching and turbidity interference were also required. Instrument-specific temperature corrections and instrument and site-specific turbidity corrections were developed prior to this study (by Khamis et al. 2017), and these were used herein. Fluorescence was temperature corrected to a reference temperature of 20°C using the following equation derived by Khamis *et al.* (2015):

$$1) \quad F_{ref} = \frac{Fmes}{1 + \rho(T_{mes} - T_{ref})}$$

where F = Fluorescence signal, ρ = ratio at the slope intercept for the reference temperature, Fmes = measured value, and T_{ref} = reference value.

For turbidity, corrections were made for HLF and TLF using linear regression models. Measurements from the fluorometer were calibrated for turbidity by collecting sediment from the study site and diluting with deionized water to create a dilution series ranging 0-500 NTU. The impact of site-specific turbidity across the dilution series was then calculated by measuring the degree of change in the TLF and HLF signal with increasing turbidity. The percentage change in the HLF and TLF signal across the range of turbidities were then calculated and could be applied to the data post-monitoring.

5.3.4 Meteorological data

Event precipitation for the catchment was estimated using radar data from the UK Met Office MIDAS radar system (Met Office, 2012), and checked against gauge data from within the catchment for accuracy. Radar precipitation data were recorded at 5-min time steps with 1km^2 spatial resolution. This enabled spatial estimates of precipitation for each storm event to be calculated for 1km^2 grid cells distributed across the catchment (Figure 5.1B).

5.3.5 Data analysis

5.3.5.1 Concentration-Discharge Data

C-Q relationships were developed for HLF and TLF. The C-Q relationship was determined by calculating the slope on logarithmically transformed data for both C and Q, as has been widely used in prior concentration-discharge studies (Evans and Davies, 1998; Bieroza et al., 2018; Godsey et al., 2009). HLF, TLF, and discharge for the entire dataset were log-transformed and TLF and HLF were then regressed against discharge to determine slope. Where a slope value was < 0.1, the relationship was defined as chemostatic, meaning that no change in concentrations occurs with increasing discharge. Where the slope was > 0.1, the relationship was defined as chemodynamic, indicating either a dilution or concentration effect with increasing discharge (Bieroza et al., 2018).

As the C-Q relationships we observed were not entirely linear, we also used segmented regression to assess whether there was a breakpoint in the C-Q relationship (Muggeo, 2008). We then tested if the difference in slope between breakpoints was significant using a Davies test. We used the Alkaike Information Criterion (AIC) index to assess if the C-Q relationship was modelled better by the linear model or segmented model.

Hysteresis analysis provides further information about the nature of the C-Q relationship during discrete storm events, specifically the potential catchment source areas and flow pathways (Lloyd et al., 2016a; Vaughan et al., 2017). In this study we used the modified Hysteresis Index (HI) developed by Lloyd et al. (2016b) to assess hysteresis. The modified HI calculates hysteresis across the loop for different flow percentiles by comparing the rising limb and falling limb values. Due to the rapid rising limb flow, which is common in urban rivers (Fletcher et al., 2013), the percentiles ranged from 20% to 33% for the study. In

calculating the modified HI, flow (Q) and fluorescence (F) for both HLF and TLF were normalized using the following equation (Lloyd et al., 2016), taking Q as an example:

$$2) \quad Normalised\ Q_i = \frac{Q_i - Q_{min}}{Q_{max} - Q_{min}}$$

where Q_i is discharge for a given timestep, Q_{min} is minimum discharge and Q_{max} is maximum discharge. Fluorescence values were normalized in the same manner. HI was calculated using the following equation:

$$3) \quad HI_i = V_r - V_f$$

where HI_i is the HI for a given percentile, V_r is the value of the rising limb for a given variable, and V_f is the corresponding value of the falling limb for the given variable. All values across the loop were then averaged, yielding a HI value between -1 and 1 for each event. Positive (negative) values indicate clockwise (anti-clockwise) hysteresis.

Each event hysteresis graph was visually inspected and classified, based on the directionality and shape, into one of the following groups: (i) figure of eight, (ii) clockwise, (iii) anti-clockwise, (iv) complex, and (v) no hysteresis. These groupings were chosen based on prior studies which have identified these as the most common forms of hysteresis (Williams, 1989).

5.3.5.2 Hydrometeorological and Landscape Analysis

Hydrometeorological and landscape metrics (Table 5.2) were determined for 22 events. Events were defined using the "*hydromad*" R package, using a threshold of >25% increase in flow for a minimum of five hours. This relatively short event duration was selected due to the flashy nature of the catchment.

Hydrometeorological metrics were chosen based on their importance in other water quality studies (Blaen et al., 2017). The following landscape metrics were derived for the catchment: average slope (percentage), percentage road cover (defined as road and associated paved surfaces), roofs (defined as area of roofs from all buildings in the catchment), urban area (defined as all paved surfaces within the catchment), vegetation (defined as all vegetation within the catchment), and woodland (defined as only wooded areas of the catchment). The classifications were selected to include land use variables that reflect the drainage properties of the basin and influence water flow pathways (Khamis et al., 2018). Vegetation, woodland, and urbanization metrics were calculated at a $25m^2$ spatial resolution using the Centre of Ecology and Hydrology Land Class 2015 dataset (Rowland et al., 2017) while road and roof cover were obtained from the Corine Land Cover 2012 dataset (EEA, 2012). Catchment slope was calculated from a catchment DEM derived from a 5m digital terrain model of the UK (Ordnance Survey, 2018).

The catchment was sub-divided into $1km^2$ grid cells that matched the grid cells of the radar precipitation dataset (Figure 5.1B). For each event, precipitation totals were determined for each gridcell, and the weighted average for the contribution of each gridcell to the total event rainfall were derived. The contributions of each land use type in every event were calculated as a function of the proportional land cover in each gridcell and each gridcell was weighted by the proportion of the total catchment precipitation that fell in that gridcell. Gridcell values were then averaged to yield a single value for each land use variable, indicating its estimated contribution to each event: indicating the relative precipitation totals falling on roads, vegetation, urban areas, roofed, and woodland areas for each event.

To assess the main hydrometeorological and landscape predictors (Table 5.2) on the fluorescence metrics (Table 5.3), ordinary least squares (OLS) multiple linear regression was undertaken. Variables were initially screened for normality and homogeneity of variance. Normality was assessed using Shapiro-Wilk tests (Shapiro and Wilk, 1965), and then visually inspected using quantile-quantile plots. All variables were found to be normally distributed. Data were then investigated for collinearity by calculating variance influence factors (VIF) (Zuur et al., 2010). If a variable had a VIF greater than three, it was removed from analysis. The R package "MuMin" was then used to fit all combinations of response models (N = 256) ranked according to corrected AICc due to the small sample size of the dataset. All models within <2AICc were considered the subset of best models. Following the law of parsimony, the model with the fewest variables was considered the best model.

Table 5.2. Summary of hydrometeorological and landscape metrics analyzed. Land use stats represent the contribution of each land use type during individual events. Descriptive statistics are shown for storm events within the study period.

Variable	Code	Metric	Unit	Max	Min	Mean
Flow	PF	Peak flow	$m^3 s^{-1}$	2.79	0.54	1.46 ± 0.77
	ED	Event duration	Hours	58.00	5.75	23.55 ± 14.15
Precipitation	RA	Rainfall amount	mm	18.40	0.40	5.57 ± 4.95
	MaI	Maximum hourly intensity	mm/hr	6.40	0.40	2.11 ± 1.64
	MeI	Mean Intensity	mm/hr	2.57	0.18	0.72 ± 0.51
Temperature	WT	Water temperature during event	˚C	14.50	9.33	12.37 ± 1.34
Antecedent Conditions	1A	Total rain 1 day before event	mm	5.60	0	1.31 ± 1.72
	7A	Total rain 7 days before event	mm	31.20	2.20	18.84 ± 9.27
	14A	Total rain 14 days before event	mm	46.40	4.80	32.68 ± 12.47
	EM	Magnitude of last event	$m^3 s^{-1}$	2.79	0.54	1.43 ± 0.79
Landscape	Ur	Average Urbanised	%	81.03	73.65	76.9 ± 1.92
	Ve	Average Vegetation	%	25.72	17.97	22.20 ± 1.95
	Wo	Average Woodland	%	13.77	7.90	11.34 ± 1.36
	Ro	Average Roofs	%	12.23	11.47	12.23 ± 0.28
	Rd	Average Roads	%	8.97	7.95	8.38 ± 0.22
	Sl	Average Slope	%	5.78	5.41	5.61 ± 0.08

Table 5.3. Definitions of fluorescence metrics used within the study

Metric	Unit	Definition	Justification
Max TLF	ppb	Maximum value for TLF during each event	Indicator of maximum amount of protein-like fluorophores mobilised during high flow
Max HLF	ppb	Maximum value for HLF during each event	Indicator of maximum amount of humic-like fluorophores mobilized.
Mean TLF:HLF ratio	None	The mean value of the ratio between TLF:HLF for each event	Indicator of shifts in flow path
HLF HI	None	HLF hysteresis index for each event	Indicator of hysteresis type
TLF HI	None	TLF hysteresis index for each event	Indicator of hysteresis type
Max TLF increase	%	The percentage increase value for peak TLF from the start of event value for TLF	Standardized peak increase across each event, allowing better comparison between events
Max HLF increase	%	The percentage increase value for peak HLF from the start of event value for HLF	Standardized peak increase across each event, allowing better comparison between events

5.4 Results

5.4.1 Water Quality Parameters Time Series

The study period included 22 discrete storm events. Daily mean discharge averaged 0.43 ± 0.17 $m^3 s^{-1}$ over this period. Baseflow was relatively stable across the duration of the study, with discharge peaks predominantly influenced by precipitation (Figure 5.2). Mean precipitation for each discrete storm event averaged 2.86 mm, with the bulk of studied events (14) occurring in September, followed by a notable drier period from the 1st to the 20th October, followed by a further 5 events in quick succession. In November, 3 discrete precipitation events were identified (Figure 5.2). Water temperature (WTemp) showed a notable decrease over time during the study (Figure 5.2), from a mean daily WTemp of 14.21 ± 2.13 °C during September, to 9.5 ± 2.33 °C in November which followed normal seasonal patterns. Turbidity remained low during baseflow, with peaks during storm events (Figure 5.2).

TLF was stable outside of storm events, with increased largely after the onset of storm events (Figure 5.2). Mean daily TLF was 61 ± 15.85 ppb, with a maximum daily mean of 85.9 ppb recorded on 11 September. Uncorrected TLF was slightly higher than the corrected TLF, with uncorrected mean daily TLF at 64.47 ± 17.3 ppb. HLF was also stable during baseflow, although a slight diurnal pattern was present with decreases in HLF throughout the day followed by increases at night (Figure 5.2). Mean daily HLF was 58.05 ± 10.65 ppb, with a maximum daily mean of 76.39 ppb observed on 1 October. Uncorrected daily HLF was higher than corrected HLF, with uncorrected mean daily HLF at 74.35 ± 17.67 ppb.

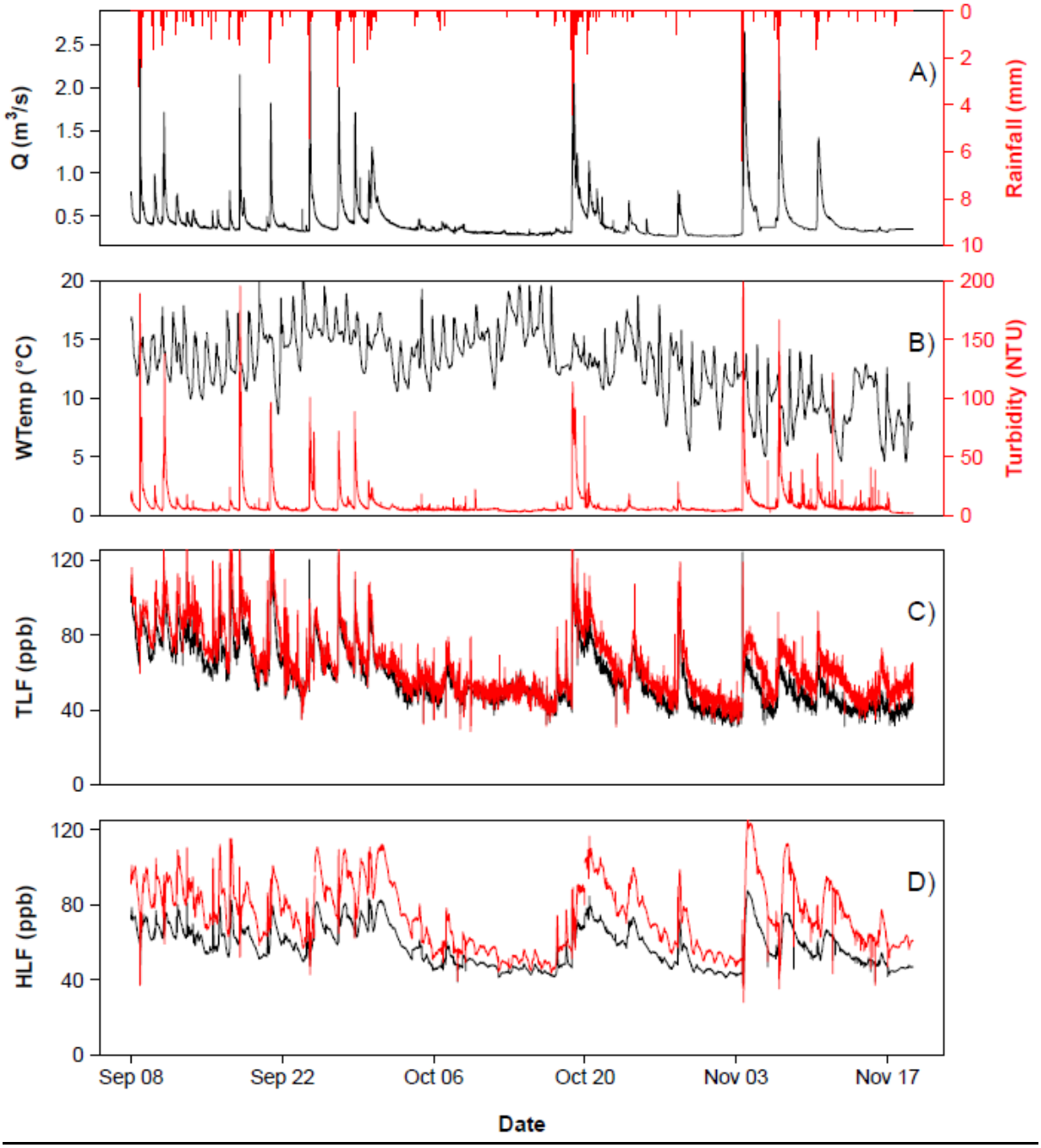

Figure 5.2. Time series of water quality and discharge for the study period: 9 Sept. to 21 Nov. 2017. A) Shows discharge (black) and precipitation (red), B) shows water temperature (black) and turbidity (red), C) shows TLF and D) shows HLF. For the TLF and HLF graphs black lines show the data corrected for temperature and turbidity, and red lines show the raw time series.

5.4.2 Concentration Controls

5.4.2.1 Concentration-Discharge Analysis

Analysis of the C-Q relationship indicates that both TLF ($P < 0.01$, slope = 0.54 ± 0.01*)* and HLF ($P < 0.01$, slope= 0.30 ± 0.01) exhibited significant chemodynamic behavior (Figure 5.3). The relationship was stronger for TLF, with greater explanatory power for the TLF linear model ($R^2 = 0.42$) compared to the HLF linear model ($R^2 = 0.36$).

However, as both the TLF and HLF C-Q relationships were non-linear, a break point analysis was undertaken to identify the flow under which chemodynamic behavior ceases and chemostatic behavior begins. For the TLF data (Figure 5.3a), the breakpoint was 0.48 ± 0.01 $m^3 s^{-1}$: before this point, the data are chemodynamic (slope = 0.85 ± 0.01), whereas subsequently chemostatic behavior is observed (slope = 0.09 ± 0.01). The slopes of the segmented regression for the TLF data were significantly different from one another, as analyzed with a Davies test ($P < 0.001$). For the HLF dataset, no chemostatic behavior threshold was reached and a breakpoint in the C-Q relationship occurred earlier at 0.46 ± 0.01 $m^3 s^{-1}$. Slopes of the segmented regression for the HLF dataset were also found to be significantly different using a Davies test ($P < 0.001$).

When ranking models using AIC, the segmented models were found to fit the C-Q relationship better than the linear models for both the TLF and HLF datasets. For the TLF data, the linear model had an AIC of -42355 compared to -46983 for the segmented model, while for HLF data, the linear model had an AIC of -55991 compared to -70403 for the segmented model.

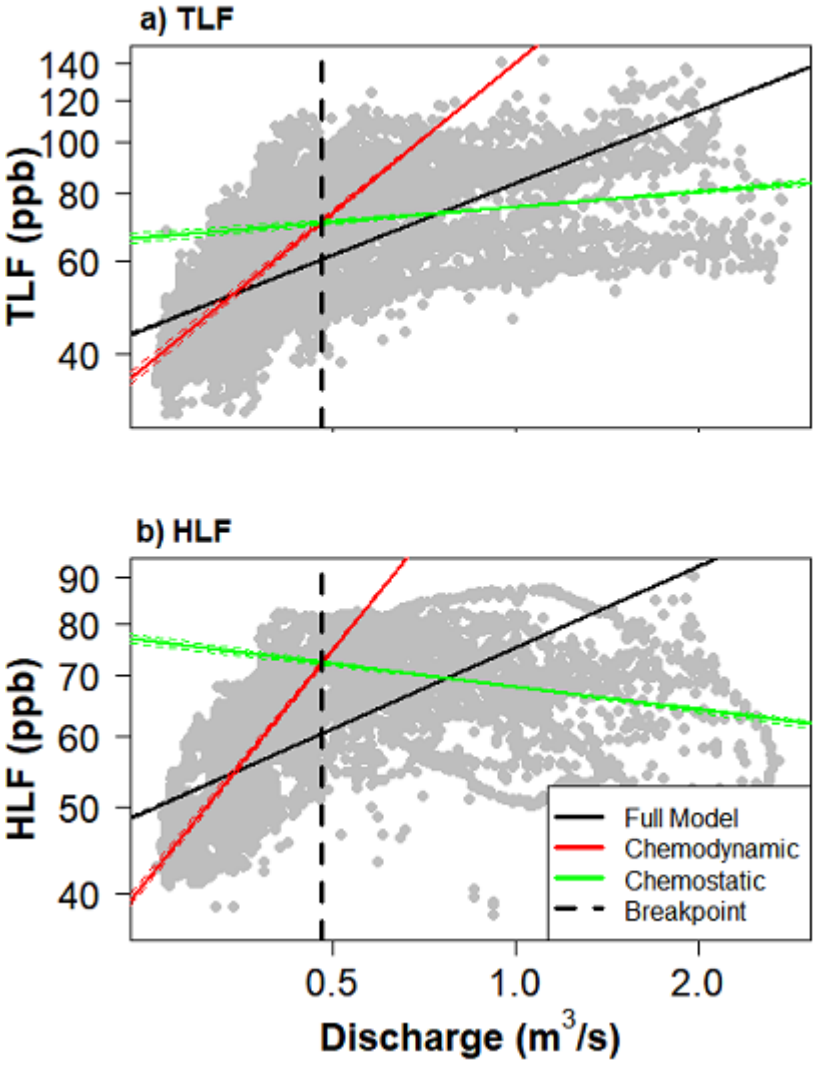

Figure 5.3. Log C-Q relationship for a) TLF against discharge and b) HLF against discharge. Overall C-Q relationships for the dataset are indicated by the black lines, red lines show the chemodynamic portion of the dataset, and green lines show the chemostatic. The breakpoint line indicates where the relationship changes from chemodynamic to chemostatic.

5.4.2.2 Hysteresis Analysis

Four forms of hysteresis were observed during the study period (Figure 5.4). A HI between -0.1 and 0.1 was most commonly observed for both the HLF (11 events) and TLF (8 events) datasets (Table 5.4). An HI of < -0.1 (indicating anti-clockwise hysteresis) was found for 8

events for TLF, and for 9 events for HLF. An event HI of > 0.1 (clockwise hysteresis), was found 6 times for the TLF dataset, but only two times for the HLF dataset.

After visual inspection, figure of eight hysteresis was determined to be the most common class in both datasets, followed by anti-clockwise, with clockwise hysteresis occurring far less frequently for both datasets (Table 5.4). While the hysteresis ratio suggested clockwise hysteresis, events were the most frequent, most clockwise and anti-clockwise hysteresis events were reclassified as figure of eight hysteresis following visual inspection. Complex hysteresis was also common in both datasets and tended to occur during storm events with multiple discharge peaks on the rising limb of the event.

Table 5.4. HI ratio shows categories for individual events for both TLF and HLF. The hysteresis categories were split as follows: >0.1 (indicating clockwise hysteresis), -0.1-0.1 (indicating no hysteresis), and < -0.1 (indicating anti-clockwise hysteresis). Hysteresis type shows the categorization of events into the four defined hysteresis categories. Hysteresis type was determined by visual inspection as a means of best identifying figure of eight hysteresis.

	HI Ratio			**Hysteresis Type**			
	>0.1	**0.1 to -0.1**	**< -0.1**	**Clockwise**	**Anti-Clockwise**	**Figure of Eight**	**Complex**
TLF	6	8	8	2	7	8	5
HLF	2	11	9	0	8	9	5

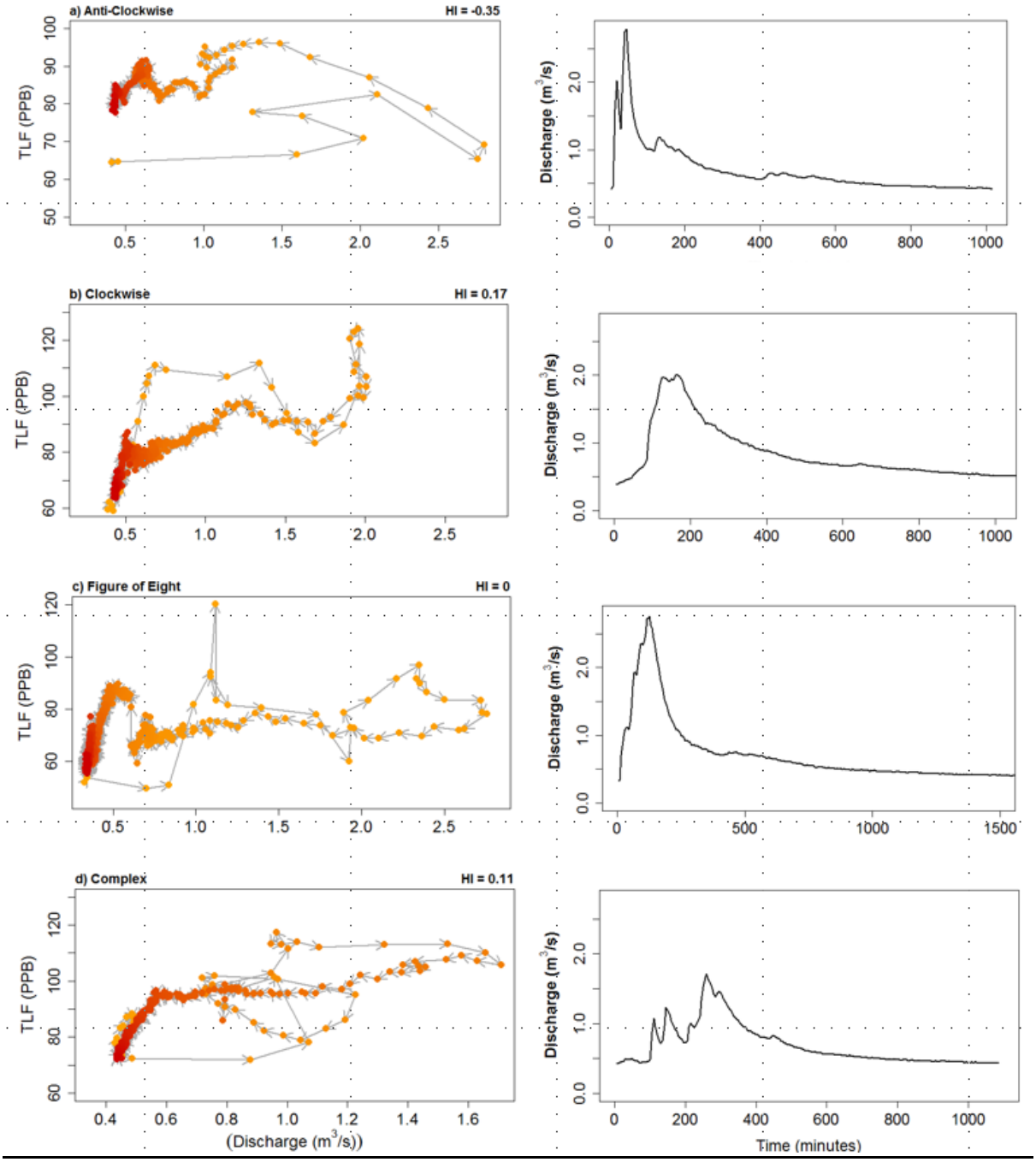

Figure 5.4. Examples of the hysteresis types observed during the study period, with event-hydrograph shown to the right of each hysteresis type. Color of the data points relates to the progression of the event (yellow = event start, red = event end), whilst arrows show direction of hysteresis. The associated HI scores are shown for each graph.

5.4.3 Landscape and hydrometeorological controls

Water Temperature was found to be the most common predictor of maximum change in

TLF and HLF, featuring in all possible model combinations (Table 5.5), with WT positively

correlated with maximum TLF and HLF in all cases. For both maximum TLF and HLF, only one model combination was identified (Table 5.5). For mean TLF: HLF ratio, event magnitude and road density were found to be significant predictors and the most commonly featured variables in the top models (Table 5.5). Peak flow (PF) was found to be the most regular candidate variable and was also a significant predictor in TLF and HLF HI models (Table 5.5). For TLF, HI peak flow featured in 17 of 20 model combinations (Table 5.5), while for the HLF HI model peak flow featured in all three combinations. For the percentage change metrics, the seven-day antecedence predictor featured in all possible model combinations (Table 5.5). In all cases seven-day antecedent rainfall had a significant ($P < 0.05$) negative relationship with maximum TLF and HLF percentage change. Mean rainfall intensity (MeI) also featured commonly in percentage change metric models and featured in the best model for maximum HLF (Table 5.5), with positive relationships observed for both metrics.

Hydrometeorological variables were the dominant variables featuring in models for the fluorescence metrics and were included in all the best fitting models shown (Table 5.5). In contrast land use metrics were found to feature in models for three of the seven fluorescence metrics. Within the land use metrics, only vegetation (VE) and road density (RD) were found in the model combinations (Table 5.5), with road density the only variable featuring in a best model (Table 5.5). Notably, both vegetation and road density featured in model combinations for the maximum percentage TLF change where they were significant ($P < 0.05$) predictors, but not for the maximum percentage HLF change. Where land use variables did feature, road density showed a positive trend with TLF metrics, while vegetation showed a negative trend.

Table 5.5. Model coefficients for best model for each metric in Table 5.3. Number of models (N) that each predictor variable featured in for models <2 AICc of top model is also shown for each fluorescence metric (see Table 5.6 in supplementary material for full list of competing models). Only predictors significant in at least one the best models are shown. A full list of predictors is found in Table 5.2. $^{*}P < 0.05$, $^{**}P < 0.01$, $^{***}P < 0.001$.

	Predictor								
Response	**PF**	**Mel**	**WT**	**1A**	**7A**	**EM**	**RD**	**Ve**	**R^2**
Max TLF			6.06 ± 2.29 N = 1		-1.28 ± 0.33 N = 1				0.46**
Max HLF		15.62 ± 7.78 N =1	7. ± 2.91 N =1						0.21*
Mean TLF:HLF ratio			N =1	N =2		-0.12 ± 0.05 N =4	-0.33 ± 0.17 N = 3		0.23*
TLF HI	0.13 ± 0.06 N = 17	N = 5	N = 3	N = 10	N = 4	N =4	N =2	N =2	0.17*
HLF HI	0.18 ± 0.06 N = 3	-0.13 ± 0.11 N = 3	N = 2	N = 1					0.20*
Max TLF increase (%)	N = 2	N = 4	N = 2		-4.87 ± 0.72 N = 7		N = 1	N = 1	0.68***
Max HLF increase (%)		18.53 ± 5.99 N = 2		N = 1	-1.27 ± 0.33 N = 2				0.69***

5.5 Discussion & Conclusions

5.5.1 Controls on DOM concentration

We found that TLF and HLF responses were chemodynamic when discharge was below a certain threshold, suggesting that small events may have a disproportionately large impact on DOM dynamics. Urban catchments have particularly strong terrestrial-riverine linkages, with drainage systems activating at relatively low precipitation totals (McGrane, 2016). Consequently, even minor events (<1mm) can lead to noticeable fluxes in both TLF and HLF (Kaushal and Belt, 2012). The strong changes in TLF and HLF at low discharge suggest that significant sources of organic fluorophores, contributing to TLF and HLF, are located either close to the channel or in-stream. Previous studies have indicated that storm drain biofilms are particularly rich sources of DOM, while road runoff is also likely to also provide an elevated DOM pulses (Zhao et al., 2015). Stream bed scouring has also been proposed as an important DOM source during storm events with benthic algae and biofilms transported (Khamis et al., 2018; Kaushal and Belt, 2012). The chemostatic nature of the relationship at higher discharges is likely a result of a variety of factors. To a large extent, it is a dilution effect, whereby increased runoff from flow pathways carrying DOM are counteracted by low DOM precipitation inputs, leading to a relatively steady chemostatic relationship. As a result, the high HLF and TLF concentrations at low discharges are likely to be a result of anti-clockwise hysteresis as they were mainly apparent on the falling limb of storms, as has previously been observed by Evans and Davies (1998). It should also be noted that the range of values observed at high discharges is very high, indicating that events of similar magnitude have a substantially different response in DOM concentration. This suggests that antecedent conditions may be a major control of DOM dynamics at high discharges

(Guarch-Ribot and Butturini, 2016; Yates et al., 2016). Where antecedent conditions are wetter, new flow paths have been found to emerge from the wider catchment, which create new potential sources of DOM within the drainage network (Haga et al., 2005). For example, after wetter antecedent conditions CSOs are more likely to be activated which means material usually transported to the sewerage system is instead transported to the river system.

The hysteresis analysis identified a range of hysteresis types in the catchment. Figure of eight hysteresis was most commonly observed for both TLF and HLF. The frequency of figure of eight hysteresis supports the results of the C-Q relationship. As discharge increases from initially low values, clockwise hysteresis occurs, possibly as in- or near-stream DOM sources are activated (Blaen et al., 2017), while at higher discharges, anti-clockwise hysteresis occurs as a result of the changing relationship between discharge and DOM (Lloyd et al., 2016a). This is possibly due to source depletion from the near-stream sources that are activated first during storm flow (Lawler et al., 2006).

It would appear that the fluorophores contributing to TLF are more prone to source depletion, whereas HLF tends to remain elevated even at long timescales after return to baseflow suggesting a long-term input from distal sources (Vaughan et al., 2017). This may indicate the importance of subsurface, slow flowing pathways which provide a steady and constant input of humic material as the main contributing source of HLF within the system. The compounds contributing to TLF meanwhile appear to be more related to more proximal sources, which reflects the influence of engineered structures on the TLF which tend to build up protein-like materials over time (Sakrabani et al., 2009), but are susceptible to exhaustion effects which can cause clockwise hysteresis. However, anti-clockwise hysteresis occurred regularly in both HLF

and TLF. Anti-clockwise hysteresis is suggestive of a lag between discharge rise and DOM activation, which suggests that distal pathways are in general a prominent source of DOM. The presence of anti-clockwise hysteresis may also result from the activation and cross-connections of CSOs, which are inactive at the beginning of the event and are activated only during heavy rainfall and when specific flow thresholds are exceeded (Chen et al., 2017).

5.5.2 Hydrometeorological and landscape controls on DOM dynamics

The study has highlighted that water temperature, peak flow and antecedent rainfall appear to be the dominant hydrometeorological drivers influencing urban DOM dynamics. Water temperature during events was found to be a strong predictor of maximum fluorescence values. The positive influence of water temperature on DOM and DOC dynamics has been observed previously with temperature having an important role in delivery and uptake (Winterdahl et al., 2011, 2016; Huang et al., 2013; Raymond et al., 2016). This is thought to be caused by higher temperatures driving increased algal production in streams during warmer parts of the year (Dawson et al., 2008). As our study ran from the start of autumn, it is likely that as the study progressed and temperatures decreased, biological activity within the stream also reduced, which reduced the amount of DOM within the systems even for storms of similar discharges (Raymond et al., 2016). TLF and HLF had higher values at the start of the study (early Autumn) and lower values at the end of the study period (late Autumn). The water temperature change within the study may therefore also represent the change in season. Hence, the reduced HLF and TLF values found for storms later during the study appear could be related to seasonal changes such as changes in leaf fall within early Autumn (Miller and

McKnight, 2010). Further, due to the large amount of rainfall events it is likely that significant source depletion occurred over the duration of the study.

The TLF and HLF HI were linked to the peak flow, with higher peak flows generally corresponding to more positive HI values. This provides further evidence of dilution effects being a strong control on DOM dynamics at high discharge, as higher HI values indicate clockwise hysteresis (Lloyd et al., 2016b). Subsequently, during higher peak flows, the amount of material transported into the river is counteracted by dilution from high discharge. (Phillips and Chalmers, 2009; Kaushal et al., 2014). However, it is also possible that the link of HI to peak flow is related to source depletion for bigger events, where during the largest events TLF and HLF concentrations the bulk of availably material has been transported on the rising limb of the storm (Sakrabani et al., 2009).

Antecedent rainfall conditions featured in all models as a predictor of percentage changes in HLF and TLF, which is in line with numerous studies showing that antecedent conditions act to control nutrient dynamics (Grand-Clement et al., 2014; Gnecco et al., 2005; Blaen et al., 2017). This provides further evidence that source depletion is linked to antecedent conditions. Wetter antecedent periods lead to source depletion, with regular rainfall events leading to exhaustion of DOM within the catchment (Carstea et al., 2009). During drier conditions organic material builds up in the catchment and in the drainage network, which can then be mobilized during events (Guarch-Ribot and Butturini, 2016).

While hydrometeorological conditions appear to represent the dominant control on DOM dynamics, land use was found to play a subsidiary role. Road density occurred in more model

combinations than any of the other land use metrics and contributed to one best model. As road drainage is directly connected to storm drain systems, the percentage of roads in the catchment provides a useful proxy for storm drain flow paths (Brabec et al., 2002). It is therefore likely a better proxy for urbanization and the density of urban infrastructure than impermeable surface cover. Roads are also a prominent source of DOM derived from the wider catchment, with petroleum spills and road dust build up representing two of the biggest urban terrestrial sources of DOM that are activated during storms (Krein and Schorer, 2000; McElmurry et al., 2014). Catchment vegetation was the only other land use variable to feature in the models. Vegetation generally featured in models for TLF, where a negative relationship with TLF was shown. This likely reflects that when vegetated areas provide higher amounts of material during storms, there is reduced impact from the engineered terrestrial sources that tend to be associated with higher TLF (Fork et al., 2018; Kaushal et al., 2014). Generally, for the HLF metrics, the land use variables were much less likely to appear as predictors. This may be because HLF in the urban environment tends to be formed from a wide range of both natural and anthropogenic sources and flow paths (Khamis et al., 2018), which is difficult to resolve using land use data alone. In contrast, the bulk of the sources contributing to TLF tend to be within the engineered network, which land use metrics appear to be able to more effectively identify.

5.5.3 Conclusions and future research

The study highlighted the main controls on DOM event dynamics and explored the links to sources and transport mechanisms. We identified how an urban stream behaves chemodynamically at lower discharge, but at higher discharge source depletion and dilution

lead to the system becoming chemostatic. The relatively low discharge required for large increases in DOM suggested inputs of terrestrial DOM to the stream are likely to represent regular, recurrent events regardless of event size. Hence current management techniques to reduce peak flow magnitude for flood control are likely to be ineffective in moderating inputs of terrestrial DOM. Further, we highlighted the potential importance of water temperature in controlling overall urban DOM dynamics. However, when standardizing storm changes in HLF and TLF to percentages, antecedent conditions seemed to exert as a particularly strong control on DOM availability. This suggests source depletion is a predominant driving mechanism of DOM dynamics in urban systems. We also showed that hydrometeorological controls were generally much stronger than land use controls. However, road density, which acts as a surrogate for more urban, engineered infrastructure was shown to be a potentially useful predictor of in-stream DOM dynamics. The controls influencing TLF were also shown to be different to the controls on HLF. The compounds contributing to TLF appeared to be more vulnerable to source depletion and exhaustion effects than HLF. We suggest this reflects that TLF is generally influenced by proximal engineered sources vulnerable to exhaustion effects, whereas a wider array of sources contribute to HLF, with vegetated areas providing inputs of slow, subsurface humic-rich waters which are less vulnerable to exhaustion effects.

Further research is required to explore the links between urban land use and DOM dynamics more fully. There is a need develop longer datasets that capture a greater range of event types to further investigate the degree of influence of land use on DOM dynamics. In conjunction with this, a wider gradient of land use over greater spatial scales, different landscape metrics (for example infrastructure age) and differing catchment types over differing latitudes and

climatic gradients are required to further strengthen or contrast our conclusions. Identification of the effectiveness of preventing degradation of DOM quality by sustainable urban drainage systems (SUDS) and other drainage interventions used to mitigate water quality issues is vital in order to better suggest remediation solutions for DOM in urban areas. Furthermore, monitoring networks with a higher spatial density of *in-situ* monitoring nodes are imperative to improve and strengthen mechanistic understanding of the linkages between DOM sources and in-stream response. This will enable better assessment of the role of catchment properties in modulating these relationships.

5.6 Supplementary Material

Table 5.6. Multiple linear regression models using ordinary least square for each fluorescence metric (Table 5.3). All models < 2 ΔAICc of the top model are presented. Candidate variables code refers to codes stated in Table 5.2.

Response	Candidate variables code	k	AICc	ΔI	Weight
Max TLF	7A + WT	4	186.10	0	0.22
Max HLF	MeI + WT	4	138.21	0	0.19
Mean TLF:HLF ratio	RD + EM	4	-20.90	0	0.09
	RD + EM + WT	5	-19.94	0.96	0.05
	RD + EM + 1A	5	-19.89	1.01	0.05
	EM + 1A	4	-19.26	1.64	0.04
TLF HI	PF + 1A	4	-1.86	0	0.08
	PF	3	-1.77	0.08	0.08
	MeI + PF + 1A	5	-1.62	0.23	0.07
	MeI + PF	4	-0.60	1.25	0.04
	RD + PF + 1A	5	-0.24	1.62	0.04
	EM + PF	4	0.51	2.36	0.02
	VE + PF + 1A	5	0.52	2.38	0.02
	VE + PF	4	0.60	2.46	0.02
	RD + PF	4	0.64	2.50	0.02
	EM + PF + 1A	5	0.67	2.52	0.02
	MeI + PF + 1A + WT	6	0.77	2.63	0.02
	1A	3	1.01	2.87	0.02
	PF + WT	4	1.02	2.87	0.02

	PF + 7A	4	1.10	2.95	0.02
	PF + 1A + 7A	5	1.29	3.15	0.02
	Mel + PF + 7A	5	1.35	3.20	0.02
	PF + 1A + WT	5	1.45	3.30	0.02
	EM	3	1.53	3.38	0.01
	7A	3	1.58	3.44	0.01
	Mel + EM + PF + 1A	6	1.77	3.63	0.01
HLF HI	Mel + PF + WT	5	-27.82	0	0.13
	Mel + PF	4	-27.09	0.73	0.09
	Mel + PF + 1A + WT	6	-26	1.82	0.05
Max TLF increase (%)	Mel + 7A	4	216.78	0	0.11
	PF + 7A	4	217.22	0.43	0.09
	PF + 7A + WT	5	217.80	1.01	0.07
	7A	3	217.94	1.16	0.06
	Mel + 7A + WT	5	218.34	1.56	0.05
	Mel + VE + 7A	5	218.43	1.65	0.05
	Mel + PF + 7A	5	218.55	1.77	0.03
Max HLF increase (%)	Mel + 7A	4	178.91	0	0.29
	Mel + 1A + 7A	5	180.69	1.78	0.12

CHAPTER 6: CONCLUSIONS AND SYNTHESIS

6.1 Conclusions

The research presented in this thesis aimed to improve understanding of the effects of urbanization and extreme events on river water quality with specific focus on water temperature and DOM. The research was conducted in urbanized, headwater catchments in Birmingham UK. The main aims of the study were addressed as follows:

1) Water temperature surges were observed in an urbanized headwater catchment. Precipitation intensity and the difference between air temperature and water temperature best predicted water temperature surges. This suggests that the prime conditions for water temperature surge events are high-intensity precipitation events on days when air temperature is substantially higher than water temperature. The surge events were predicted best by catchment averaged precipitation data rather than the more commonly-used point-source data. Catchment-averaged precipitation measured with rainfall radar was a stronger predictor of water temperature surges than the other precipitation datasets (i.e. based on official and citizen-science rain gauges), likely because it best captures the high spatial and temporal variability of precipitation (Chapter 2).

2) Daily water temperature anomalies were significantly higher during low flow events compared to average flow and high flow events, but no significant differences were found between average flow and high flow events. The metrics that best predicted daily water temperature anomalies during low flow events were those related to urbanization: road buffer percentage and urban land use in a 1km buffer. Both metrics had a negative relationship with

temperature anomalies suggesting urbanization is associated with reduced water temperature change during low flow. During high flow events, the metric that best predicted water temperature anomalies was elevation, which may be a proxy of river discharge and distance from source which indicates water temperature changes during high flows mostly occur in lower order rivers (Chapter 3)

3) Flume experiments showed shading of urban streams alters DOM composition over sub-daily timescales. Shading prevents photodegradation which stops removal and transformation in the fluorescing humic component of DOM over daily timescales. However, shading had minimal effect on degradation of the proteinaceous component of DOM. Extreme temperature events had minimal impact on photodegradation and biodegradation rates over sub-daily timescales. At sub-daily scales photodegradation appears to be the main removal and transformation process in urban streams, however this is altered through practices such as stream burial (Chapter 4).

4) In an urban headwater stream, TLF (Tryptophan-like fluorescence) and HLF (Humic-like fluorescence) were strongly chemodynamic at low discharges and chemostatic for TLF and weakly chemodynamic for HLF at higher discharges. This suggests that DOM in headwater urban rivers is strongly influenced by dilution effects and source depletion. Consequently, small events often had as large increases in TLF and HLF as large events. Figure of eight hysteresis was the dominant hysteresis type for both TLF and HLF, which suggests that the contributing sources of DOM shift throughout events. The main predictors of HLF and TLF were water temperature, which likely represents the increased microbial activity with higher temperature and the effects of changes in DOM inputs leaf fall in autumn, and antecedent rainfall

conditions, which suggests urban headwater systems experience exhaustion effects. Landscape metrics were weaker predictors of DOM dynamics. Only road density was identified as important, probably acting as a proxy of the storm drain system with denser storm drain systems contributing more DOM (Chapter 5).

6.2 Discussion

The research in chapter two identifies water temperatures surges in UK headwater sites. These temperature surges have not regularly been recognized in a temperate maritime climate. The study provides evidence of experimental work showing impermeable surfaces can cause heating of surface runoff due to heat transfer from low-specific heat capacity surfaces (Herb et al., 2008). Chapter two also highlights the importance of the temporal and spatial resolution of precipitation data to adequately quantify the surge effect. Whereas previous studies have identified surges as a result of thermal dissipation downstream (Somers et al., 2016; Wilby et al., 2015), chapter two proposes spatial variation of storms is the main governing process of temperature surges. This implies water quality studies should consider the spatial and temporal variation of measured variables in order to better represent water quality processes.

The potential for urbanization to influence water temperature was demonstrated in chapter two. Building on this, the impacts of extreme events and land use on river temperature over daily timescales was discussed in chapter three. Increased water temperature at low discharges were found, however no significant differences in water temperature between high flow and average flow were identified likely because the increased thermal capacity during higher flows reduces the likelihood of temperature anomalies. Urbanization was associated

with reduced water temperature during low flows, although urbanization has been linked to increased water temperature elsewhere (Kaushal et al., 2010; Wagner et al., 2017; McGrane, 2016). From the results, it was suggested that urbanization alters the main processes governing water temperature at low flows. This may occur by reducing the atmospheric influence on streams through urban infrastructure like stream burial while inputs from pipe leakages may also moderate water temperature at baseflow in urban streams.

Chapter four considered the impacts of stream infrastructure (through stream burial) and extreme water temperatures on photodegradation and biodegradation of DOM. The research in chapter four confirmed findings from field experiments by showing that the humic-like component of DOM was the most prone to photodegradation, with this process inhibited by stream burial (Arango et al., 2017; Beaulieu et al., 2014). Although temperature has previously been identified to accelerate biodegradation processes through increasing microbial activities (Mao and Li, 2018), over the timescale of this study, high water temperatures had minimal effects on photodegradation and biodegradation rates. This suggests that land use change that alters shading, such as stream burial, has a larger influence on photodegradation and biodegradation than temperature.

After chapter four identified the main autochthonous processes acting on DOM, chapter five focused on the allochthonous processes contributing to DOM in urban areas during storm events. The C-Q (concentration-discharge) relationships developed for TLF and HLF confirm previous work for other nutrients (Blaen et al., 2016; Bieroza et al., 2018). The chemostatic behavior developing after initial chemodynamic behavior provides evidence for the source-limitation theory put forward in previous DOM studies (Fork et al., 2018; Khamis et al., 2018),

while it also suggests dilution effects at high discharge. Further, the identification of temperature and antecedent rainfall as predominant drivers of DOM dynamics provides evidence for the importance of biological activity (for example, increased algal activity at higher temperatures contributes more DOM) and exhaustion effects as key controls on DOM dynamics (Kaushal et al., 2014; Gnecco et al., 2005; Miller and McKnight, 2010). Landscape was less of a control than hydrometeorological effects but some land use metrics such as road density may be useful proxies of the influence of land use on DOM pathways.

The thesis further identified that water quality dynamics in urban headwaters differ substantially to those reported in previous studies for rural headwaters. The response of water quality variables to extreme events were more pronounced in the urban headwaters compared to previous studies on rural headwaters. For example, in rural catchments temperature surges were found to be much lower and inputs of DOM in natural streams were lower compared to the urban catchments in this thesis (Wilby et al., 2015). Urban headwaters are hence shown to be particularly sensitive to extreme high flow events, with subsequent increased influence on downstream reaches. For the low-flow events, urbanization led to lower water temperature anomalies compared to rural catchments (Wilbers et al., 2009), possibly due to increased underground connectivity due to pipe leakages and other point source outputs.

6.3 Synthesis & Implications

6.3.1 Urbanization and Extreme Events

Water quality degradation from urbanization hinders efforts at maintaining rivers as healthy ecosystems. In the UK, only 14% of rivers were defined as good ecological status in 2016 under

the EU Water Framework Directive, while 53% were defined as good chemical status (Environment Agency, 2018). Over 1000 water bodies in the UK were identified to have urban-related pollution problems. Diffuse pollution is responsible for 49% of missed water quality targets, while point source pollution accounts for 36% of missed water quality targets in the UK (DEFRA, 2012). Hence, despite the implementation of directives to improve water quality, it appears that urbanization has confounded most management attempts thus far.

Urbanization is difficult to develop management strategies for as the impacts of urbanization on water quality can be more diverse than often considered. The impact of urbanization on hydrological processes varies depending on the catchment characteristics. Urbanization is assumed to cause increased warming through removal of riparian vegetation, heated effluents, and increased stormwater runoff (Whitehead *et al.*, 2009; Hannah and Garner, 2015). However, urban infrastructure, such as stream burial and pipe leakage, may lead to reductions in stream temperature, although urban streams are still susceptible to storm surges. Many of the assumptions about the influence of urbanization on temperature such as increased temperatures from reduced riparian shading are not accurate for many urban catchments (Webb et al., 2008), particularly in the context of headwater catchments. Hence, grouping streams into "urban" is likely to be too general and may lead to contradictory conclusions in water quality studies. Developing effective management strategies for improving water quality in urban rivers is therefore likely to require catchment specific management strategies. To improve outcomes, identifying the main water quality variables affected by urbanization is required to better inform management efforts. Management practices for water quality

mitigation must further consider the potential trade-offs between different water quality variables when choosing stream restoration techniques.

The need to identify more targeted metrics that better characterize urbanization has been raised in the hydrological literature (Walsh et al., 2016). Despite the importance of engineered flow pathways in urban rivers (Kaushal and Belt, 2012), they are not well categorized by simple impermeable surface land cover metrics. To better identify the impacts of urbanization in rivers, several further land use metrics should be developed, in particular for stream burial cover. In this thesis, stream burial was observed to impact DOM dynamics and also speculated to impact water temperature, and it has been identified as a dominant control on urban stream processes (Arango et al., 2017). Buried stream metrics are difficult to develop however due to difficulties in identifying buried streams from aerial imagery, therefore buried stream coverage would likely require manual calculation. But it may yield important information to inform water quality studies. Furthermore, road density may represent a useful proxy of the storm drainage system that depicts a more accurate estimation of the engineered pathways than other measures of land cover (Blaszczak et al., 2019). From a hydrology perspective, river buffer land use is likely to be much more important for altering water quality processes than wider catchment land use (Jackson et al., 2015).

Urban environments are more susceptible to the effects of extreme events which poses a further barrier to achieving good water quality (Fletcher et al., 2013; Mosley, 2015). Floods are noted as a stronger immediate control on hydrological processes in urban rivers than other extreme events and from a biogeochemistry perspective they are far better studied (Miller and Hutchins, 2017). For example, high transport of polluting material from the catchment was

highlighted as a regular pulse disturbance to urban streams, with storm drains providing a direct pipeline from the catchment to the river (Raymond et al., 2016). However, although floods cause more immediate changes in processes, the prolonged nature of drought events means they alter hydrological processes over longer timespans (Van Loon, 2015). Recent research hence highlights the importance of studying droughts from a water quality perspective (Tilburg et al., 2015). The importance of drought as a water quality control is often overlooked as a contributor to the urban stream syndrome. The separation of extreme events such as floods and droughts can be problematic as the impacts of one can influence the other. For example, in this thesis dry antecedent periods were identified as a strong predictor of DOM dynamics in urban streams. Drought conditions are therefore influential on water quality response during storm events. Mitigation of extreme events is therefore required to reduce their impact on water quality in urban catchments. Hence for storm events, infrastructure that captures and slows down rainfall runoff in urban areas is required to better mitigate stormwater quality (Czemiel Berndtsson, 2010; Bliss et al., 2009; Razzaghmanesh et al., 2014). Increasing green infrastructure such as wetlands may also help to increase resilience to drought conditions by providing gradual releases of water to sustain baseflow (Güneralp et al., 2015). The prevention of urban sprawl has been highlighted elsewhere as imperative to reduce urban water quality degradation (Miller and Hutchins, 2017). The demands for urban growth often override water quality concerns however, hence management strategies in urban areas are often overwhelmed by urban sprawl.

The impacts of extreme events and urbanization on water quality are most severe in developing countries (Cohen, 2006). However, water quality is not well studied in developing nations,

although recently increasing attention has been focused on outreach and collaboration with developing regions (McMillan et al., 2016). Resultantly, results from developed regions are regularly used to inform policy in developing nations. The impact of urbanization on river temperature may be of particular interest to developing regions as increased river temperatures prompt microbial growth which increases disease risk (Karvonen et al., 2010), although the processes that lead to changes in water temperature in urban regions during extreme events may be different between developed and developing regions. Water temperature surges during storms are likely to combine with the high export of DOM to degrade water quality. This effect is likely to be exacerbated in developing regions, as 90% of sewage is discharged directly into water bodies (UN-Water, 2015). However, it is important to not over-generalize the applicability of results between regions, and further research on water quality in urban regions in developing countries is an urgent requirement.

6.3.2 Importance of High-Frequency Monitoring

Studies of storm events require high temporal resolution datasets in order to capture initial water quality dynamics (Fletcher et al., 2013). In this thesis, the largest change in water quality occurred at sub-hourly scales. The dominant processes acting on water quality were found to depend on the temporal resolution, for example storms cause water temperature surges at sub-hourly scales, but at daily scales their impact is minimal.

The development of high-frequency sensors is a means of providing higher temporal resolution datasets, while also increasing the potential for long-term deployment of sensors as they can be left *in-situ* (Halliday et al., 2015; Rode et al., 2016). High frequency sensors are more readily

available than previously, while developments in homemade sensors have also reduced instrumentation costs (Mao, Khamis, Krause, Clark, & Hannah, 2019). High-frequency datasets are highlighted as particularly required for monitoring water quality during extreme events when large changes in water quality often occur (Blaen et al., 2017). Furthermore, high-frequency datasets are a means of providing increased understanding of the processes influencing water quality dynamics. High-frequency sensors do usually require more maintenance therefore their benefits must be balanced with the need for regular upkeep (Rode et al., 2016). However, where available, *in-situ* high-frequency sensors should be considered by river managers to yield more meaningful monitoring data.

Renewed focus on the importance of long-term catchment-scale monitoring to understand hydrological processes has also been recently highlighted (Tetzlaff et al., 2017). Building longer datasets for water quality variables is crucial to understanding long-term variability and dynamics, however hydrological variables are often monitored for the duration of projects based on grant lengths and hence do not capture long-term trends and variability in processes (Shanley et al., 2018). Long water temperature datasets are sparse although water temperature is relatively easy to monitor *in-situ*, while extremely few long DOM datasets exists. Resultantly, more long site-specific datasets need to be developed, but maintenance and instrumentation costs have hindered progress. Nonetheless, development of long-term datasets is crucial to the development of evidence-based management strategies. To measure the long-term impact of water quality projects, long-term datasets provide the most useful form of evidence to evaluate the success of projects (Pinto et al., 2013).

Citizen science has been increasingly promoted as a means of maintaining long-term datasets and increasing the spatial density of data collection (Bonney et al., 2016). For variables like water temperature and precipitation where instrumentation is relatively simple and low maintenance, citizen science is most likely to be useful. As demonstrated in this thesis, citizen science rain gauges provide a means of increasing the spatial density of precipitation datasets for water quality studies, however issues with data quality may limit their usage. Maintaining the motivation of citizen scientists may also provide a barrier to providing long-term datasets (Conrad and Hilchey, 2011), therefore maintaining awareness is required for projects aiming to use citizen science. For more complex instrumentation, such as for DOM, citizen science is of minimal use due to difficulties in the maintenance of the instruments. Although relying on citizen science entirely is likely to be problematic, there is some value to be found in citizen science datasets. Increasing data coverage in data-sparse regions is one of the chief advantages of citizen science. Citizen science activity should therefore be further encouraged and promoted as a means of complementing long-term data records from other sources.

6.4 Future research suggestions

To build on the results of this study, which focused on headwater catchments, water quality monitoring from source to sea is crucial. The dominant processes controlling water quality dynamics are likely to shift with distance downstream due to changes in stream size, surrounding land uses, and catchment size (Foley et al., 2005; Pilgrim et al., 1982). This source-to-sea monitoring will allow identification of areas where extreme events often lead to water quality degradation, therefore informing where efforts for stream management and restoration should focus.

The understanding of when different flow paths activate and of residence time of water in different stores remains extremely limited, which has hindered efforts to increase understanding of water quality processes (Kaushal and Belt, 2012). Hence, future research should investigate flow-path activation and residence times and effects on urban water quality to build upon the results of this thesis. Tracer studies using conservative tracers are recommended to identify timing of flow path activation and these should be linked to high-frequency in-stream water-quality measurements to build greater confidence in our understanding of flow pathways and water quality dynamics.

To improve understanding of urban water quality dynamics, future research should also focus on a broader geographical range. Most previous research on water quality has been based in the developed world (Fletcher et al., 2013; Bhaskar et al., 2016), however the water quality dynamics and processes are likely to be highly variable between countries due to large differences in the characteristics and quality of urban infrastructure. In particular, countries with poorer infrastructure are likely to experience different responses during extreme events (Webster and Jian, 2011).

Having identified that storm events can lead to substantial changes in water quality, research on the relative impact of mitigation strategies to reduce water quality degradation is required. Currently, much of the proposed green infrastructure is designed around reducing surface runoff (Czemiel Berndtsson, 2010). The influence of green infrastructure on water quality is much less understood (Hashemi et al., 2015). To better inform future management strategies, evaluation of the best methods of stormwater mitigation for water quality variables is required.

Furthermore, as extreme events are likely to become more severe due to climate change and urbanization is going to continue (Güneralp et al., 2015), resultantly the impacts of extreme events on urban water quality are likely to become more severe in the future. To assess possible trends, future research should seek to develop long datasets for field sites in order to assess the long-term impact of extreme events and urbanization on water quality dynamics. Currently, research tends to revolve round relatively short studies, but these are ineffective at identifying long-term trends, which are required to better identify the global pressures on water quality arising from multiple stressors.

Future research should also consider the use of metabolomics as a tool to better understand the role of DOM composition in riverine ecology. Metabolomics offer a means of analyzing phenotypes using a range of tools. Mass spectrometry methods such as Liquid chromatography mass-spectrometry (LC-MS) and gas chromatography mass-spectrometry (GC-MS) offer a means of analyzing the entire metabolic network which allows for changing trends in metabolites to be identified (Burgess et al., 2014). Limited metabolomic work has currently been carried on DOM, however initial results have indicated that non-targeted metabolomics are capable of profiling metabolites in DOM and have been shown as useful as a means of exploring the link between land use and DOM complexity (Lynch et al., 2019). Future research involving metabolomics is therefore suggested as a means of complimenting the results in this thesis and allowing more precise characterization of DOM.

7.0 REFERENCES

Agency, E. (2019) *LIDAR Composite DTM - 1m*. Available at: https://data.gov.uk/dataset/6a117171-5c59-4c7d-8e8b-8e7aefe8ee2e/lidar-composite-dtm-1m (Accessed: 4 August 2019).

Alexander, M.D. and Caissie, D. (2003) Variability and comparison of hyporheic water temperatures and seepage fluxes in a small Atlantic salmon stream. *Ground Water*, 41 (1): 72–82. doi:10.1111/j.1745-6584.2003.tb02570.x.

Anderson, W.P., Anderson, J.L., Thaxton, C.S., et al. (2010) Changes in stream temperatures in response to restoration of groundwater discharge and solar heating in a culverted, urban stream. *Journal of Hydrology*, 393 (3–4): 309–320. doi:10.1016/j.jhydrol.2010.08.030.

Arango, C.P., Beaulieu, J.J., Fritz, K.M., et al. (2017) Urban infrastructure influences dissolved organic matter quality and bacterial metabolism in an urban stream network. *Freshwater Biology*, 62 (11): 1917–1928. doi:10.1111/fwb.13035.

Arora, R., Toffolon, M., Tockner, K., et al. (2018) Thermal discontinuities along a lowland river: The importance of urban areas and lakes. *Journal of Hydrology*, 564: 811–823. doi:10.1016/J.JHYDROL.2018.05.066.

Baines, S.B. and Pace, M.L. (1991) The production of dissolved organic matter by phytoplankton and its importance to bacteria: Patterns across marine and freshwater systems. *Limnology and Oceanography*, 36 (6): 1078–1090. doi:10.4319/lo.1991.36.6.1078.

Baker, A. (2001) Fluorescence excitation-emission matrix characterization of some sewage-impacted rivers. *Environmental Science & Technology*, 35 (5): 948–53. Available at: http://www.ncbi.nlm.nih.gov/pubmed/11351540 (Accessed: 6 December 2018).

Baker, A., Bolton, L., Newson, M., et al. (2008) Spectrophotometric properties of surface water dissolved organic matter in an afforested upland peat catchment. *Hydrological Processes*, 22 (13): 2325–2336. doi:10.1002/hyp.6827.

Baker, A. and Inverarity, R. (2004) Protein-like fluorescence intensity as a possible tool for determining river water quality. *Hydrological Processes*, 18: 2927–2945. doi:10.1002/hyp.5597.

Baker, A., Inverarity, R., Charlton, M., et al. (2003) Detecting river pollution using fluorescence spectrophotometry: case studies from the Ouseburn, NE England. *Environmental Pollution*, 124 (1): 57–70. doi:10.1016/S0269-7491(02)00408-6.

Baker, A., Ward, D., Lieten, S.H., et al. (2004) Measurement of protein-like fluorescence in river and waste water using a handheld spectrophotometer. *Water Research*, 38 (12): 2934–2938. doi:10.1016/j.watres.2004.04.023.

Ball, J.E. and Luk, K.C. (1998) Modeling Spatial Variability of Rainfall over a Catchment. *Journal of Hydrologic Engineering*, 3 (2): 122–130. doi:10.1061/(ASCE)1084-0699(1998)3:2(122).

Barthel, R., Seidl, R., Nickel, D., et al. (2016) Global change impacts on the Upper Danube

Catchment (Central Europe): a study of participatory modeling. *Regional Environmental Change*, 16 (6): 1595–1611. doi:10.1007/s10113-015-0895-x.

Beaulieu, J.J., Mayer, P.M., Kaushal, S.S., et al. (2014) Effects of urban stream burial on organic matter dynamics and reach scale nitrate retention. *Biogeochemistry*, 121 (1): 107–126. doi:10.1007/s10533-014-9971-4.

Beggs, K.M.H. and Summers, R.S. (2011) Character and Chlorine Reactivity of Dissolved Organic Matter from a Mountain Pine Beetle Impacted Watershed. *Environmental Science & Technology*, 45 (13): 5717–5724. doi:10.1021/es1042436.

Berne, A., Delrieu, G., Creutin, J.-D., et al. (2004) Temporal and spatial resolution of rainfall measurements required for urban hydrology. *Journal of Hydrology*, 299 (3–4): 166–179. doi:10.1016/J.JHYDROL.2004.08.002.

Bhaskar, A.S., Beesley, L., Burns, M.J., et al. (2016) Will it rise or will it fall? Managing the complex effects of urbanization on base flow. *Freshwater Science*, 35 (1): 293–310. doi:10.1086/685084.

Bieroza, M.Z., Heathwaite, A.L., Bechmann, M., et al. (2018) The concentration-discharge slope as a tool for water quality management. *Science of The Total Environment*, 630: 738–749. doi:10.1016/J.SCITOTENV.2018.02.256.

Biggs, E.M. and Atkinson, P.M. (2011) A comparison of gauge and radar precipitation data for simulating an extreme hydrological event in the Severn Uplands, UK. *Hydrological Processes*, 25 (5): 795–810. doi:10.1002/hyp.7869.

Blaen, P.J., Khamis, K., Lloyd, C., et al. (2017) High-frequency monitoring of catchment nutrient exports reveals highly variable storm event responses and dynamic source zone activation. *Journal of Geophysical Research: Biogeosciences*, 122 (9): 2265–2281. doi:10.1002/2017JG003904.

Blaen, P.J., Khamis, K., Lloyd, C.E.M., et al. (2016) Real-time monitoring of nutrients and dissolved organic matter in rivers: Capturing event dynamics, technological opportunities and future directions. *Science of The Total Environment*, 569–570: 647–660. doi:10.1016/J.SCITOTENV.2016.06.116.

Blaszczak, J.R., Delesantro, J.M., Zhong, Y., et al. (2019) Watershed urban development controls on urban streamwater chemistry variability. *Biogeochemistry*, 144 (1): 61–84. doi:10.1007/s10533-019-00572-7.

Bliss, D.J., Neufeld, R.D., Ries, R.J., et al. (2009) Storm Water Runoff Mitigation Using a Green Roof. *ENVIRONMENTAL ENGINEERING SCIENCE*, 26 (2). doi:10.1089/ees.2007.0186.

Blöschl, G., Bierkens, M.F.P., Chambel, A., et al. (2019) Twenty-three unsolved problems in hydrology (UPH) – a community perspective. *Hydrological Sciences Journal*, 64 (10): 1141–1158. doi:10.1080/02626667.2019.1620507.

Bond, N.R., Lake, P.S. and Arthington, A.H. (2008) The impacts of drought on freshwater

ecosystems: An Australian perspective. *Hydrobiologia*. doi:10.1007/s10750-008-9326-z.

Bonney, R., Phillips, T.B., Ballard, H.L., et al. (2016) Can citizen science enhance public understanding of science? *Public Understanding of Science*, 25 (1): 2–16. doi:10.1177/0963662515607406.

Borisover, M., Laor, Y., Parparov, A., et al. (2009) Spatial and seasonal patterns of fluorescent organic matter in Lake Kinneret (Sea of Galilee) and its catchment basin. *Water Research*, 43 (12): 3104–3116. doi:10.1016/J.WATRES.2009.04.039.

Bowes, M.J., Jarvie, H.P., Halliday, S.J., et al. (2015) Characterising phosphorus and nitrate inputs to a rural river using high-frequency concentration–flow relationships. *Science of The Total Environment*, 511: 608–620. doi:10.1016/J.SCITOTENV.2014.12.086.

Brabec, E., Schulte, S. and Richards, P.L. (2002) Impervious Surfaces and Water Quality: A Review of Current Literature and Its Implications for Watershed Planning. *Journal of Planning Literature*, 16 (4): 499–514. doi:10.1177/088541202400903563.

Brack, W., Dulio, V., Ågerstrand, M., et al. (2017) Towards the review of the European Union Water Framework management of chemical contamination in European surface water resources. *Science of the Total Environment*. 576 pp. 720–737. doi:10.1016/j.scitotenv.2016.10.104.

Braud, I., Fletcher, T.D. and Andrieu, H. (2013) Hydrology of peri-urban catchments: Processes and modelling. *Journal of Hydrology*, 485: 1–4. doi:10.1016/j.jhydrol.2013.02.045.

Brett, M.T., Bunn, S.E., Chandra, S., et al. (2017) How important are terrestrial organic carbon inputs for secondary production in freshwater ecosystems? *Freshwater Biology*, 62 (5): 833–853. doi:10.1111/fwb.12909.

Brown, L.E. and Hannah, D.M. (2007) Alpine Stream Temperature Response to Storm Events. *Journal of Hydrometeorology*, 8 (4): 952–967. doi:10.1175/JHM597.1.

Bunn, S.E. (1986) *Origin and Fate of Organic Matter in Australian Upland Streams*. In Springer, Dordrecht. pp. 277–291. doi:10.1007/978-94-009-4820-4_17.

Van Buren, M.A., Watt, W.E., Marsalek, J., et al. (2000) Thermal enhancement of stormwater runoff by paved surfaces. *Water Research*, 34 (4): 1359–1371. doi:10.1016/S0043-1354(99)00244-4.

Burgess, K., Rankin, N. and Weidt, S. (2014) "Metabolomics." In *Handbook of Pharmacogenomics and Stratified Medicine*. Elsevier Inc. pp. 181–205. doi:10.1016/B978-0-12-386882-4.00010-4.

Bushaw, K.L., Zepp, R.G., Tarr, M.A., et al. (1996) Photochemical release of biologically available nitrogen from aquatic dissolved organic matter. *Nature*, 381: 404–407. doi:10.1038/381404a0.

Buytaert, W., Zulkafli, Z., Grainger, S., et al. (2014) Citizen science in hydrology and water resources: opportunities for knowledge generation, ecosystem service management, and sustainable development. *Frontiers in Earth Science*, 2: 26. doi:10.3389/feart.2014.00026.

Caissie, D. (2006) The thermal regime of rivers: a review. *Freshwater Biology*, 51 (8): 1389–1406. doi:10.1111/j.1365-2427.2006.01597.x.

Carstea, E.M., Baker, A., Bieroza, M., et al. (2010) Continuous fluorescence excitation–emission matrix monitoring of river organic matter. *Water Research*, 44 (18): 5356–5366. doi:10.1016/j.watres.2010.06.036.

Carstea, E.M., Baker, A., Pavelescu, G., et al. (2009) Continuous fluorescence assessment of organic matter variability on the Bournbrook River, Birmingham, UK. *Hydrological Processes*, 23 (13): 1937–1946. doi:10.1002/hyp.7335.

Catalán, N., Casas-Ruiz, J.P., von Schiller, D., et al. (2017) Biodegradation kinetics of dissolved organic matter chromatographic fractions in an intermittent river. *Journal of Geophysical Research: Biogeosciences*, 122 (1): 131–144. doi:10.1002/2016JG003512.

Challis, J.K., Hanson, M.L., Friesen, K.J., et al. (2014) A critical assessment of the photodegradation of pharmaceuticals in aquatic environments: defining our current understanding and identifying knowledge gaps. *Environmental Science: Processes & Impacts*, 16 (4): 672. doi:10.1039/c3em00615h.

Chang, H. and Psaris, M. (2013) Local landscape predictors of maximum stream temperature and thermal sensitivity in the Columbia River Basin, USA. *Science of The Total Environment*, 461–462: 587–600. doi:10.1016/j.scitotenv.2013.05.033.

Chen, H., Liao, Z., Gu, X., et al. (2017) Anthropogenic Influences of Paved Runoff and Sanitary Sewage on the Dissolved Organic Matter Quality of Wet Weather Overflows: An Excitation–Emission Matrix Parallel Factor Analysis Assessment. *Environmental Science & Technology*, 51 (3): 1157–1167. doi:10.1021/acs.est.6b03727.

Coble, A.A., Marcarelli, A.M., Kane, E.S., et al. (2016) Temporal patterns of dissolved organic matter biodegradability are similar across three rivers of varying size. *Journal of Geophysical Research: Biogeosciences*, 121 (6): 1617–1631. doi:10.1002/2015JG003218.

Coble, P.G. (1996) Characterization of marine and terrestrial DOM in seawater using excitation-emission matrix spectroscopy. *Marine Chemistry*, 51 (4): 325–346. doi:10.1016/0304-4203(95)00062-3.

Cohen, B. (2006) Urbanization in developing countries: Current trends, future projections, and key challenges for sustainability. *Technology in Society*, 28 (1–2): 63–80. doi:10.1016/J.TECHSOC.2005.10.005.

Conrad, C.C. and Hilchey, K.G. (2011) A review of citizen science and community-based environmental monitoring: issues and opportunities. *Environmental Monitoring and Assessment*, 176 (1–4): 273–291. doi:10.1007/s10661-010-1582-5.

Constantz, J. (1998) *Interaction between stream temperature, streamflow, and groundwater exchanges in alpine streams*. doi:10.1029/98WR00998.

Countway, R.E., Dickhut, R.M. and Canuel, E.A. (2003) Polycyclic aromatic hydrocarbon (PAH)

distributions and associations with organic matter in surface waters of the York River, VA Estuary. *Organic Geochemistry*, 34 (2): 209–224. doi:10.1016/S0146-6380(02)00162-6.

Croghan, D., Van Loon, A.F., Sadler, J.P., et al. (2018) Prediction of river temperature surges is dependent on precipitation method. *Hydrological Processes*. doi:10.1002/hyp.13317.

Czemiel Berndtsson, J. (2010) Green roof performance towards management of runoff water quantity and quality: A review. *Ecological Engineering*, 36 (4): 351–360. doi:10.1016/J.ECOLENG.2009.12.014.

Daniels, E., Lenderink, G., Hutjes, R., et al. (2016) Relative impacts of land use and climate change on summer precipitation in the Netherlands. *Hydrology and Earth System Sciences*, 20 (10): 4129–4142. doi:10.5194/hess-20-4129-2016.

Dawson, J.J.C., Soulsby, C., Tetzlaff, D., et al. (2008) Influence of hydrology and seasonality on DOC exports from three contrasting upland catchments. *Biogeochemistry*, 90 (1): 93–113. doi:10.1007/s10533-008-9234-3.

DEFRA (2012) *Tackling water pollution from the urban environment Consultation on a strategy to address diffuse water pollution from the built environment*. Available at: www.defra.gov.ukwww.defra.gov.uk/consult (Accessed: 26 August 2019).

Demars, B.O.L., Russell Manson, J., Ólafsson, J.S., et al. (2011) Temperature and the metabolic balance of streams. *Freshwater Biology*, 56 (6): 1106–1121. doi:10.1111/j.1365-2427.2010.02554.x.

Descy, J.P., Darchambeau, F., Lambert, T., et al. (2017) Phytoplankton dynamics in the Congo River. *Freshwater Biology*, 62 (1): 87–101. doi:10.1111/fwb.12851.

Dixon, P.G. and Mote, T.L. (2003) Patterns and Causes of Atlanta's Urban Heat Island–Initiated Precipitation. *Journal of Applied Meteorology*, 42 (9): 1273–1284. doi:10.1175/1520-0450(2003)042<1273:PACOAU>2.0.CO;2.

Dosskey, M. and Bertsch, P. (1994) Forest sources and pathways of organic matter transport to a blackwater stream: a hydrologic approach. *Biogeochemistry*, 24 (1): 1–19. doi:10.1007/BF00001304.

Downing, B.D., Pellerin, B.A., Bergamaschi, B.A., et al. (2012) Seeing the light: The effects of particles, dissolved materials, and temperature on in situ measurements of DOM fluorescence in rivers and streams. *Limnology and Oceanography: Methods*, 10 (10): 767–775. doi:10.4319/lom.2012.10.767.

Du, Y., Zhang, Y., Chen, F., et al. (2016) Photochemical reactivities of dissolved organic matter (DOM) in a sub-alpine lake revealed by EEM-PARAFAC: An insight into the fate of allochthonous DOM in alpine lakes affected by climate change. *Science of The Total Environment*, 568: 216–225. doi:10.1016/J.SCITOTENV.2016.06.036.

Dugdale, S.J., Malcolm, I.A. and Hannah, D.M. (2019) Drone-based Structure-from-Motion provides accurate forest canopy data to assess shading effects in river temperature models.

Science of the Total Environment, 678: 326–340. doi:10.1016/j.scitotenv.2019.04.229.

Eckard, R.S., Pellerin, B.A., Bergamaschi, B.A., et al. (2017) Dissolved Organic Matter Compositional Change and Biolability During Two Storm Runoff Events in a Small Agricultural Watershed. *Journal of Geophysical Research: Biogeosciences*, 122 (10): 2634–2650. doi:10.1002/2017JG003935.

EEA (2012) *Corine Land Cover 2012*. Available at: https://www.eea.europa.eu/data-and-maps/data/clc-2012-vector.

Einfalt, T., Arnbjerg-Nielsen, K., Golz, C., et al. (2004) Towards a roadmap for use of radar rainfall data in urban drainage. *Journal of Hydrology*, 299 (3–4): 186–202. doi:10.1016/J.JHYDROL.2004.08.004.

Elmore, A.J. and Kaushal, S.S. (2008) Disappearing headwaters: Patterns of stream burial due to urbanization. *Frontiers in Ecology and the Environment*, 6 (6): 2008. doi:10.1890/070101.

Environment Agency (2018) *The state of the environment: water quality*.

European, C. (2019) *Introduction to the EU Water Framework Directive - Environment*. Available at: https://ec.europa.eu/environment/water/water-framework/info/intro_en.htm (Accessed: 20 January 2020).

Evans, C. and Davies, T.D. (1998) Causes of concentration/discharge hysteresis and its potential as a tool for analysis of episode hydrochemistry. *Water Resources Research*, 34 (1): 129–137. doi:10.1029/97WR01881.

Fasching, C., Behounek, B., Singer, G.A., et al. (2015) Microbial degradation of terrigenous dissolved organic matter and potential consequences for carbon cycling in brown-water streams. *Scientific Reports*, 4 (1): 4981. doi:10.1038/srep04981.

Fellman, J.B., Hood, E., Edwards, R.T., et al. (2009) Changes in the concentration, biodegradability, and fluorescent properties of dissolved organic matter during stormflows in coastal temperate watersheds. *Journal of Geophysical Research*, 114 (G1): G01021. doi:10.1029/2008JG000790.

Fellman, J.B., Hood, E. and Spencer, R.G.M. (2010) Fluorescence spectroscopy opens new windows into dissolved organic matter dynamics in freshwater ecosystems: A review. *Limnology and Oceanography*, 55 (6): 2452–2462. doi:10.4319/lo.2010.55.6.2452.

Fierer, N., Craine, J.M., Mclauchlan, K., et al. (2005) Litter quality and the temperature sensitivity of decomposition. *Ecology*, 86 (2): 320–326. doi:10.1890/04-1254.

Finkenbine, J.K., Atwater, J.W. and Mavinic, D.S. (2000) Stream health after urbanization. *Journal of the American Water Resources Association*, 36 (5): 1149–1160. doi:10.1111/j.1752-1688.2000.tb05717.x.

Fletcher, T.D., Andrieu, H. and Hamel, P. (2013) Understanding, management and modelling of urban hydrology and its consequences for receiving waters: A state of the art. *Advances in Water Resources*, 51: 261–279. doi:10.1016/j.advwatres.2012.09.001.

Folegot, S., Hannah, D.M., Dugdale, S.J., et al. (2018) Low flow controls on stream thermal dynamics. *Limnologica*, 68: 157–167. doi:10.1016/j.limno.2017.08.003.

Foley, J.A., DeFries, R., Asner, G.P., et al. (2005) Global consequences of land use. *Science*, 309 (5734): 570–574. doi:10.1126/science.1111772.

Fork, M.L., Blaszczak, J.R., Delesantro, J.M., et al. (2018) Engineered headwaters can act as sources of dissolved organic matter and nitrogen to urban stream networks. *Limnology and Oceanography Letters*, 3 (3): 215–224. doi:10.1002/lol2.10066.

Freitas, C., Olsen, E.M., Knutsen, H., et al. (2016) Temperature-associated habitat selection in a cold-water marine fish. *Journal of Animal Ecology*, 85 (3): 628–637. doi:10.1111/1365-2656.12458.

Gabriele, S., Chiaravalloti, F. and Procopio, A. (2017) Radar–rain-gauge rainfall estimation for hydrological applications in small catchments. *Advances in Geosciences*, 44: 61–66. doi:10.5194/adgeo-44-61-2017.

Garner, G., Malcolm, I.A., Sadler, J.P., et al. (2017) The role of riparian vegetation density, channel orientation and water velocity in determining river temperature dynamics. *Journal of Hydrology*, 553: 471–485. doi:10.1016/j.jhydrol.2017.03.024.

Gemini Data Loggers (2017) *Tinytag Aquatic 2 Data Sheet*. Available at: http://gemini2.assets.d3r.com/pdfs/original/2921-tg-4100.pdf (Accessed: 22 November 2017).

Giakoumis, T. and Voulvoulis, N. (2019) Water Framework Directive programmes of measures: Lessons from the 1st planning cycle of a catchment in England. *Science of the Total Environment*, 668: 903–916. doi:10.1016/j.scitotenv.2019.01.405.

Gnecco, I., Berretta, C., Lanza, L.G., et al. (2005) Storm water pollution in the urban environment of Genoa, Italy. *Atmospheric Research*, 77 (1–4): 60–73. doi:10.1016/J.ATMOSRES.2004.10.017.

Godsey, S.E., Kirchner, J.W. and Clow, D.W. (2009) Concentration-discharge relationships reflect chemostatic characteristics of US catchments. *Hydrological Processes*, 23 (13): 1844–1864. doi:10.1002/hyp.7315.

Golding, B.. (2000) Quantitative precipitation forecasting in the UK. *Journal of Hydrology*, 239 (1–4): 286–305. doi:10.1016/S0022-1694(00)00354-1.

Golding, B.W. (1998) Nimrod: A system for generating automated very short range forecasts. *Meteorological Applications*, 5 (1): S1350482798000577. doi:10.1017/S1350482798000577.

Golroudbary, V.R., Zeng, Y., Mannaerts, C.M., et al. (2019) Response of extreme precipitation to urbanization over the Netherlands. *Journal of Applied Meteorology and Climatology*, 58: 645–661. doi:10.1175/JAMC-D-18-0180.1.

Gonçalves-Araujo, R., Stedmon, C.A., Heim, B., et al. (2015) From Fresh to Marine Waters: Characterization and Fate of Dissolved Organic Matter in the Lena River Delta Region, Siberia. *Frontiers in Marine Science*, 2: 108. doi:10.3389/fmars.2015.00108.

Grand-Clement, E., Luscombe, D.J., Anderson, K., et al. (2014) Antecedent conditions control carbon loss and downstream water quality from shallow, damaged peatlands. *Science of The Total Environment*, 493: 961–973. doi:10.1016/J.SCITOTENV.2014.06.091.

Grimm, N.B., Foster, D., Groffman, P., et al. (2008) The changing landscape: Ecosystem responses to urbanization and pollution across climatic and societal gradients. *Frontiers in Ecology and the Environment*, 6 (5): 264–272. doi:10.1890/070147.

Guarch-Ribot, A. and Butturini, A. (2016) Hydrological conditions regulate dissolved organic matter quality in an intermittent headwater stream. From drought to storm analysis. *Science of The Total Environment*, 571: 1358–1369. doi:10.1016/J.SCITOTENV.2016.07.060.

Güneralp, B., Güneralp, I. and Liu, Y. (2015) Changing global patterns of urban exposure to flood and drought hazards. *Global Environmental Change*, 31: 217–225. doi:10.1016/j.gloenvcha.2015.01.002.

Gurnell, A., Lee, M. and Souch, C. (2007) Urban Rivers: Hydrology, Geomorphology, Ecology and Opportunities for Change. *Geography Compass*, 1 (5): 1118–1137. doi:10.1111/j.1749-8198.2007.00058.x.

Haag, D. and Matschonat, G. (2001) Limitations of controlled experimental systems as models for natural systems: a conceptual assessment of experimental practices in biogeochemistry and soil science. *Science of The Total Environment*, 277 (1–3): 199–216. doi:10.1016/S0048-9697(00)00878-0.

Haga, H., Matsumoto, Y., Matsutani, J., et al. (2005) Flow paths, rainfall properties, and antecedent soil moisture controlling lags to peak discharge in a granitic unchanneled catchment. *Water Resources Research*, 41 (12). doi:10.1029/2005WR004236.

Halliday, S.J., Skeffington, R.A., Wade, A.J., et al. (2015) High-frequency water quality monitoring in an urban catchment: hydrochemical dynamics, primary production and implications for the Water Framework Directive. *Hydrological Processes*, 29 (15): 3388–3407. doi:10.1002/hyp.10453.

Halstead, J.A., Kliman, S., Berheide, C.W., et al. (2014) Urban stream syndrome in a small, lightly developed watershed: A statistical analysis of water chemistry parameters, land use patterns, and natural sources. *Environmental Monitoring and Assessment*, 186 (6): 3391–3414. doi:10.1007/s10661-014-3625-9.

Hannah, D.M. and Garner, G. (2015a) River water temperature in the United Kingdom: Changes over the 20th century and possible changes over the 21st century. *Progress in Physical Geography*, 39 (1). doi:10.1177/0309133314550669.

Hannah, D.M. and Garner, G. (2015b) River water temperature in the United Kingdom. *Progress in Physical Geography*, 39 (1): 68–92. doi:10.1177/0309133314550669.

Hannah, D.M., Malcolm, I.A. and Bradley, C. (2009) Seasonal hyporheic temperature dynamics over riffle bedforms. *Hydrological Processes*, 23 (15): 2178–2194. doi:10.1002/hyp.7256.

Hannah, D.M., Malcolm, I.A., Soulsby, C., et al. (2004) Heat exchanges and temperatures within a salmon spawning stream in the Cairngorms, Scotland: Seasonal and sub-seasonal dynamics. *River Research and Applications*, 20 (6): 635–652. doi:10.1002/rra.771.

Hannah, D.M., Webb, B.W. and Nobilis, F. (2008) River and stream temperature: dynamics, processes, models and implications. *Hydrological Processes*, 22 (7): 899–901. doi:10.1002/hyp.6997.

Hansen, A.M., Kraus, T.E.C., Pellerin, B.A., et al. (2016) Optical properties of dissolved organic matter (DOM): Effects of biological and photolytic degradation. *Limnology and Oceanography*, 61 (3): 1015–1032. doi:10.1002/lno.10270.

Harjung, A., Ejarque, E., Battin, T., et al. (2019) Experimental evidence reveals impact of drought periods on dissolved organic matter quality and ecosystem metabolism in subalpine streams. *Limnology and Oceanography*, 64 (1): 46–60. doi:10.1002/lno.11018.

Harrison, D.L., Scovell, R.W. and Kitchen, M. (2009) High-resolution precipitation estimates for hydrological uses. *Proceedings of the Institution of Civil Engineers - Water Management*, 162 (2): 125–135. doi:10.1680/wama.2009.162.2.125.

Harrison, X.A., Donaldson, L., Correa-Cano, M.E., et al. (2018) A brief introduction to mixed effects modelling and multi-model inference in ecology. *PeerJ*, 6: e4794. doi:10.7717/peerj.4794.

Harvey, R., Lye, L., Khan, A., et al. (2011) The Influence of Air Temperature on Water Temperature and the Concentration of Dissolved Oxygen in Newfoundland Rivers. *Canadian Water Resources Journal*, 36 (2): 171–192. doi:10.4296/cwrj3602849.

Hashemi, S.S.G., Mahmud, H. Bin and Ashraf, M.A. (2015) Performance of green roofs with respect to water quality and reduction of energy consumption in tropics: A review. *Renewable and Sustainable Energy Reviews*, 52: 669–679. doi:10.1016/J.RSER.2015.07.163.

Helms, J.R., Stubbins, A., Ritchie, J.D., et al. (2008) Absorption spectral slopes and slope ratios as indicators of molecular weight, source, and photobleaching of chromophoric dissolved organic matter. *Limnology and Oceanography*, 53 (3): 955–969. doi:10.4319/lo.2008.53.3.0955.

Henderson, R.K., Baker, A., Parsons, S.A., et al. (2008) Characterisation of algogenic organic matter extracted from cyanobacteria, green algae and diatoms. *Water Research*, 42 (13): 3435–3445. doi:10.1016/j.watres.2007.10.032.

Herb, W.R., Janke, B., Mohseni, O., et al. (2008) Thermal pollution of streams by runoff from paved surfaces. *Hydrological Processes*, 22 (7): 987–999. doi:10.1002/hyp.6986.

Hester, E.T. and Bauman, K.S. (2013) Stream and Retention Pond Thermal Response to Heated Summer Runoff From Urban Impervious Surfaces [1]. *JAWRA Journal of the American Water Resources Association*, 49 (2): 328–342. doi:10.1111/jawr.12019.

Hester, E.T. and Doyle, M.W. (2011) Human impacts to river temperature and their effects on biological processes: A quantitative synthesis. *Journal of the American Water Resources*

Association, 47 (3): 571–587. doi:10.1111/j.1752-1688.2011.00525.x.

Hofmeister, K.L., Cianfrani, C.M. and Hession, W.C. (2015) Complexities in the stream temperature regime of a small mixed-use watershed, Blacksburg, VA. *Ecological Engineering*, 78: 101–111. doi:10.1016/J.ECOLENG.2014.05.019.

Hogg, I.D., Williams, D.D., Eadie, J.M., et al. (1995) The consequences of global warming for stream invertebrates: A field simulation. *Journal of Thermal Biology*, 20 (1–2): 199–206. doi:10.1016/0306-4565(94)00057-P.

Hook, A.M. and Yeakley, J.A. (2005) Stormflow Dynamics of Dissolved Organic Carbon and Total Dissolved Nitrogen in a Small Urban Watershed. *Biogeochemistry*, 75 (3): 409–431. doi:10.1007/s10533-005-1860-4.

Hosen, J.D., McDonough, O.T., Febria, C.M., et al. (2014) Dissolved Organic Matter Quality and Bioavailability Changes Across an Urbanization Gradient in Headwater Streams. *Environmental Science & Technology*, 48 (14): 7817–7824. doi:10.1021/es501422z.

Hrachowitz, M., Soulsby, C., Imholt, C., et al. (2010) Thermal regimes in a large upland salmon river: A simple model to identify the influence of landscape controls and climate change on maximum temperatures. *Hydrological Processes*, 24 (23): 403–419. doi:10.1002/hyp.7756.

Hrdinka, T., Novický, O., Hanslík, E., et al. (2012) Possible impacts of floods and droughts on water quality. *Journal of Hydro-environment Research*, 6 (2): 145–150. doi:10.1016/J.JHER.2012.01.008.

Huang, W., McDowell, W.H., Zou, X., et al. (2013) Dissolved Organic Carbon in Headwater Streams and Riparian Soil Organic Carbon along an Altitudinal Gradient in the Wuyi Mountains, China Wang, X. (ed.). *PLoS ONE*, 8 (11): e78973. doi:10.1371/journal.pone.0078973.

Hudson, N., Baker, A. and Reynolds, D. (2007) Fluorescence analysis of dissolved organic matter in natural, waste and polluted waters—a review. *River Research and Applications*, 23 (6): 631–649. doi:10.1002/rra.1005.

Imholt, C., Soulsby, C., Malcolm, I.A., et al. (2013) Influence of scale on thermal characteristics in a large montane river basin. *River Research and Applications*, 29 (4): 403–419. doi:10.1002/rra.1608.

Jackson, F.L., Hannah, D.M., Fryer, R.J., et al. (2017) Development of spatial regression models for predicting summer river temperatures from landscape characteristics: Implications for land and fisheries management. *Hydrological Processes*, 31 (6): 1225–1238. doi:10.1002/hyp.11087.

Jackson, F.L., Malcolm, I.A. and Hannah, D.M. (2015) A novel approach for designing large-scale river temperature monitoring networks. *Hydrology Research*, 47 (3): 569–590. doi:10.2166/nh.2015.106.

Jacobson, C.R. (2011) Identification and quantification of the hydrological impacts of imperviousness in urban catchments: A review. *Journal of Environmental Management*, 92 (6): 1438–1448. doi:10.1016/j.jenvman.2011.01.018.

Johnson, M.F. and Wilby, R.L. (2015) Seeing the landscape for the trees: Metrics to guide riparian shade management in river catchments. *Water Resources Research*, 51 (5): 3754–3769. doi:10.1002/2014WR016802.

Jones, M.P., Hunt, W.F. and Winston, R.J. (2012) Effect of Urban Catchment Composition on Runoff Temperature. *Journal of Environmental Engineering*, 138 (12): 1231–1236. doi:10.1061/(ASCE)EE.1943-7870.0000577.

Karvonen, A., Rintamäki, P., Jokela, J., et al. (2010) Increasing water temperature and disease risks in aquatic systems: Climate change increases the risk of some, but not all, diseases. *International Journal for Parasitology*, 40 (13): 1483–1488. doi:10.1016/j.ijpara.2010.04.015.

Kaushal, S.S. and Belt, K.T. (2012) The urban watershed continuum: evolving spatial and temporal dimensions. *Urban Ecosystems*, 15 (2): 409–435. doi:10.1007/s11252-012-0226-7.

Kaushal, S.S., Gold, A.J., Bernal, S., et al. (2018a) Diverse water quality responses to extreme climate events: an introduction. *Biogeochemistry*, 141 (3): 273–279. doi:10.1007/s10533-018-0527-x.

Kaushal, S.S., Gold, A.J., Bernal, S., et al. (2018b) Watershed 'chemical cocktails': forming novel elemental combinations in Anthropocene fresh waters. *Biogeochemistry*, 141 (3): 281–305. doi:10.1007/s10533-018-0502-6.

Kaushal, S.S., Likens, G.E., Jaworski, N.A., et al. (2010) Rising stream and river temperatures in the United States. *Frontiers in Ecology and the Environment*, 8 (9): 461–466. doi:10.1890/090037.

Kaushal, S.S., McDowell, W.H. and Wollheim, W.M. (2014) Tracking evolution of urban biogeochemical cycles: past, present, and future. *Biogeochemistry*, 121 (1): 1–21. doi:10.1007/s10533-014-0014-y.

Keeler, B.L., Polasky, S., Brauman, K.A., et al. (2012) Linking water quality and well-being for improved assessment and valuation of ecosystem services. *Proceedings of the National Academy of Sciences*, 109 (45): 18619–18624. doi:10.1073/pnas.1215991109.

Keiser, D.A. and Shapiro, J.S. (2019) Consequences of the Clean Water Act and the Demand for Water Quality*. *The Quarterly Journal of Economics*, 134 (1): 349–396. doi:10.1093/qje/qjy019.

Kelleher, C., Wagener, T., Gooseff, M., et al. (2012) Investigating controls on the thermal sensitivity of Pennsylvania streams. *Hydrological Processes*, 26 (5): 771–785. doi:10.1002/hyp.8186.

Khamis, K., Bradley, C. and Hannah, D.M. (2018) Understanding dissolved organic matter dynamics in urban catchments: insights from *in situ* fluorescence sensor technology. *Wiley Interdisciplinary Reviews: Water*, 5 (1): e1259. doi:10.1002/wat2.1259.

Khamis, K., Bradley, C., Stevens, R., et al. (2017) Continuous field estimation of dissolved organic carbon concentration and biochemical oxygen demand using dual-wavelength fluorescence, turbidity and temperature. *Hydrological Processes*, 31 (3): 540–555.

doi:10.1002/hyp.11040.

Khamis, K., Sorensen, J.P.R., Bradley, C., et al. (2015) In situ tryptophan-like fluorometers: assessing turbidity and temperature effects for freshwater applications. *Environmental Science: Processes & Impacts*, 17 (4): 740–752. doi:10.1039/C5EM00030K.

King, K.W., Smiley, P.C. and Fausey, N.R. (2010) Hydrology of channelized and natural headwater streams. *Hydrological Sciences Journal*, 54 (5): 929–948. doi:10.1623/hysj.54.5.929.

Kobe, K.A. and Dutton, F.B. (1961) The effect of temperature on solubility. *Journal of Chemical Education*, 38 (2). doi:10.1021/ed038pa99.1.

Koch, J. and Stisen, S. (2017) Citizen science: A new perspective to advance spatial pattern evaluation in hydrology Schumann, G.J.-P. (ed.). *PLOS ONE*, 12 (5): e0178165. doi:10.1371/journal.pone.0178165.

Kothawala, D.N., von Wachenfeldt, E., Koehler, B., et al. (2012) Selective loss and preservation of lake water dissolved organic matter fluorescence during long-term dark incubations. *Science of The Total Environment*, 433: 238–246. doi:10.1016/J.SCITOTENV.2012.06.029.

Krause, S., Blume, T. and Cassidy, N.J. (2012) Investigating patterns and controls of groundwater up-welling in a lowland river by combining Fibre-optic Distributed Temperature Sensing with observations of vertical hydraulic gradients. *Hydrology and Earth System Sciences*, 16: 1775–1792. doi:10.5194/hess-16-1775-2012.

Krein, A. and Schorer, M. (2000) Road runoff pollution by polycyclic aromatic hydrocarbons and its contribution to river sediments. *Water Research*, 34 (16): 4110–4115. doi:10.1016/S0043-1354(00)00156-1.

Kritzberg, E.S., Cole, J.J., Pace, M.L., et al. (2004) Autochthonous versus allochthonous carbon sources of bacteria: Results from whole-lake 13C addition experiments. *Limnology and Oceanography*, 49 (2): 588–596. doi:10.4319/lo.2004.49.2.0588.

Laanaya, F., St-Hilaire, A. and Gloaguen, E. (2017) Water temperature modelling: comparison between the generalized additive model, logistic, residuals regression and linear regression models. *Hydrological Sciences Journal*, 62 (7): 1–16. doi:10.1080/02626667.2016.1246799.

Lambert, T., Bouillon, S., Darchambeau, F., et al. (2017) Effects of human land use on the terrestrial and aquatic sources of fluvial organic matter in a temperate river basin (The Meuse River, Belgium). *Biogeochemistry*, 136 (2): 191–211. doi:10.1007/s10533-017-0387-9.

Landrigan, P.J., Fuller, R., Acosta, N.J.R., et al. (2018) The Lancet Commission on pollution and health. *The Lancet*, 391 (101119): 462–512. doi:10.1016/S0140-6736(17)32345-0.

Lange, J. and Haensler, A. (2012) Runoff generation following a prolonged dry period. *Journal of Hydrology*, 464–465: 157–164. doi:10.1016/J.JHYDROL.2012.07.010.

Larson, J.H., Frost, P.C., Lodge, D.M., et al. (2007) Photodegradation of dissolved organic matter in forested streams of the northern Great Lakes region. *Journal of the North American Benthological Society*, 26 (3): 416–425. doi:10.1899/06-097.1.

Lavelle, A.M., Bury, N.R., O'Shea, F.T., et al. (2019) Influence of urban river restoration on nitrogen dynamics at the sediment-water interface Cañedo-Argüelles Iglesias, M. (ed.). *PLOS ONE*, 14 (3): e0212690. doi:10.1371/journal.pone.0212690.

Lawler, D.M., Petts, G.E., Foster, I.D.L., et al. (2006) Turbidity dynamics during spring storm events in an urban headwater river system: The Upper Tame, West Midlands, UK. *Science of The Total Environment*, 360 (1–3): 109–126. doi:10.1016/j.scitotenv.2005.08.032.

LeBlanc, R.T., Brown, R.D. and FitzGibbon, J.E. (1997) Modeling the effects of land use change on the water temperature in unregulated urban streams. *Journal of Environmental Management*, 49 (4): 445–469. doi:10.1006/jema.1996.0106.

Leenheer, J.A. and Croué, J.-P. (2003) Peer Reviewed: Characterizing Aquatic Dissolved Organic Matter. *Environmental Science & Technology*, 37 (1): 18A-26A. doi:10.1021/es032333c.

Liu, C., Du, Y., Yin, H., et al. (2019) Exchanges of nitrogen and phosphorus across the sediment-water interface influenced by the external suspended particulate matter and the residual matter after dredging. *Environmental Pollution*, 246: 207–216. doi:10.1016/j.envpol.2018.11.092.

Lloyd, C.E.M., Freer, J.E., Johnes, P.J., et al. (2016a) Technical Note: Testing an improved index for analysing storm discharge-concentration hysteresis. *Hydrol. Earth Syst. Sci*, 20: 625–632. doi:10.5194/hess-20-625-2016.

Lloyd, C.E.M., Freer, J.E., Johnes, P.J., et al. (2016b) Using hysteresis analysis of high-resolution water quality monitoring data, including uncertainty, to infer controls on nutrient and sediment transfer in catchments. *Science of The Total Environment*, 543: 388–404. doi:10.1016/J.SCITOTENV.2015.11.028.

Logvinova, C.L., Frey, K.E., Mann, P.J., et al. (2015) Assessing the potential impacts of declining Arctic sea ice cover on the photochemical degradation of dissolved organic matter in the Chukchi and Beaufort Seas. *Journal of Geophysical Research: Biogeosciences*, 120 (11): 2326–2344. doi:10.1002/2015JG003052.

Van Loon, A.F. (2015) Hydrological drought explained HYDROLOGICAL DROUGHT IN CONTEXT. *WIREs Water*, 2: 359–392. doi:10.1002/wat2.1085.

Van Loon, A.F., Gleeson, T., Clark, J., et al. (2016) Drought in the Anthropocene. *Nature Geoscience*, 9 (2): 89–91. doi:10.1038/ngeo2646.

Lu, Y., Bauer, J.E., Canuel, E.A., et al. (2013) Photochemical and microbial alteration of dissolved organic matter in temperate headwater streams associated with different land use. *Journal of Geophysical Research: Biogeosciences*, 118 (2): 566–580. doi:10.1002/jgrg.20048.

Lynch, L.M., Sutfin, N.A., Fegel, T.S., et al. (2019) River channel connectivity shifts metabolite composition and dissolved organic matter chemistry. *Nature Communications*, 10 (1). doi:10.1038/s41467-019-08406-8.

Malcolm, I.A., Soulsby, C., Hannah, D.M., et al. (2008) The influence of riparian woodland on

stream temperatures: Implications for the performance of juvenile salmonids. *Hydrological Processes*, 22 (7): 968–979. doi:10.1002/hyp.6996.

Mallin, M.A., Johnson, V.L. and Ensign, S.H. (2009) Comparative impacts of stormwater runoff on water quality of an urban, a suburban, and a rural stream. *Environmental Monitoring and Assessment*, 159 (1–4): 475–491. doi:10.1007/s10661-008-0644-4.

Manning, C., Widmann, M., Bevacqua, E., et al. (2018) Soil Moisture Drought in Europe: A Compound Event of Precipitation and Potential Evapotranspiration on Multiple Time Scales. *Journal of Hydrometeorology*, 19 (8): 1255–1271. doi:10.1175/JHM-D-18-0017.1.

Mao, F., Khamis, K., Krause, S., et al. (2019) Low-cost environmental sensor networks: recent advances and future directions. *Frontiers in Earth Science*, 7: 221. doi:10.3389/FEART.2019.00221.

Mao, R. and Li, S.-Y. (2018) Temperature sensitivity of biodegradable dissolved organic carbon increases with elevating humification degree in subtropical rivers. *Science of The Total Environment*, 635: 1367–1371. doi:10.1016/J.SCITOTENV.2018.04.256.

Massiccotte, P. (2017) *eemR: Tools for Pre-Processing Emission-Excitation-Matrix (EEM) Fluorescence Data*. Available at: https://cran.r-project.org/web/packages/eemR/index.html.

Massicotte, P., Asmala, E., Stedmon, C., et al. (2017) Global distribution of dissolved organic matter along the aquatic continuum: Across rivers, lakes and oceans. *Science of The Total Environment*, 609: 180–191. doi:10.1016/J.SCITOTENV.2017.07.076.

McElmurry, S.P., Long, D.T. and Voice, T.C. (2014) Stormwater Dissolved Organic Matter: Influence of Land Cover and Environmental Factors. *Environmental Science & Technology*, 48 (1): 45–53. doi:10.1021/es402664t.

McGrane, S.J. (2016) Impacts of urbanisation on hydrological and water quality dynamics, and urban water management: a review. *Hydrological Sciences Journal*, 61 (13): 2295–2311. doi:10.1080/02626667.2015.1128084.

McKnight, D.M., Boyer, E.W., Westerhoff, P.K., et al. (2001) Spectrofluorometric characterization of dissolved organic matter for indication of precursor organic material and aromaticity. *Limnology and Oceanography*, 46 (1): 38–48. doi:10.4319/lo.2001.46.1.0038.

McMillan, H., Montanari, A., Cudennec, C., et al. (2016) Panta Rhei 2013–2015: global perspectives on hydrology, society and change. *Hydrological Sciences Journal*, 61 (7): 1–18. doi:10.1080/02626667.2016.1159308.

Met Office (2012) *Met Office Integrated Data Archive System (MIDAS) Land and Marine Surface Stations Data (1853-current).* Available at: http://catalogue.ceda.ac.uk/uuid/220a65615218d5c9cc9e4785a3234bd0 (Accessed: 12 August 2018).

Met Office (2018) *Weather Observations Website*. Available at: http://wow.metoffice.gov.uk/ (Accessed: 15 June 2018).

Meyer, J.L. and Edwards, R.T. (1990) Ecosystem metabolism and turnover of organic carbon along a blackwater river continuum. *Ecology*, 71 (2): 668–677. doi:10.2307/1940321.

Meyer, J.L., Wallace, J.B. and Eggert, S.L. (1998) Leaf Litter as a Source of Dissolved Organic Carbon in Streams. *Ecosystems*. 1 pp. 240–249. doi:10.2307/3658761.

Miller, J.D. and Hutchins, M. (2017) The impacts of urbanisation and climate change on urban flooding and urban water quality: A review of the evidence concerning the United Kingdom. *Journal of Hydrology: Regional Studies*, 12: 345–362. doi:10.1016/J.EJRH.2017.06.006.

Miller, J.D., Kim, H., Kjeldsen, T.R., et al. (2014) Assessing the impact of urbanization on storm runoff in a peri-urban catchment using historical change in impervious cover. *Journal of Hydrology*, 515: 59–70. doi:10.1016/J.JHYDROL.2014.04.011.

Miller, M.P. and McKnight, D.M. (2010) Comparison of seasonal changes in fluorescent dissolved organic matter among aquatic lake and stream sites in the Green Lakes Valley. *Journal of Geophysical Research*, 115 (G1): G00F12. doi:10.1029/2009JG000985.

Minor, E.C., Swenson, M.M., Mattson, B.M., et al. (2014) Structural characterization of dissolved organic matter: a review of current techniques for isolation and analysis. *Environmental Science: Processes & Impacts*, 16 (9): 2064–2079. doi:10.1039/c4em00062e.

Mohajerani, A., Bakaric, J. and Jeffrey-Bailey, T. (2017) The urban heat island effect, its causes, and mitigation, with reference to the thermal properties of asphalt concrete. *Journal of Environmental Management*, 197: 522–538. doi:10.1016/j.jenvman.2017.03.095.

Mohseni, O., Stefan, H.G. and Eaton, J.G. (2003) Global Warming and Potential Changes in Fish Habitat in U.S. Streams. *Climatic Change*, 59 (3): 389–409. doi:10.1023/A:1024847723344.

Monteith, D.T., Stoddard, J.L., Evans, C.D., et al. (2007) Dissolved organic carbon trends resulting from changes in atmospheric deposition chemistry. *Nature*, 450 (7169): 537–540. doi:10.1038/nature06316.

Moody, C.S. and Worrall, F. (2017) Modeling rates of DOC degradation using DOM composition and hydroclimatic variables. *Journal of Geophysical Research: Biogeosciences*, 122 (5): 1175–1191. doi:10.1002/2016JG003493.

Moody, C.S., Worrall, F., Evans, C.D., et al. (2013) The rate of loss of dissolved organic carbon (DOC) through a catchment. *Journal of Hydrology*, 492: 139–150. doi:10.1016/J.JHYDROL.2013.03.016.

Moran, M.A. and Zepp, R.G. (1997) Role of photoreactions in the formation of biologically labile compounds from dissolved organic matter. *Limnology and Oceanography*, 42 (6): 1307–1316. doi:10.4319/lo.1997.42.6.1307.

Mosley, L.M. (2015) Drought impacts on the water quality of freshwater systems; review and integration. *Earth-Science Reviews*, 140: 203–214. doi:10.1016/J.EARSCIREV.2014.11.010.

Muggeo, V.M.. (2008) segmented: an R Package to Fit Regression Models with Broken-Line Relationships. *R News*, 8 (1): 20–25. Available at: https://cran.r-project.org/doc/Rnews/.

Muller, C.L., Chapman, L., Grimmond, C.S.B., et al. (2013) Sensors and the city: a review of urban meteorological networks. *International Journal of Climatology*, 33 (7): 1585–1600. doi:10.1002/joc.3678.

Murase, H., Nagashima, H., Yonezaki, S., et al. (2009) Application of a generalized additive model (GAM) to reveal relationships between environmental factors and distributions of pelagic fish and krill: a case study in Sendai Bay, Japan. *ICES Journal of Marine Science*, 66 (6): 1417–1424. doi:10.1093/icesjms/fsp105.

Murphy, K.R., Butler, K.D., Spencer, R.G.M., et al. (2010) Measurement of Dissolved Organic Matter Fluorescence in Aquatic Environments: An Interlaboratory Comparison. *Environmental Science & Technology*, 44 (24): 9405–9412. doi:10.1021/es102362t.

Napieralski, J.A. and Carvalhaes, T. (2016) Urban stream deserts: Mapping a legacy of urbanization in the United States. *Applied Geography*, 67: 129–139. doi:10.1016/J.APGEOG.2015.12.008.

Nélieu, S., Perreau, F., Bonnemoy, F., et al. (2009) Sunlight Nitrate-Induced Photodegradation of Chlorotoluron: Evidence of the Process in Aquatic Mesocosms. *Environmental Science & Technology*, 43 (9): 3148–3154. doi:10.1021/es8033439.

Nelson, K.C. and Palmer, M.A. (2007) Stream Temperature Surges under Urbanization and Climate Change: Data, Models, and Responses. *Journal of the American Water Resources Association*, 43 (2): 440–452. doi:10.1111/j.1752-1688.2007.00034.x.

NRFA (2018) *28039 - Rea at Calthorpe Park*. Available at: https://nrfa.ceh.ac.uk/data/station/spatial/28039 (Accessed: 22 April 2018).

O'Driscoll, M., Clinton, S., Jefferson, A., et al. (2010a) Urbanization effects on watershed hydrology and in-stream processes in the southern United States. *Water*. doi:10.3390/w2030605.

O'Driscoll, M., Clinton, S., Jefferson, A., et al. (2010b) Urbanization Effects on Watershed Hydrology and In-Stream Processes in the Southern United States. *Water*, 2 (3): 605–648. doi:10.3390/w2030605.

O'Gorman, E.J., Ólafsson, Ó.P., Demars, B.O.L., et al. (2016) Temperature effects on fish production across a natural thermal gradient. *Global change biology*, 22 (9): 3206–3220. doi:10.1111/gcb.13233.

Obernosterer, I. and Benner, R. (2004) Competition between biological and photochemical processes in the mineralization of dissolved organic carbon. *Limnology and Oceanography*, 49 (1): 117–124. doi:10.4319/lo.2004.49.1.0117.

Ockenden, M.C., Deasy, C.E., Benskin, C.M.H., et al. (2016) Changing climate and nutrient transfers: Evidence from high temporal resolution concentration-flow dynamics in headwater catchments. *Science of The Total Environment*, 548–549: 325–339. doi:10.1016/J.SCITOTENV.2015.12.086.

Ohno, T. (2002) Fluorescence Inner-Filtering Correction for Determining the Humification Index of Dissolved Organic Matter. *Environmental Science & Technology*, 36 (4): 742–746. doi:10.1021/ES0155276.

Old, G.H., Naden, P.S., Harman, M., et al. (2019) Using dissolved organic matter fluorescence to identify the provenance of nutrients in a lowland catchment; the River Thames, England. *Science of The Total Environment*, 653: 1240–1252. doi:10.1016/J.SCITOTENV.2018.10.421.

Osburn, C.L., Handsel, L.T., Mikan, M.P., et al. (2012) Fluorescence Tracking of Dissolved and Particulate Organic Matter Quality in a River-Dominated Estuary. *Environmental Science & Technology*, 46 (16): 8628–8636. doi:10.1021/es3007723.

Paerl, H., Pinckney, J., Fear, J., et al. (1998) Ecosystem responses to internal and watershed organic matter loading: consequences for hypoxia in the eutrophying Neuse River Estuary, North Carolina, USA. *Marine Ecology Progress Series*, 166: 17–25. Available at: https://scholarcommons.sc.edu/biol_facpub/18 (Accessed: 6 December 2018).

Para, J., Coble, P.G., Charrière, B., et al. (2010) Fluorescence and absorption properties of chromophoric dissolved organic matter (CDOM) in coastal surface waters of the northwestern Mediterranean Sea, influence of the Rhône River. *Biogeosciences*, 7 (12): 4083–4103. doi:10.5194/bg-7-4083-2010.

Parr, T.B., Cronan, C.S., Ohno, T., et al. (2015) Urbanization changes the composition and bioavailability of dissolved organic matter in headwater streams. *Limnology and Oceanography*, 60 (3): 885–900. doi:10.1002/lno.10060.

Pedersen, L., Jensen, N.E., Christensen, L.E., et al. (2010) Quantification of the spatial variability of rainfall based on a dense network of rain gauges. *Atmospheric Research*, 95: 441–454. doi:10.1016/j.atmosres.2009.11.007.

Peleato, N.M., McKie, M., Taylor-Edmonds, L., et al. (2016) Fluorescence spectroscopy for monitoring reduction of natural organic matter and halogenated furanone precursors by biofiltration. *Chemosphere*, 153: 155–161. doi:10.1016/J.CHEMOSPHERE.2016.03.018.

Pennino, M.J., Kaushal, S.S., Beaulieu, J.J., et al. (2014) Effects of urban stream burial on nitrogen uptake and ecosystem metabolism: implications for watershed nitrogen and carbon fluxes. *Biogeochemistry*, 121 (1): 247–269. doi:10.1007/s10533-014-9958-1.

Pereda, O., Acuña, V., von Schiller, D., et al. (2019) Immediate and legacy effects of urban pollution on river ecosystem functioning: A mesocosm experiment. *Ecotoxicology and Environmental Safety*, 169: 960–970. doi:10.1016/J.ECOENV.2018.11.103.

Petrone, K.C., Fellman, J.B., Hood, E., et al. (2011) The origin and function of dissolved organic matter in agro-urban coastal streams. *Journal of Geophysical Research: Biogeosciences*, 116 (G1). doi:10.1029/2010JG001537.

Phillips, P. and Chalmers, A. (2009) Wastewater Effluent, Combined Sewer Overflows, and Other Sources of Organic Compounds to Lake Champlain. *JAWRA Journal of the American Water Resources Association*, 45 (1): 45–57. doi:10.1111/j.1752-1688.2008.00288.x.

Phong, D.D. and Hur, J. (2015) Insight into photocatalytic degradation of dissolved organic matter in UVA/TiO2 systems revealed by fluorescence EEM-PARAFAC. *Water Research*, 87: 119–126. doi:10.1016/J.WATRES.2015.09.019.

Pilgrim, D.H., Cordery, I. and Baron, B.C. (1982) Effects of catchment size on runoff relationships. *Journal of Hydrology*, 58 (3–4): 205–221. doi:10.1016/0022-1694(82)90035-X.

Pinheiro, J., Bates, D., DebRoy, S., et al. (2019) *nlme: Linear and Nonlinear Mixed Effects Model*. Available at: https://cran.r-project.org/package=nlme.

Pinto, U., Maheshwari, B.L. and Ollerton, R.L. (2013) Analysis of long-term water quality for effective river health monitoring in peri-urban landscapes—a case study of the Hawkesbury–Nepean river system in NSW, Australia. *Environmental Monitoring and Assessment*, 185 (6): 4551–4569. doi:10.1007/s10661-012-2888-2.

Pluhowski, E.J. and Pecora, W.T. (1970) *Urbanization and Its Eifect on the Temperature of the Streams on Long Island, New York*. Professional Paper 627-D. Available at: https://pubs.usgs.gov/pp/0627d/report.pdf (Accessed: 22 November 2017).

Porcal, P., Dillon, P.J. and Molot, L.A. (2015) Temperature Dependence of Photodegradation of Dissolved Organic Matter to Dissolved Inorganic Carbon and Particulate Organic Carbon Almeida, A. (ed.). *PLOS ONE*, 10 (6): e0128884. doi:10.1371/journal.pone.0128884.

Qu, F., Liang, H., He, J., et al. (2012) Characterization of dissolved extracellular organic matter (dEOM) and bound extracellular organic matter (bEOM) of Microcystis aeruginosa and their impacts on UF membrane fouling. *Water Research*, 46 (9): 2881–2890. doi:10.1016/j.watres.2012.02.045.

Raymond, P. and Bauer, J. (2000) Bacterial consumption of DOC during transport through a temperate estuary. *Aquatic Microbial Ecology*, 22 (1): 1–12. doi:10.3354/ame022001.

Raymond, P.A., Saiers, J.E. and Sobczak, W. V. (2016) Hydrological and biogeochemical controls on watershed dissolved organic matter transport: Pulse- shunt concept. *Ecology*, 97 (1): 5–16. doi:10.1890/14-1684.1.

Razzaghmanesh, M., Beecham, S. and Kazemi, F. (2014) Impact of green roofs on stormwater quality in a South Australian urban environment. *Science of The Total Environment*, 470–471: 651–659. doi:10.1016/J.SCITOTENV.2013.10.047.

Réalis-Doyelle, E., Pasquet, A., De Charleroy, D., et al. (2016) Strong Effects of Temperature on the Early Life Stages of a Cold Stenothermal Fish Species, Brown Trout (Salmo trutta L.). *PloS one*, 11 (5): e0155487. doi:10.1371/journal.pone.0155487.

Rice, J.S., Anderson, W.P. and Thaxton, C.S. (2011) Urbanization influences on stream temperature behavior within low-discharge headwater streams. *Hydrological Research Letters*, 5: 27–31. doi:10.3178/HRL.5.27.

Rico-Ramirez, M.A., Liguori, S. and Schellart, A.N.A. (2015) Quantifying radar-rainfall uncertainties in urban drainage flow modelling. *Journal of Hydrology*, 528: 17–28.

doi:10.1016/J.JHYDROL.2015.05.057.

Rode, M., Wade, A.J., Cohen, M.J., et al. (2016) Sensors in the Stream: The High-Frequency Wave of the Present. *Environmental Science & Technology*, 50 (19): 10297–10307. doi:10.1021/acs.est.6b02155.

Romera-Castillo, C., Álvarez-Salgado, X.A., Galí, M., et al. (2013) Combined effect of light exposure and microbial activity on distinct dissolved organic matter pools. A seasonal field study in an oligotrophic coastal system (Blanes Bay, NW Mediterranean). *Marine Chemistry*, 148: 44–51. doi:10.1016/J.MARCHEM.2012.10.004.

Rowland, C., Morton, R., Carrasco, L., et al. (2017) *Land Cover Map 2015 (25m raster, GB)*. Available at: https://doi.org/10.5285/bb15e200-9349-403c-bda9-b430093807c7.

Rutherford, J.C., Blackett, S., Blackett, C., et al. (1997) Predicting the effects of shade on water temperature in small streams. *New Zealand Journal of Marine and Freshwater Research*, 31 (5): 707–721. doi:10.1080/00288330.1997.9516801.

Sakrabani, R., Vollertsen, J., Ashley, R.M., et al. (2009) Biodegradability of organic matter associated with sewer sediments during first flush. *Science of The Total Environment*, 407 (8): 2989–2995. doi:10.1016/J.SCITOTENV.2009.01.008.

Salvadore, E., Bronders, J. and Batelaan, O. (2015) Hydrological modelling of urbanized catchments: A review and future directions. *Journal of Hydrology*, 529: 62–81. doi:10.1016/j.jhydrol.2015.06.028.

Samuel, J., Coulibaly, P. and Metcalfe, R.A. (2011) Estimation of Continuous Streamflow in Ontario Ungauged Basins: Comparison of Regionalization Methods. *Journal of Hydrologic Engineering*, 16 (5): 447–459. doi:10.1061/(ASCE)HE.1943-5584.0000338.

Sandoval, S., Torres, A., Duarte, M., et al. (2014) Assessment of rainfall influence over water quality effluent of an urban catchment: a data driven approach. *Urban Water Journal*, 11 (2): 116–126. doi:10.1080/1573062X.2013.765492.

Sankar, M.S., Dash, P., Singh, S., et al. (2019) Effect of photo-biodegradation and biodegradation on the biogeochemical cycling of dissolved organic matter across diverse surface water bodies. *Journal of Environmental Sciences*, 77: 130–147. doi:10.1016/J.JES.2018.06.021.

Saraceno, J.F., Pellerin, B.A., Downing, B.D., et al. (2009) High-frequency in situ optical measurements during a storm event: Assessing relationships between dissolved organic matter, sediment concentrations, and hydrologic processes. *Journal of Geophysical Research: Biogeosciences*, 114 (G4): G00F09. doi:10.1029/2009JG000989.

Saraceno, J.F., Shanley, J.B., Downing, B.D., et al. (2017) Clearing the waters: Evaluating the need for site-specific field fluorescence corrections based on turbidity measurements. *Limnology and Oceanography: Methods*, 15 (4): 408–416. doi:10.1002/lom3.10175.

Schuster, P.F., Shanley, J.B., Marvin-Dipasquale, M., et al. (2007) Mercury and Organic Carbon

Dynamics During Runoff Episodes from a Northeastern USA Watershed. *Water, Air, and Soil Pollution*, 187 (1–4): 89–108. doi:10.1007/s11270-007-9500-3.

Schwarz, N., Schlink, U., Franck, U., et al. (2012) Relationship of land surface and air temperatures and its implications for quantifying urban heat island indicators—An application for the city of Leipzig (Germany). *Ecological Indicators*, 18: 693–704. doi:10.1016/J.ECOLIND.2012.01.001.

Seto, K.C., Güneralp, B. and Hutyra, L.R. (2012) Global forecasts of urban expansion to 2030 and direct impacts on biodiversity and carbon pools. *Proceedings of the National Academy of Sciences of the United States of America*, 109 (40): 16083–16088. doi:10.1073/pnas.1211658109.

Shank, G.C., Nelson, K. and Montagna, P.A. (2009) Importance of CDOM Distribution and Photoreactivity in a Shallow Texas Estuary. *Estuaries and Coasts*, 32 (4): 661–677. doi:10.1007/s12237-009-9159-7.

Shanley, J.B., Sebestyen, S.D., McDowell, W.H., et al. (2018) "The scientific and societal value of long-term watershed research." In *American Geophysical Union, Fall Meeting 2018*. 2018. Available at: http://adsabs.harvard.edu/abs/2018AGUFM.H12D..06S (Accessed: 22 August 2019).

Shapiro, S.S. and Wilk, ; M B (1965) *An Analysis of Variance Test for Normality (Complete Samples)*. Available at: http://www.bios.unc.edu/~mhudgens/bios/662/2008fall/Backup/wilkshapiro1965.pdf (Accessed: 27 January 2019).

Shutova, Y., Baker, A., Bridgeman, J., et al. (2014) Spectroscopic characterisation of dissolved organic matter changes in drinking water treatment: From PARAFAC analysis to online monitoring wavelengths. *Water Research*, 54: 159–169. doi:10.1016/J.WATRES.2014.01.053.

Sieczko, A., Maschek, M. and Peduzzi, P. (2015) Algal extracellular release in river-floodplain dissolved organic matter: Response of extracellular enzymatic activity during a post-flood period. *Frontiers in Microbiology*, 6: 80. doi:10.3389/fmicb.2015.00080.

Singh, S., Inamdar, S., Mitchell, M., et al. (2014) Seasonal pattern of dissolved organic matter (DOM) in watershed sources: influence of hydrologic flow paths and autumn leaf fall. *Biogeochemistry*, 118 (1–3): 321–337. doi:10.1007/s10533-013-9934-1.

Smith, R.M. and Kaushal, S.S. (2015) Carbon cycle of an urban watershed: exports, sources, and metabolism. *Biogeochemistry*, 126 (1–2): 173–195. doi:10.1007/s10533-015-0151-y.

Sohrabi, M.M., Benjankar, R., Tonina, D., et al. (2017) Estimation of daily stream water temperatures with a Bayesian regression approach. *Hydrological Processes*, 31 (9): 1719–1733. doi:10.1002/hyp.11139.

Soltani, A. and Sharifi, E. (2017) Daily variation of urban heat island effect and its correlations to urban greenery: A case study of Adelaide. *Frontiers of Architectural Research*, 6 (4): 529–538. doi:10.1016/j.foar.2017.08.001.

Somers, K.A., Bernhardt, E.S., Grace, J.B., et al. (2013) Streams in the urban heat island: spatial and temporal variability in temperature. *Freshwater Science*, 32 (1): 309–326. doi:10.1899/12-046.1.

Somers, K.A., Bernhardt, E.S., McGlynn, B.L., et al. (2016) Downstream Dissipation of Storm Flow Heat Pulses: A Case Study and its Landscape-Level Implications. *JAWRA Journal of the American Water Resources Association*, 52 (2): 281–297. doi:10.1111/1752-1688.12382.

Søndergaard, M., Stedmon, C.A. and Borch, N.H. (2003) Fate of terrigenous dissolved organic matter (DOM) in estuaries: Aggregation and bioavailability. *Ophelia*, 57 (3): 161–176. doi:10.1080/00785236.2003.10409512.

Spencer, R.G.M., Stubbins, A., Hernes, P.J., et al. (2009) Photochemical degradation of dissolved organic matter and dissolved lignin phenols from the Congo River. *Journal of Geophysical Research: Biogeosciences*, 114 (G3): G03010. doi:10.1029/2009JG000968.

Sprague, L.A. (2005) Drought effects on water quality in the South Platte River Basin, Colorado. *Journal of the American Water Resources Association*, 41 (1): 11–24. doi:10.1111/j.1752-1688.2005.tb03713.x.

Starkey, E., Parkin, G., Birkinshaw, S., et al. (2017) Demonstrating the value of community-based ('citizen science') observations for catchment modelling and characterisation. *Journal of Hydrology*, 548: 801–817. doi:10.1016/j.jhydrol.2017.03.019.

Stedmon, C.A. and Bro, R. (2008) Characterizing dissolved organic matter fluorescence with parallel factor analysis: a tutorial. *Limnology and Oceanography: Methods*, 6 (11): 572–579. doi:10.4319/lom.2008.6.572.

Stedmon, C.A., Markager, S. and Bro, R. (2003) Tracing dissolved organic matter in aquatic environments using a new approach to fluorescence spectroscopy. *Marine Chemistry*, 82 (3–4): 239–254. doi:10.1016/S0304-4203(03)00072-0.

Stedmon, C.A., Thomas, D.N., Papadimitriou, S., et al. (2011) Using fluorescence to characterize dissolved organic matter in Antarctic sea ice brines. *Journal of Geophysical Research: Biogeosciences*, 116 (G3): G03027. doi:10.1029/2011JG001716.

Stepanauskas, R., Moran, M.A., Bergamaschi, B.A., et al. (2005) Sources, bioavailability, and photoreactivity of dissolved organic carbon in the Sacramento–San Joaquin River Delta. *Biogeochemistry*, 74 (2): 131–149. doi:10.1007/s10533-004-3361-2.

Stott, P.A., Christidis, N., Otto, F.E.L., et al. (2016) Attribution of extreme weather and climate-related events. *Wiley Interdisciplinary Reviews: Climate Change*, 7 (1): 23–41. doi:10.1002/wcc.380.

Survey, O. (2018) *OS Terrain 5m*. Available at: https://www.ordnancesurvey.co.uk/business-and-government/products/os-terrain-5.html.

Tague, C.L., Farrell, M., Grant, G., et al. (2007) Hydrogeologic controls on summer stream temperatures in the McKenzie River basin, Oregon. *Hydrological Processes*, 21 (24): 3288–3300.

doi:10.1002/hyp.6538.

Talmage, P.J., Lee, K.E., Goldstein, R.M., et al. (1999) *Water quality, physical habitat, and fish community composition in streams in the Twin Cities metropolitan area, Minnesota, 1997-98*. doi:10.3133/wri994247.

Tam, V.T. and Nga, T.T.V. (2018) Assessment of urbanization impact on groundwater resources in Hanoi, Vietnam. *Journal of environmental management*, 227: 107–116. doi:10.1016/j.jenvman.2018.08.087.

Tank, J.L., Rosi-Marshall, E.J., Griffiths, N.A., et al. (2010) A review of allochthonous organic matter dynamics and metabolism in streams. *Journal of the North American Benthological Society*, 29 (1): 118–146. doi:10.1899/08-170.1.

Tetzlaff, D., Carey, S.K., McNamara, J.P., et al. (2017) The essential value of long-term experimental data for hydrology and water management. *Water Resources Research*, 53 (4): 2598–2604. doi:10.1002/2017WR020838.

Thorndahl, S., Einfalt, T., Willems, P., et al. (2017) Weather radar rainfall data in urban hydrology. *Hydrol. Earth Syst. Sci*, 21: 1359–1380. doi:10.5194/hess-21-1359-2017.

Thorp, J.H. and Delong, M.D. (2002) Dominance of autochthonous autotrophic carbon in food webs of heterotrophic rivers. *Oikos*, 96 (3): 543–550. doi:10.1034/j.1600-0706.2002.960315.x.

Tilburg, C.E., Jordan, L.M., Carlson, A.E., et al. (2015) The effects of precipitation, river discharge, land use and coastal circulation on water quality in coastal Maine. *Royal Society open science*, 2 (7): 140429. doi:10.1098/rsos.140429.

Toffolon, M. and Piccolroaz, S. (2015) A hybrid model for river water temperature as a function of air temperature and discharge. *Environmental Research Letters*, 10. doi:10.1088/1748-9326/10/11/114011.

Tu, J. (2009) Combined impact of climate and land use changes on streamflow and water quality in eastern Massachusetts, USA. *Journal of Hydrology*, 379 (3–4): 268–283. doi:10.1016/j.jhydrol.2009.10.009.

UKTAG (2008) *UK Environmental Standards and Conditions*. Available at: https://www.wfduk.org/sites/default/files/Media/Environmental standards/Environmental standards phase 2_Final_110309.pdf.

Ummenhofer, C.C. and Meehl, G.A. (2017) Extreme weather and climate events with ecological relevance: A review. *Philosophical Transactions of the Royal Society B: Biological Sciences*, 372 (1723). doi:10.1098/rstb.2016.0135.

UN-Water (2015) *The United Nations world water development report 2015.* Available at: https://unesdoc.unesco.org/ark:/48223/pf0000231823 (Downloaded: 26 August 2019).

UNESCO (2019) *The United Nations world water development report 2019: leaving no one behind*.

United Nations (2018) *World Urbanization Prospects 2018*.

Vannote, R.L., Minshall, G.W., Cummins, K.W., et al. (1980) The River Continuum Concept. *Canadian Journal of Fisheries and Aquatic Sciences*, 37 (1): 130–137. doi:10.1139/f80-017.

Vaughan, M.C.H., Bowden, W.B., Shanley, J.B., et al. (2017) High-frequency dissolved organic carbon and nitrate measurements reveal differences in storm hysteresis and loading in relation to land cover and seasonality. *Water Resources Research*, 53 (7): 5345–5363. doi:10.1002/2017WR020491.

Vaughn, C.C. (2010) Biodiversity Losses and Ecosystem Function in Freshwaters: Emerging Conclusions and Research Directions. *BioScience*, 60 (1): 25–35. doi:10.1525/bio.2010.60.1.7.

Del Vecchio, R. and Blough, N. V (2002) Photobleaching of chromophoric dissolved organic matter in natural waters: kinetics and modeling. *Marine Chemistry*, 78 (4): 231–253. doi:10.1016/S0304-4203(02)00036-1.

Vicente-Serrano, S.M., Zabalza-Martínez, J., Borràs, G., et al. (2017) Extreme hydrological events and the influence of reservoirs in a highly regulated river basin of northeastern Spain. *Journal of Hydrology: Regional Studies*, 12: 13–32. doi:10.1016/j.ejrh.2017.01.004.

Villarini, G. and Krajewski, W.F. (2010) Review of the Different Sources of Uncertainty in Single Polarization Radar-Based Estimates of Rainfall. *Surveys in Geophysics*, 31 (1): 107–129. doi:10.1007/s10712-009-9079-x.

Villarini, G., Mandapaka, P. V., Krajewski, W.F., et al. (2008) Rainfall and sampling uncertainties: A rain gauge perspective. *Journal of Geophysical Research*, 113 (D11): D11102. doi:10.1029/2007JD009214.

Van Vliet, M.T.., Franssen, W.H.P., Yearsley, J.R., et al. (2013) Global river discharge and water temperature under climate change. *Global Environmental Change*, 23 (2): 450–464. doi:10.1016/J.GLOENVCHA.2012.11.002.

Van Vliet, M.T.H. and Zwolsman, J.J.G. (2008) Impact of summer droughts on the water quality of the Meuse river. *Journal of Hydrology*, 353 (1–2): 1–17. doi:10.1016/J.JHYDROL.2008.01.001.

Wagner, T., Midway, S.R., Whittier, J.B., et al. (2017) Annual changes in seasonal riverwater temperatures in the Eastern and Western United States. *Water*, 9 (90). doi:10.3390/w9020090.

Wakode, H.B., Baier, K., Jha, R., et al. (2018) Impact of urbanization on groundwater recharge and urban water balance for the city of Hyderabad, India. *International Soil and Water Conservation Research*, 6 (1): 51–62. doi:10.1016/j.iswcr.2017.10.003.

Walsh, C.J., Fletcher, T.D. and Burns, M.J. (2012) Urban Stormwater Runoff: A New Class of Environmental Flow Problem Gilbert, J.A. (ed.). *PLoS ONE*, 7 (9): e45814. doi:10.1371/journal.pone.0045814.

Walsh, C.J., Fletcher, T.D. and Vietz, G.J. (2016) Variability in stream ecosystem response to urbanization. *Progress in Physical Geography: Earth and Environment*, 40 (5): 714–731. doi:10.1177/0309133316671626.

Walsh, C.J., Roy, A.H., Feminella, J.W., et al. (2005) The urban stream syndrome: current knowledge and the search for a cure. *Journal of the North American Benthological Society*, 24 (3): 706–723. doi:10.1899/04-028.1.

Wang, L. and Kanehl, P. (2003) INFLUENCES OF WATERSHED URBANIZATION AND INSTREAM HABITAT ON MACROINVERTEBRATES IN COLD WATER STREAMS. *Journal of the American Water Resources Association*, 39 (5): 1181–1196. doi:10.1111/j.1752-1688.2003.tb03701.x.

Warren, L. and Zimmerman, A. (1994) Suspended particulate oxides and organic matter interactions in trace metal sorption reactions in a small urban river. *Biogeochemistry*, 24 (1): 21–34. doi:10.1007/BF00001305.

Webb, B.W., Clack, P.D. and Walling, D.E. (2003) Water-air temperature relationships in a Devon river system and the role of flow. *Hydrological Processes*, 17 (15): 3069–3084. doi:10.1002/hyp.1280.

Webb, B.W., Hannah, D.M., Moore, R.D., et al. (2008) Recent advances in stream and river temperature research. *Hydrological Processes*, 22 (7): 902–918. doi:10.1002/hyp.6994.

Webster, P.J. and Jian, J. (2011) Environmental prediction, risk assessment and extreme events: adaptation strategies for the developing world. *Philosophical Transactions of the Royal Society A: Mathematical, Physical and Engineering Sciences*, 369 (1956): 4768–4797. doi:10.1098/rsta.2011.0160.

Weishaar, J.L., Aiken, G.R., Bergamaschi, B.A., et al. (2003) Evaluation of Specific Ultraviolet Absorbance as an Indicator of the Chemical Composition and Reactivity of Dissolved Organic Carbon. *Environmental Science & Technology*, 37 (20): 4702–4708. doi:10.1021/ES030360X.

Whitehead, P.G., Wilby, R.L., Battarbee, R.W., et al. (2009) A review of the potential impacts of climate change on surface water quality A review of the potential impacts of climate change on surface water quality A review of the potential impacts of climate change on surface water quality. *Hydrological Sciences Journal*, 54 (1): 101–123. doi:10.1623/hysj.54.1.101.

Whitfield, P.H., Wang, J.Y. and Cannon, A.J. (2009) Modelling Future Streamflow Extremes — Floods and Low Flows in Georgia Basin, British Columbia. *Canadian Water Resources Journal / Revue canadienne des ressources hydriques*, 28 (4). doi:10.4296/cwrj2804633.

Wilbers, G.-J., Zwolsman, G., Klaver, G., et al. (2009) Effects of a drought period on physico-chemical surface water quality in a regional catchment area. *Journal of Environmental Monitoring*, 11 (6): 1298. doi:10.1039/b816109g.

Wilby, R.L., Johnson, M.F. and Toone, J.A. (2015) Thermal shockwaves in an upland river. *Weather*, 70 (3): 92–100. doi:10.1002/wea.2435.

Williams, C.J., Frost, P.C., Morales-Williams, A.M., et al. (2016) Human activities cause distinct dissolved organic matter composition across freshwater ecosystems. *Global Change Biology*, 22 (2): 613–626. doi:10.1111/gcb.13094.

Williams, C.J., Yamashita, Y., Wilson, H.F., et al. (2010) Unraveling the role of land use and

microbial activity in shaping dissolved organic matter characteristics in stream ecosystems. *Limnology and Oceanography*, 55 (3): 1159–1171. doi:10.4319/lo.2010.55.3.1159.

Williams, G.P. (1989) Sediment concentration versus water discharge during single hydrologic events in rivers. *Journal of Hydrology*, 111 (1–4): 89–106. doi:10.1016/0022-1694(89)90254-0.

Winterdahl, M., Futter, M., Köhler, S., et al. (2011) Riparian soil temperature modification of the relationship between flow and dissolved organic carbon concentration in a boreal stream. *Water Resources Research*, 47 (8). doi:10.1029/2010WR010235.

Winterdahl, M., Laudon, H., Lyon, S.W., et al. (2016) Sensitivity of stream dissolved organic carbon to temperature and discharge: Implications of future climates. *Journal of Geophysical Research: Biogeosciences*, 121 (1): 126–144. doi:10.1002/2015JG002922.

Wood, S.N. (2017) *Generalized additive models : an introduction with R*.

Wood, S.N. (2018) *Package 'mgcv'*. Available at: https://cran.r-project.org/web/packages/mgcv/mgcv.pdf.

Woodward, G., Perkins, D.M. and Brown, L.E. (2010a) Climate change and freshwater ecosystems: impacts across multiple levels of organization. *Philosophical Transactions of the Royal Society B: Biological Sciences*, 365 (1549): 2093–2106. doi:10.1098/rstb.2010.0055.

Woodward, G., Perkins, D.M. and Brown, L.E. (2010b) Climate change and freshwater ecosystems: Impacts across multiple levels of organization. *Philosophical Transactions of the Royal Society B: Biological Sciences*, 365 (1549): 2093–2106. doi:10.1098/rstb.2010.0055.

Worrall, F. and Burt, T. (2004) Time series analysis of long-term river dissolved organic carbon records. *Hydrological Processes*, 18: 893–911. doi:10.1002/hyp.1321.

Wymore, A.S., Rodríguez-Cardona, B. and McDowell, W.H. (2016) Understanding Dissolved Organic Matter Biogeochemistry Through In Situ Nutrient Manipulations in Stream Ecosystems. *Journal of Visualized Experiments*, 116. doi:10.3791/54704.

Yamashita, Y., Boyer, J.N. and Jaffé, R. (2013) Evaluating the distribution of terrestrial dissolved organic matter in a complex coastal ecosystem using fluorescence spectroscopy. *Continental Shelf Research*, 66: 136–144. doi:10.1016/J.CSR.2013.06.010.

Yang, D., Marsh, P. and Ge, S. (2014) Heat flux calculations for Mackenzie and Yukon Rivers. *Polar Science*, 8 (3): 232–241. doi:10.1016/j.polar.2014.05.001.

Yates, C.A., Johnes, P.J. and Spencer, R.G.M. (2016) Assessing the drivers of dissolved organic matter export from two contrasting lowland catchments, U.K. *Science of The Total Environment*, 569–570: 1330–1340. doi:10.1016/J.SCITOTENV.2016.06.211.

Ye, F., Guo, W., Wei, G., et al. (2018) The Sources and Transformations of Dissolved Organic Matter in the Pearl River Estuary, China, as Revealed by Stable Isotopes. *Journal of Geophysical Research: Oceans*, 123 (9): 6893–6908. doi:10.1029/2018JC014004.

Zhang, F., Cai, X. and Thornes, J.E. (2014) Birmingham's air and surface urban heat islands

associated with Lamb weather types and cloudless anticyclonic conditions. *Progress in Physical Geography*, 38 (4): 431–447. doi:10.1177/0309133314538725.

Zhao, C., Wang, C.-C., Li, J.-Q., et al. (2015) Dissolved organic matter in urban stormwater runoff at three typical regions in Beijing: chemical composition, structural characterization and source identification. *RSC Advances*, 5 (90): 73490–73500. doi:10.1039/C5RA14993B.

Zhou, Y., Davidson, T.A., Yao, X., et al. (2018) How autochthonous dissolved organic matter responds to eutrophication and climate warming: Evidence from a cross-continental data analysis and experiments. *Earth-Science Reviews*, 185: 928–937. doi:10.1016/J.EARSCIREV.2018.08.013.

Zuur, A.F., Ieno, E.N. and Elphick, C.S. (2010) A protocol for data exploration to avoid common statistical problems. *Methods in Ecology and Evolution*, 1 (1): 3–14. doi:10.1111/j.2041-210X.2009.00001.x.

Zwolsman, J.J.G. and van Bokhoven, A.J. (2007) Impact of summer droughts on water quality of the Rhine River - a preview of climate change? *Water Science and Technology*, 56 (4): 45–55. doi:10.2166/wst.2007.535.